Multicomponent Simulation of Wastewater-Derived Nitrogen and Carbon in Shallow Unconfined Aquifers

by Kerry T.B. MacQuarrie

A thesis
presented to the University of Waterloo
in fulfilment of the
thesis requirement for the degree of
Doctor of Philosophy
in
Earth Sciences

Waterloo, Ontario, Canada, 1997

The University of Waterloo requires the signatures of all persons using or photocopying this thesis. Please sign below, and give address and date.

Abstract

One of the most common methods to dispose of domestic wastewater involves the release of septic effluent from drains located in the unsaturated zone. Nitrogen from such systems is currently of concern because of nitrate contamination of drinking water supplies and eutrophication of coastal waters. The objectives of this study were to develop and apply a mechanistic flow and reactive transport model which couples the most relevant physical, geochemical and biochemical processes involved in wastewater plume evolution in sandy aquifers. This is the first application of multicomponent reactive transport modelling to wastewater plume evolution in shallow groundwater. The work focuses on nitrogen and carbon species in wastewater because of the environmental relevance of nitrogen and the important interactions between the nitrogen and carbon chemistry systems.

The numerical model solves for variably-saturated flow and reactive transport of multiple species. Individual drains are represented in the model by using a new method based on discretization of a one-dimensional open channel flow equation; the numerical contributions to the global system of equations from the one-dimensional equation are added to the three-dimensional, porous medium contributions. The reactive transport equations are solved using the Strang splitting method which is shown to be accurate for Monod and first- and second-order kinetic reactions, and two to four times more efficient than sequential iterative splitting. The reaction system is formulated as a fully-kinetic chemistry problem which allows for the use of several special-purpose ordinary differential equation solvers. For reaction systems containing both fast and slow kinetic reactions, such as the combined nitrogen-carbon system, it is found that a specialized stiff explicit solver fails to obtain a solution. An implicit solver is more robust and its computational performance is improved by scaling of the fastest reaction rates.

The model results were compared to geochemical data obtained from a well-studied wastewater plume in a sandy aquifer near Cambridge, Ontario. It is shown that the oxidation of ammonium and dissolved organic carbon (DOC) goes to completion in the 1.5 m distance between the drain field and the water table, and that only a minor pH

reduction occurs. The overall behaviour of the reactive species in the model simulations agrees well with the geochemical data obtained below the drain field and it is concluded that the major physical and biochemical processes have been correctly captured in the current model. The model is then used to examine the impact of several key physical and chemical factors on the evolution of the wastewater plume. It is shown that depth to the water table and wastewater chemistry can have important repercussions on groundwater chemistry beneath septic drain fields. Interestingly, it is demonstrated that low-pH plumes may not always develop in noncalcarious aquifers. It is concluded that the model developed here is a useful tool to assess the impacts of onsite wastewater release into shallow aquifers.

As a final contribution the performance of an alternative drain field design is investigated. It is shown that a fine-grained layer, supplemented with labile organic carbon in the form of wood wastes, located beneath the drains is an effective means to create denitrifying conditions which eliminate nitrogen loading to shallow groundwater. It is also shown that in noncalcarious aquifers the denitrification reaction provides sufficient buffering capacity to maintain near neutral pH conditions beneath and down gradient of the drain field. Leaching of excess *DOC* from the denitrification layer is problematic and causes an anaerobic plume to develop in situations where the water table is less than five to six metres below ground surface; this anaerobic plume may lead to other down gradient changes in groundwater quality. A drain field and denitrification layer of smaller dimensions is shown to be just as effective for reducing nitrate, but has the benefit of reducing the excess *DOC* leached from the layer. This configuration will minimize the impact of wastewater disposal in areas where the water table is as shallow as 3.5 *m*.

Acknowledgments

I would like to thank my supervisor, Dr. E.A. Sudicky, for his advice and support during the course of my Doctoral program. This is my second post graduate degree under Ed's supervision and my academic career has been strongly influenced by his guidance and enthusiasm.

I am grateful for the many discussions and technical assistance provided by fellow PhD candidates Joel VanderKwaak, Uli Mayer, and André Unger, by Rob McLaren of the Waterloo Centre for Groundwater Research, and by Dr. Will Robertson of the Department of Earth Sciences, University of Waterloo. Without their contributions the work would have progressed much slower, and would definitely have been less enjoyable.

Foremost I would like to thank my wife Carol for her support throughout the last four years. She has managed to successfully balance her own career and the upbringing of our two daughters, and at the same time have the patience to deal with an often absent husband.

Funding support for this work was provided through scholarships provided by the Natural Sciences and Engineering Research Council of Canada (NSERC), the Waterloo Center for Groundwater Research, the Canadian Council of Professional Engineers, North American Life, and the Association of Professional Engineers of New Brunswick. Support was also provided by NSERC research grants awarded to Dr. E.A. Sudicky. My present employer, the University of New Brunswick (Department of Civil Engineering), also contributed substantially by granting me an extended leave of absence to complete my Doctoral studies.

Contents

List of Tables

List of Figures

Chapter 1

Introduction

In the United States approximately 25 million private residences utilize on onsite wastewater treatment systems, most consisting of septic tanks and drain distribution fields [*US Bureau of the Census*, 1993]. Effluent from the distribution fields is released to the shallow subsurface at a total rate of approximately 3.8 billion cubic metres per year [*US Environmental Protection Agency*, 1986]. The wastewater can contain a number of potential groundwater contaminants: inorganic salts, nitrogen, phosphate, detergent-derived surfactants, infectious bacteria, and viruses. Of these, nitrogen (N) is currently of environmental concern for a number of reasons. Nitrate in drinking water is a health concern because of a link with the occurrence of methaemoglobinaemia in infants, and its possible role as a pro-carcinogen. In many jurisdictions the maximum acceptable concentration for nitrate in drinking water is 10 mg/L (as N) and this concentration may be exceeded by factors of 5 to 10 in plumes from drain fields depending on the effluent composition and hydrogeological conditions [*Postma et al.*, 1992; *Wilhelm et al.*, 1994a; *Harman et al.*, 1996]. In the province of Ontario, nitrate concentrations in groundwater at the property boundary must be less than 2.5 mg/L (as N) for distribution fields releasing more than 4500 litres/day. A typical regulated separation distance between distribution fields and drinking water wells is 30 m, and it is rarely required that a water supply well be sited hydraulically up gradient of a nearby septic drain field.

For most inland surface waters phosphorus is the limiting nutrient in determining productivity; however, *Weiskel and Howes* [1992] point out that coastal marine systems are more often *N*-limited and that because an increasing amount of septic effluent is discharged to coastal watersheds, septic systems may contribute substantially to eutrophication. Dissolved *N* concentrations may be 100 to 1000 times higher in septic tank effluent than in typical receiving water bodies. Coastal eutrophication in areas of the Florida Keys and the New England states has been linked to movement of septic-derived nutrients (*N* in particular) through groundwater flow systems [*Lapointe and Clark*, 1992; *Valiela et al.*, 1992]. Impacts include increased frequency of anoxic events and algal blooms, change of fauna composition, and loss of reef cover. A major focus of current coastal research is determining the groundwater contribution of wastewater-derived nitrogen to estuaries, bays and harbors [*DeSimone and Howes*, 1996; *Valiela et al.*, 1997]. *Valiela et al.* [1997] emphasize that the largest and most poorly understood of all issues related to coastal eutrophication is the fate of nitrogen in aquifers.

Despite the possible negative impacts of onsite wastewater systems, such systems have traditionally been installed based on regulations which are often adopted from other jurisdictions, and once in place the treatment performance is not monitored. This regulation-driven process is currently being called into question [*Smithson*, 1995] and it appears that performance-based regulations may be necessary, at least in areas where onsite systems may have severe impacts on water quality. Thus, there is a need to better understand the interaction between physical and biochemical processes which occur during wastewater transport from drain distribution fields. A better understanding of onsite systems will indicate where traditional designs are acceptable, and situations where alternative designs may be necessary.

A schematic of a typical onsite wastewater disposal system, and associated biochemical transformations, is given in Figure 1.1. Unlike atmospheric deposition and fertilizer use, disposal of wastewater via septic drain fields inserts nitrogen and carbon below the normal root zone and directly into the vadose zone. The biogeochemical processes occurring after discharge of wastewater from drain fields have been presented by *Reneau et al.* [1989] and *Wilhelm et al.* [1994a, 1994b]. Nitrogen in septic tank effluent is almost

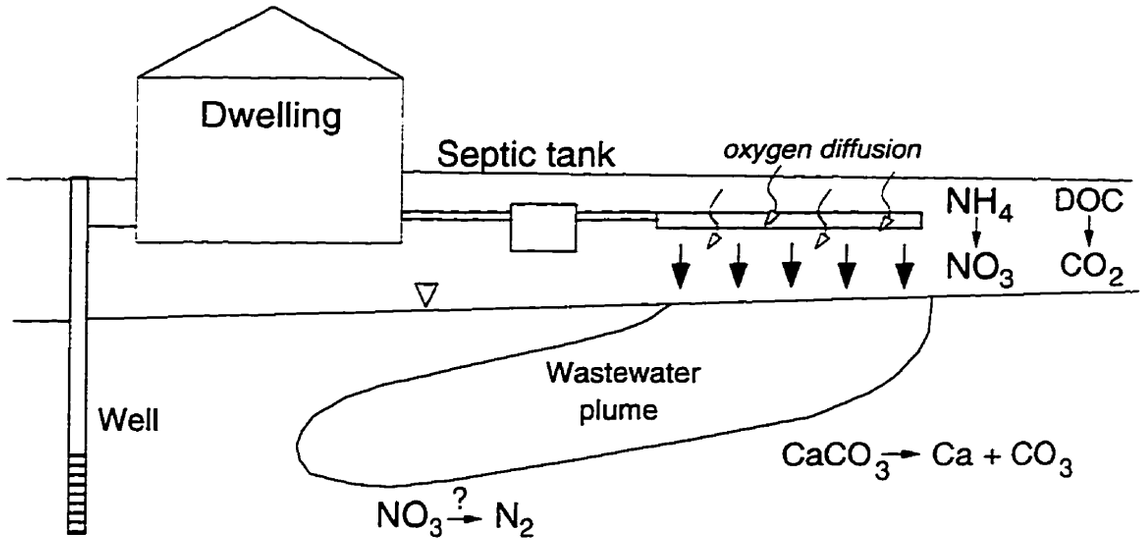

Figure 1.1: Typical onsite wastewater disposal system and associated biochemical transformations.

entirely in the form of dissolved ammonium (NH_4^+) [*Wilhelm et al.*, 1994a; *Whelan and Titamnis*, 1982], which can be oxidized to nitrate (NO_3^-) by autotrophic bacteria utilizing dissolved oxygen. In the vadose zone oxygen will be supplied primarily via gaseous O_2 diffusion from the atmosphere. Oxidation of NH_4^+ and septic organic matter may depress the pH of the aqueous solution unless carbonate minerals are present in the aquifer solids [*Whelan*, 1988]. The NO_3^- produced by nitrification is mobile in the subsurface and is generally only attenuated by biochemical reactions such as heterotrophic denitrification, which requires anoxic conditions and labile organic carbon [*e.g. Robertson and Cherry*, 1992], or pyrite oxidation [*Appelo and Postma*, 1994]. These reactions will therefore be restricted primarily to the saturated zone or soil layers near complete saturation.

In addition to ammonium oxidation, the degradation of dissolved organic carbon (*DOC*) will consume dissolved oxygen in the unsaturated and saturated zones beneath septic drain fields. This aerobic oxidation will produce dissolved CO_2 which can partition between the aqueous and gaseous phases (if present). The increased CO_2 may

affect aqueous carbonate chemistry and carbonate mineral solubility [*e.g. Robertson and Cherry*, 1992]. If the *DOC* is completely consumed by aerobic degradation in the unsaturated zone then denitrification further down gradient may not occur: the availability of labile organic carbon appears to be the primary controlling factor for denitrification in anaerobic groundwater [*Starr and Gillham*, 1989; *Hiscock et al.*, 1991; *Bradley et al.*, 1992; *DeSimone and Howes*, 1996]. Conversely, if *DOC* is present in excess of that required for denitrification, then more reducing conditions may develop and oxidation-reduction reactions involving *Mn*-oxides, *Fe*-oxides, or sulfates may occur down gradient of the drain fields.

Previous investigations of wastewater behaviour have generally involved laboratory column experiments or field studies, which provide valuable but case-specific information. In many studies the transport and fate of septic tank effluent were investigated only in unsaturated soils; the findings were then extrapolated to the groundwater zone [*e.g. Magdoff et al.*, 1974; *Whelan*, 1988]. Only a limited number of field evaluations have been conducted which follow the wastewater-derived plumes after they enter the saturated zone [*e.g. Viraraghavan and Warnock*, 1976; *Robertson and Cherry*, 1992; *Wilhelm et al.*, 1994a]. These detailed studies have shown that there is a complex interaction between physical transport and geochemical and biochemical reactions involving organic carbon, inorganic solutes (*e.g.* nitrogen, phosphate), dissolved gases, and aquifer minerals. In some circumstances these factors can lead to plumes of nitrate above 10 mg/L which extend over 100 metres down gradient from the septic drain field [*Robertson et al.*, 1991; *Harman et al.*, 1996]. Recent studies have shown that the impact of wastewater-derived *N* can be controlled to some extent by using reactive barriers to promote *in situ* denitrification [*Carmichael*, 1994; *Robertson and Cherry*, 1995]. Such alternative septic system designs require further investigation to determine their applicability in various hydrogeological situations.

Numerical models that simulate transport and biogeochemical processes are useful for integrating field observations and studying the relative importance of simultaneous processes. Numerical modelling studies of septic effluent plumes have been very limited, both in number and the level of detail considered. *Harmsen et al.* [1991a, 1991b] devel-

oped a three-dimensional pathline model to simulate advective transport of a conservative contaminant from a rectangular contaminant source (the drain field) to a pumping well. Their analysis estimated separation distances and minimum well depths required to avoid contamination of a water supply well; however, unsaturated zone transport and potential contaminant transformation mechanisms were not considered in the model. *Shutter et al.* [1994] applied a variably-saturated flow and transport model to investigate the movement of a conservative solute (Na^+) and a reactive solute (anionic surfactant) from a well-studied septic drain field. Biodegradation of the reactive solute was represented by first-order kinetics and therefore the effects of electron acceptor limitations could not be studied. Neither of these models are appropriate for simulating nitrogen transport and transformations as discussed above because nitrification and denitrification in groundwater must be represented by kinetic expressions which take the form of multiple nutrient, Monod-type equations. Several groups of researchers have recently simulated heterotrophic denitrification in one- or two-dimensional saturated groundwater flow systems [*e.g. Widdowson et al.*, 1988; *Kindred and Celia*, 1989; *Kinzelbach et al.*, 1991; *Lensing et al.*, 1994]; however, nitrogen and carbon transport from onsite wastewater systems has not been simulated and this will require consideration of important unsaturated zone transport and biogeochemical processes.

The objectives of this study are to develop and apply a mechanistic flow and reactive transport model which will couple the most relevant physical, geochemical and biochemical processes involved in wastewater plume evolution. Such a model can be used to obtain a more detailed understanding of how wastewater plumes evolve in shallow aquifers, and will allow for a systematic investigation into the relative importance of factors which control the concentration of contaminants which may potentially impact groundwater or surface water. Aspects related to watertable depth, unsaturated-zone soil properties, gas transport, reaction kinetics, and alternative designs can be investigated relatively economically with a realistic numerical model. For example, the presence of dissolved oxygen is considered to be of major importance in controlling the biogeochemical processes affecting N; however there are currently few, if any, nitrogen transport and fate models which also include O_2 transport in the unsaturated zone. Field and labo-

ratory studies have clearly shown that such coupling will be required in order to realistically simulate wastewater-derived *N*. To simulate the behaviour of contaminants in septic effluent a multicomponent approach is imperative because of the aforementioned interactions among the important chemical species.

In the next chapter the theoretical basis and related simplifying assumptions of the model are presented. The model simulates variably-saturated flow in porous media with discrete representation of drains. The transport of reactive species is represented by conventional advection-dispersion theory, while reactions are handled by a unique fully-kinetic formulation. Although any arbitrary number of reactions and species can be considered, this work focuses on the nitrogen and carbon species in wastewater because of the environmental relevance of nitrogen and the known interactions between the nitrogen and carbon chemistry systems. Simulation of pathogenic (disease-causing) microorganisms is beyond the scope of this study. The numerical solution approach and verification problems are presented next. The model results are compared with simplified analytical solution results and previously published numerical model results. A solution of the reactive transport problem using Strang operator splitting is shown to be both accurate and efficient. The model is then applied to a well-studied field site in southern Ontario and the simulation results for the major reactive species are discussed and compared with data from the site. A deterministic sensitivity analysis is then conducted using the model; this portion of the work investigates the influence of several key physical and biochemical parameters on the nature of the wastewater plume. The final contribution of this work is a numerical investigation of an alternative septic-system design which consists of an *in situ* reactive porous media barrier located below the drain field. The fine-grained barrier promotes nitrate attenuation by heterotrophic denitrification [*Robertson and Cherry*, 1995]. To complete the thesis the major contributions, conclusions and implications of the work are presented.

Chapter 2

Theoretical Development

The governing equations used as a basis for this research are presented in this chapter. The equation used to represent three-dimensional, variably-saturated flow in a porous medium is coupled with a one-dimensional open channel flow equation for fluid flow in drains. Transport of multiple solutes in the porous medium and drains is represented by advection-dispersion equations with appropriate modifications for variably-saturated conditions. Lastly, the biogeochemical reactions, which form source/sink terms for the transport equations, are formulated entirely as systems of nonlinear ordinary differential equations. A passive air phase is a fundamental assumption made in this work. *Massmann and Farrier* [1992] suggest that for long time periods (*e.g.* months to years) the effects of vapour diffusion will likely be more significant that atmospherically-induced advective air movement.

2.1 Porous Medium Flow

The governing equation for variably-saturated groundwater flow in a three-dimensional, non-deforming porous medium can be expressed by a modified form of Richards' equa-

tion [*Neuman*, 1973; *Cooley*, 1983; *Huyakorn et al.*, 1984]:

$$\frac{\partial}{\partial x_i}\left(K_{ij}\, k_{rw}\frac{\partial(\psi+z)}{\partial x_j}\right) = S_w S_s \frac{\partial \psi}{\partial t} + \theta_S \frac{\partial S_w}{\partial t} \qquad i,j = x,y,z \tag{2.1}$$

where K_{ij} is the saturated hydraulic conductivity tensor (L/T), $k_{rw} = k_{rw}(S_w)$ is the relative permeability of the medium, which is a function of the water saturation S_w, $\psi = \psi(x_i, t)$ is the pressure head (L), z is the elevation above an arbitrary datum (L), θ_S is the saturated moisture content, and S_s is the specific storage coefficient $(1/L)$. In order to obtain a solution to equation (2.1), the $\psi - S_w$ relationship and the $k_{rw} - S_w$ relationship must be established. These are usually determined experimentally and are often well described by the analytical expressions of *Brooks and Corey* [1964] or *van Genuchten* [1980].

2.2 Drain Flow

The general equation of continuity for flow in an open channel (*i.e.* a drain) is [*Dingman*, 1994]:

$$-\frac{\partial Q}{\partial l} + Q'\delta(l - l') + q_n = \frac{\partial A}{\partial t} \tag{2.2}$$

where Q is the discharge (L^3/T), Q' is the specified fluid flow rate in or out of the drain at location l' (L^3/T), $\delta(l - l')$ is the Dirac delta function, q_n is the rate of lateral inflow or outflow per unit channel length (L^2/T), l is distance along the drain (L), and A is the cross sectional area (L^2). For a channel in which the width, w, is constant but the depth of fluid, ψ', can vary, equation (2.2) can be written as:

$$-\frac{\partial Q}{\partial l} + Q'\delta(l - l') + q_n = w\,\frac{\partial \psi'}{\partial t} \tag{2.3}$$

The Q term in equation (2.3) will in general depend on factors such as the fluid depth, pressure gradient, channel slope, fluid properties, and channel roughness. I will simplify the present development by assuming a laminar flow regime; this allows one to neglect kinetic energy terms and express Q as [*MacQuarrie and Sudicky*, 1996]:

$$Q = -\,w\,\psi'\,K(\psi')\left(\frac{\partial \psi'}{\partial l} + \frac{\partial z}{\partial l}\right) \tag{2.4}$$

where $K(\psi')$ is the drain conductivity. The drain conductivity can be approximated by assuming shallow laminar flow in, for example, a rectangular section [*Dingman*, 1994]:

$$K(\psi') = \frac{\rho g(\psi')^2}{3\mu} \tag{2.5}$$

where μ and ρ are the fluid viscosity and density, respectively, and g is the gravitational acceleration constant. It should be noted that any arbitrary cross-sectional shape can be used to determine the drain conductivity-depth relationship; the form given by (2.5) is used because of its simplicity and because drains used for subsurface waste disposal are often placed in rectangular trenches which are filled with very coarse granular material. For transitional or turbulent flow in the drain other flow rules, including factors such as wall roughness, can be implemented [*Dingman*, 1994].

With the above assumptions in mind, the one-dimensional transient flow equation for a drain is now expressed as [*MacQuarrie and Sudicky*, 1996]:

$$w\frac{\partial}{\partial l}\left(\psi' K(\psi')\left(\frac{\partial \psi'}{\partial l}+\frac{\partial z}{\partial l}\right)\right)+Q'\delta(l-l')+q_n = w\frac{\partial \psi'}{\partial t} \tag{2.6}$$

Note that q_n may be variable with distance l due to porous medium heterogeneity or other hydraulic factors.

2.3 Porous Medium Solute Transport

The macroscopic equations governing aqueous- and air-phase transport in a variably-saturated porous medium can be derived from a mass balance applied to a unit volume of porous medium. This yields for species n:

$$\frac{\partial(\theta_w C_n{}^w+\theta_g C_n{}^g+\rho_b C_n{}^s)}{\partial t}+\frac{\partial}{\partial x_i}(q_i C_n{}^w)$$

$$-\frac{\partial}{\partial x_i}\left(\theta_w D_{ij}{}^w\frac{\partial C_n{}^w}{\partial x_j}+\theta_g D_{ij}{}^g\frac{\partial C_n{}^g}{\partial x_j}\right)$$

$$+ \lambda_n(\mathbf{C^w}, \mathbf{X}) = 0 \qquad i, j = x, y, z \tag{2.7}$$

where $\mathbf{C^w} = C_n{}^w$, $n = 1 \ldots . N_R$ is the aqueous phase concentration vector (M/L^3 *water*), $C_n{}^g$ is the gaseous phase concentration of species n (M/L^3 *air*), $C_n{}^s$ is the solid phase concentration of species n (M/M *solids*), $\theta_w = (\theta_S S_w)$ is the volumetric water content, $\theta_g = (\theta_S - \theta_w)$ is the volumetric air content, and ρ_b is the porous medium bulk density (M *solids*$/L^3$ *medium*). The fluid flux, q_i, is obtained from Darcy's law:

$$q_i = -K_{ij}\, k_{rw} \frac{\partial(\psi + z)}{\partial x_j} \tag{2.8}$$

The aqueous dispersion coefficient, $\theta_w D_{ij}{}^w$, is given by [*Bear*, 1972]:

$$\theta_w D_{ij}{}^w = (\alpha_l - \alpha_t)\frac{q_i q_j}{|q|} + \alpha_t |q| \delta_{ij} + \theta_w \left(\frac{\theta_w{}^{7/3}}{\theta_S{}^2}\right) D_w{}^o \delta_{ij} \tag{2.9}$$

where α_l and α_t are the longitudinal and transverse dispersivities (L), respectively, $|q|$ is the absolute magnitude of the Darcy flux (L^3/T), and δ_{ij} is the Kronecker delta. A modified form of (2.9), as proposed by *Burnett and Frind* [1987], is used to allow for two different transverse dispersivity values, that is, α_{th} for transverse horizontal and α_{tv} for transverse vertical dispersivity.

The product:

$$\left(\frac{\theta_w{}^{7/3}}{\theta_S{}^2}\right) D_w{}^o$$

in (2.9) is the effective diffusion coefficient for the variably-saturated medium, where $D_w{}^o$ is the free solution diffusion coefficient (L^2/T) for species n. For tortuosity, the *Millington and Quirk* [1961] expression based on water content and total porosity has been used; the effects of pressure and temperature on the effective diffusion coefficient are generally small [*Washington et al.*, 1994] and are not accounted for here.

The air phase dispersion coefficient is also expressed in terms of the *Millington and Quirk* [1961] relationship:

$$\theta_g D_{ij}{}^g = \theta_g \left(\frac{\theta_g{}^{7/3}}{\theta_S{}^2}\right) D_g{}^o \delta_{ij} \tag{2.10}$$

where D_g^o is the free air diffusion coefficient (L^2/T) for the species of interest.

The last term on the left hand side of (2.7) represents a general biogeochemical reaction term which is a function of aqueous phase concentrations and the immobile species concentrations, $\mathbf{X} = X_m$, $m = 1, \ldots, N_M$ (M/L^3 *medium*). Possible forms for this term will be discussed in Section 2.5.

Several common assumptions are made in order to simplify the system of equations given by (2.7). Partitioning between the aqueous and gaseous phases is assumed to be at local equilibrium, with the dimensionless Henry's law coefficient [*Stumm and Morgan*, 1981], $H_n = C_n{}^g/C_n{}^w$, being used for dilute aqueous systems. Aqueous/solid phase partitioning is also treated as an equilibrium process, capable of description with a linear sorption isotherm. Such an assumption implies that the distribution coefficient is $K_{dn} = C_n{}^s/C_n{}^w$ (L^3 *water*/M *solids*). With these assumptions in mind, equation (2.7) is now written as:

$$\frac{\partial[(\theta_w + \theta_g H_n + \rho_b K_{dn}) C_n{}^w]}{\partial t} + q_i \frac{\partial C_n{}^w}{\partial x_i} - \frac{\partial}{\partial x_i}\left[(\theta_w D_{ij}{}^w + \theta_g H_n D_{ij}{}^g)\frac{\partial C_n{}^w}{\partial x_j}\right] + \lambda_n(\mathbf{C^w}, \mathbf{X}) = 0 \qquad i, j = x, y, z \tag{2.11}$$

It should be noted that each mobile species in the system will have an equation of the form of (2.11); however, for nonvolatile solutes the Henry's constant will be zero, as will the distribution coefficient for nonsorbing solutes. The coupling among the various N_R species is assumed to be restricted to the reaction term in (2.11).

2.4 Drain Solute Transport

Transport in the drains is developed in a manner similar to that presented by *Lacombe et al.* [1995] for transport in vertical wells. Again application of a mass balance yields the following equation for species n:

$$w\,\psi'\left[\frac{\partial C_n{}^w}{\partial t} + Q\frac{\partial C_n{}^w}{\partial l} - \frac{\partial}{\partial l}\left(D_{ld}\frac{\partial C_n{}^w}{\partial l}\right)\right]$$

$$+ w \psi' \lambda_n(\mathbf{C}^w, \mathbf{X}) + \Gamma_n = 0 \tag{2.12}$$

where Γ_n is the rate of solute mass transfer per unit length of drain (M/LT) and solute partitioning has been ignored. Longitudinal dispersion in the drain is approximated by the *Taylor* [1953] expression for dispersion in a fluid-filled tube under laminar flow conditions:

$$D_{ld} = (r_e^2 Q^2 / 48 D_n^o) + D_n^o \tag{2.13}$$

where r_e is an equivalent radius computed from the saturated cross-sectional area of the drain.

2.5 Biogeochemical Reactions

In this section, a system of nonlinear biologically-mediated and abiotic reactions is formulated entirely in a kinetic framework. Previous formulations of relatively slow (*e.g.* microbial) and fast abiotic reactions have used a combined kinetic and equilibrium approach [*e.g. Lensing et al.*, 1994; *Marzal et al.*, 1994] which leads to multiple iteration loops (for solution of the combined system within a time step). *Zysett et al.* [1994] suggest that imposing equilibrium chemistry constraints during each time level of kinetic chemistry integration will lead to excessive computational requirements and they propose formulating all chemical problems using purely kinetic expressions. To the author's knowledge such an approach has not been previously used in subsurface reactive transport modelling involving both biologically-mediated and aqueous inorganic reactions; however, a fully-kinetic formulation is the usual approach taken in atmospheric reactive transport models [*e.g. Sandu et al.*, in press].

The microbiological reactions, which include nitrification, aerobic biodegradation, and other oxidation-reduction reactions, are handled using a multiple-Monod expression [*e.g. Essaid et al.*, 1995]. Although other expressions are possible, for example minimum-Monod kinetics [*Kindred and Celia*, 1989], recent kinetic and physiological

studies by *Bae and Rittmann* [1996] support the multiple-Monod formulation. Multiple-Monod kinetics have been successfully applied in previous subsurface microbiological reaction modelling [*e.g. Borden and Bedient*, 1986; *MacQuarrie et al.*, 1990; *Kinzelbach et al.* , 1991; *Chen et al.*, 1992].

In general terms the multiple-Monod expression for process p is given by [*Chen et al.*, 1992; *Essaid et al.*, 1995]:

$$\lambda^p = k_{max}{}^p X_m F(X_M) \left[\frac{C_1}{C_1 + K_1{}^p}\right] \left[\frac{C_2}{C_2 + K_2{}^p}\right] \cdots \left[\frac{C_{N_R}}{C_{N_R} + K_{N_R}{}^p}\right] F(C_I) \tag{2.14}$$

where $k_{max}{}^p$ is the maximum specific substrate utilization rate for process p $(1/T)$, X_m is the biomass of the population m responsible for the reaction, per unit volume of porous medium (M *biomass*$/L^3$), C_1, C_2, ..., C_{N_R} are the aqueous species concentrations (M/L^3 *water*), and $K_1{}^p$, $K_2{}^p$, ..., $K_{N_R}{}^p$ are the half-saturation constants for the respective species (M *species*$/L^3$ *water*). The total reaction rate for species n is equal to the sum of the rates for all processes in which n is involved, that is:

$$\lambda_n(\mathbf{C}^{\mathbf{w}}, \mathbf{X}) = \sum_p \lambda^p r_n^p \tag{2.15}$$

where r_n^p is an appropriate stoichiometric coefficient. For example, if 2.0 *mg* of oxygen are consumed for each 1.0 *mg* of organic carbon oxidized, then r for oxygen in the aerobic biodegradation process would be 2.0.

Noncompetitive inhibition, an example being the inhibition of an anaerobic biodegradation process (*e.g.* denitrification) by the presence of oxygen, is represented in (2.14) using a hyperbolic function [*Widdowson et al.*, 1988]:

$$F(C_I) = \frac{K_{C_I}}{K_{C_I} + C_I} \tag{2.16}$$

where C_I is the aqueous concentration of the inhibiting species, and K_{C_I} is the inhibition coefficient (M *species*$/L^3$ *water*).

Often one of the aqueous species involved in a microbiological reaction acts as a primary substrate. That is, it supplies the needed nutrients and energy for biomass growth. The rate of growth for a population m is linked to (2.14) and can be expressed as:

$$\frac{dX_m}{dt} = \lambda^p Y_m - X_m k_m{}^d \tag{2.17}$$

where Y_m is the microbial yield coefficient for bacteria m when mediating reaction p (*M biomass/M substrate*), and $k_m{}^d$ is the specific biomass decay or maintenance constant ($1/T$). It should be noted that the classical Monod equation combined with (2.17) are empirically based representations of biomass dynamics, and as such there is no mechanism to limit biomass growth in situations where all required nutrients are supplied in excess. Clearly, in a porous medium, there will be physical and hydrodynamic constraints on the maximum biomass concentration. Therefore, biomass growth inhibition has been incorporated in (2.14) using the expression given by *Kindred and Celia* [1989], which has the same form as (2.16):

$$F(X_m) = \frac{K_{b_m}}{K_{b_m} + X_m} \tag{2.18}$$

where K_{b_m} is an empirical biomass inhibition constant (*M biomass/L^3 porous medium*). Thus as X_m becomes larger than K_{b_m}, the kinetic expression (2.14) is controlled by a constant biomass of K_{b_m}. This representation of biomass inhibition has been used by *Essaid et al.* [1995] to simulate degradation processes at a crude oil spill site.

The Monod-based formulation presented here assumes that the reaction rates are controlled by the bulk aqueous phase (macroscopic) species concentrations. An alternative approach would be to consider mass transfer limitations caused by diffusion of species into a biophase or biofilm [*Molz et al.*, 1986; *Widdowson et al.*, 1988; *Wood et al.*, 1994]. The differences between the macroscopic and diffusion-limited conceptual models have been discussed in detail elsewhere [*Baveye and Valocchi*, 1989; *Wood et al.*, 1994]; however, a direct comparison of these models made by *Odencrantz* [1992] indicated that there was no noticeable differences in terms of aqueous phase species concentrations or total mass for realistic field-scale scenarios. In addition, laboratory observations by *Vandevivere and Baveye* [1992] showed that several aerobic biomass strains do not form

biofilm coatings on the solid surface of sand grains. Based on these findings, and the fact that classical biofilm models require many additional and difficult to determine parameters, the macroscopic conceptual model is adopted in this work. As such, the biomass is assumed to be an immobile population, as can be seen from (2.17), which has the ability to directly utilize aqueous species.

2.6 Microbial and Abiotic Reaction Coupling

The basic description of the kinetics of abiotic reactions follows the discussions on chemical kinetics given by *Stumm and Morgan* [1981] and *Stone and Morgan* [1990]. These authors discuss a wide variety of mechanisms for elementary aqueous reactions, as well as the influence of ionic strength and temperature. In this development isothermal conditions are assumed. As well, the ionic strength is considered to be low and thus concentrations are taken as equivalent to activities, although this is not a necessary assumption. As an example, many important reactions in groundwater systems are reversible reactions:

$$C_1 + C_2 \rightleftharpoons C_3 \tag{2.19}$$

for which the rate of change of C_1 (or C_2) can be described by:

$$\frac{dC_1}{dt} = -k_f C_1 C_2 + k_b C_3 \tag{2.20}$$

where k_f is a second-order forward reaction constant $(1/MT)$, and k_b is a first-order backward reaction constant $(1/T)$. Theoretically (2.20) can reach equilibrium, at which point the reaction is defined by:

$$\frac{k_f}{k_b} = \frac{C_3}{C_1 C_2} \tag{2.21}$$

where the ratio k_f/k_b is the thermodynamic equilibrium constant [*Stumm and Morgan*, 1981].

For a system of reactions, a set of ordinary differential equations can be written by considering the production and loss of each species over all reactions. This is illustrated below for a simple two-reaction example, where the first irreversible reaction (aerobic

degradation of CH_2O) is microbially-mediated and the second is a reversible abiotic reaction (hydration of CO_2):

$$CH_2O + O_{2_{aq}} \rightarrow CO_{2_{aq}} + H_2O$$

$$CO_{2_{aq}} + H_2O \rightleftharpoons HCO_3^- + H^+$$

The ordinary differential equation for $CO_{2_{aq}}$ is thus formed by combining a multiple-Monod expression, with first- and second-order rate equations:

$$\frac{dCO_{2_{aq}}}{dt} = r\, k_{max}\, X_m F(X_M) \left[\frac{CH_2O}{CH_2O + K_{CH_2O}}\right] \left[\frac{O_{2_{aq}}}{O_{2_{aq}} + K_{O_{2_{aq}}}}\right]$$

$$- k_f \left(CO_{2_{aq}}\right) + k_b \left(HCO_3^-\right)\left(H^+\right) \qquad (2.22)$$

where noncompetitive inhibition has been ignored and the concentration of water is assumed reaction invariant. Any additional reactions involving $CO_{2_{aq}}$ can be included by adding or subtracting the appropriate rate expression from (2.22). The overall rate equation for $CO_{2_{aq}}$ is then inserted for $\lambda_n(\mathbf{C}^{\mathbf{w}}, \mathbf{X})$ in (2.11). Other chemical processes, such as kinetic hydrophobic sorption, can easily be included in the chemical system; in such a case the equilibrium distribution coefficient in (2.11) could be omitted.

Formulating a combined biotic and abiotic system of reactions in the manner presented above leads to a consistent set of mass balance equations. For example, a charge balance is automatically satisfied. The method does; however, require rate constants for all elementary reactions; for groundwater systems many abiotic rate constants can be found in the literature [*e.g. Crooks*, 1975; *Chou et al.*, 1989] or estimated from ion diffusion theory [*Stumm and Morgan*, 1981] and thermodynamic equilibrium constants. As will be discussed in the following chapter, for a very fast reversible reaction it may not be necessary to use the actual reaction rates so long as the ratio of the forward and backward rate constants yield the correct thermodynamic equilibrium constant.

Chapter 3

Numerical Solution Approach and Verification Problems

The numerical methods employed to solve the mathematical model presented in the previous chapter are detailed below. Emphasis is placed on techniques which will provide accurate solutions; however, computational efficiency is also of great importance given that the intended application of the model is for field-scale simulation of multi-species reactive transport.

3.1 Variably-Saturated Flow

The most important aspects to resolve with respect to the flow solution are obtaining accurate saturations and Darcy fluxes, as these quantities are directly utilized in subsequent transport computations. For this work the three-dimensional variably-saturated flow model presented by *Therrien and Sudicky* [1996] has been modified to incorporate drain flow. In this model, equation (2.1) is efficiently solved using a control volume finite-element technique with Newton linearization, which in combination with upstream weighting yields a monotone solution (*i.e.* saturations remain between 0.0 and 1.0) [*Forsyth et al.*, 1995; *Therrien and Sudicky*, 1996].

Galerkin's method is used to discretize equations (2.1) and (2.6) over the domain of interest. As the details of this method can be found elsewhere [*e.g. Huyakorn and Pinder*, 1983; *Therrien and Sudicky*, 1996] only the final discretized form of (2.1) and (2.6) are presented here. Approximate solutions are defined for the primary unknowns (ψ, S_w, and ψ') according to the general equation:

$$u(x_i,t) \simeq \hat{u}(x_i,t) = \sum_{J=1}^{n} N_J(x_i)\, u_J(t) \tag{3.1}$$

where u is the unknown function ($\equiv \psi$, S_w, and ψ') , J is the nodal index, n is the total number of nodes in the mesh, and N_J are linearly independent interpolation functions. Substituting equations of the form of (3.1) for ψ, S_w, and ψ' into (2.1) and (2.6), and then applying Green's theorem (divergence theorem) to reduce the order of derivatives leads to the system of equations for the superimposed porous medium and drain elements:

$$\left[S_w{}^{L+1} S_s \frac{\left(\psi^{L+1} - \psi^{L}\right)}{\Delta t} + \theta_S \frac{\left(S_w{}^{L+1} - S_w{}^{L}\right)}{\Delta t} \right]_I v_I$$

$$- \sum_{J \in n_I} \left(\gamma_{IJ} \lambda_{IJ}\right)^{L+1} \Gamma_{IJ} + \left[w \frac{\left(\psi'^{L+1} - \psi'^{L}\right)}{\Delta t} \right]_M l_M$$

$$- w \sum_{J \in n_M} \left(\gamma^*_{MJ} \lambda^*_{MJ}\right)^{L+1} \Gamma^*_{MJ} + Q'^{L+1}_M = 0 \tag{3.2}$$

where $I = 1.....n$, $M = 1.....nd$, L is the time step level, v_I is the three-dimensional volume of influence (control volume) for porous medium node I, n_I is the set of porous medium nodes connected to node I, M is the index of nodes along the drains, nd is the total number of drain nodes, l_M is the drain element length associated with node M, and n_M is the set of drain nodes connected to drain node M. Note that q_n does not appear explicitly in (3.2) because it is an internal flux between elements which is automatically accommodated for during assembly of the global matrix equations.

The quantities in the fluid flux terms in (3.2) are:

$$\gamma_{IJ} = (\psi_J + z_J) - (\psi_I + z_I) \tag{3.3}$$

$$\gamma^*_{MJ} = (\psi'_J + z_J) - (\psi'_M + z_M) \tag{3.4}$$

$$\Gamma_{IJ} = -\int_v K_{ij} \frac{\partial N_I}{\partial x_i} \frac{\partial N_J}{\partial x_j} \, dv \tag{3.5}$$

$$\Gamma^*_{MJ} = -\int_l \frac{\partial N_M}{\partial l} \frac{\partial N_J}{\partial l} \, dl \tag{3.6}$$

where the summation convention is assumed with respect to direction i and j when evaluating spatial derivatives, and

$$\lambda_{IJ} = k_{rwI} \quad \text{or} \quad k_{rwJ} \tag{3.7}$$

$$\lambda^*_{MJ} = \psi' K(\psi')_M \quad \text{or} \quad \psi' K(\psi')_J \tag{3.8}$$

where the value of λ_{IJ} and λ^*_{MJ} is determined by upstream weighting, for example $\lambda_{IJ} = k_{rwJ}$ if $\gamma_{IJ} > 0$.

Because of the nonlinear nature of the soil characteristic functions and the drain conductivity, equation (3.2) must be solved by Newton iteration. *Therrien and Sudicky* [1996] provide a detailed description of the Newton iteration scheme which is used here. To improve the performance of the algorithm presented by *Therrien and Sudicky* [1996] several of the numerical strategies presented by *Forsyth et al.* [1995] have been implemented. These include variable substitution, in which the primary variable at a node can be either pressure or saturation, and linear interpolation of the $\psi - S_w$ and $k_{rw} - S_w$ relationships at locations where S_w tends to the residual value or to unity. While (3.2) is based on a control volume finite element discretization, *Therrien and Sudicky* [1996] and *Panday et al.* [1993] provide a modified influence coefficient approach which mimics a seven-point finite difference operator.

Several special considerations arise in the present work which require some discussion. The term on the right-hand side of (2.6) represents the change in fluid storage in the drain due to changes in fluid level. If fluid compressibility effects are ignored, then this term will vanish if the drain is submerged (*i.e.* the top of the drain is below the water table). In situations where the drain lies above the water table and an inflow Q' is specified at one end of the drain, the specified flow rate may be insufficient to maintain a positive ψ' along the entire length of the drain. In such cases the conductivity of elements with

$\psi' = 0$ will be zero and no drain contribution will be made to the global matrix equations; however, in some circumstances flow from the drain to the surrounding unsaturated matrix may be restricted, for example by partially clogged openings in the drain wall, and thus there will be a nonzero depth of fluid along the entire drain. In simulating such cases ψ' in the drain is not allowed to fall below some small positive value (*e.g.* $0.01w$).

The preconditioned CGSTAB acceleration method [*van der Vorst*, 1992; *VanderKwaak et al.*, 1995] is used for solving the sparse matrix equations which arise during Newton linearization. For a variety of test problems involving variably-saturated flow with and without drains, total simulation times using CGSTAB acceleration were found to be 0.75 to 0.9 of the simulation times obtained with ORTHOMIN [*Vinsome*, 1976] or GMRES [*Saad and Schultz*, 1986] acceleration. Generally an incomplete factorization (ILU) preconditioner with level-zero fill performed well.

An absolute convergence criterion for the Newton iteration of 10^{-4} *m* was found to produce excellent mass balances for all simulations presented here. Variable time step sizes, as discussed by *Therrien and Sudicky* [1996], were employed for transient problems.

3.2 Reactive Solute Transport

The problem of multicomponent transport has generally been approached in one of two ways. In the first strategy, the relationships which represent the chemical reactions are incorporated directly into the advection-dispersion equations. Because of the nonlinear nature of the resulting transport equations a linearization method such as Newton iteration is required. This coupled method can therefore be very computationally demanding for multi-dimensional problems involving complex chemistry [*Yeh and Tripathi*, 1989]. Some example applications of this method include one-dimensional multicomponent simulations incorporating equilibrium reactions [e.g. *Valocchi et al.*, 1981; *Jennings et al.*, 1982]. *Steefel and Lasaga* [1994] present a two-dimensional multicomponent transport model in which aqueous equilibrium reactions are directly coupled with the

transport equations, while computation of solid-phase concentrations are decoupled.

For field-scale simulation of domestic drain fields, spatial domains with approximate dimensions of 5 *m* by 20 *m* by 100 *m* could easily be envisioned; adequate discretization may require on the order of 150,000 nodes and CPU storage requirements for a fully-coupled formulation could easily exceed 500 or 1000 MB. This large memory requirement makes the fully-coupled approach unattractive at this time.

The second method of solving for physical transport and chemical reactions is to use operator splitting to separate the transport and reaction operators and solve each sequentially, and sometimes iteratively, within each time step. This "two-step" approach makes use of the fact that reaction terms do not contain spatial derivatives. The method has a number of advantages when compared to the fully-coupled method and these have been discussed by *Valocchi and Malmstead* [1992], *Miller and Rabideau* [1993], and *Steefel and Lasaga* [1994], among others. Most importantly with respect to the problem at hand, is that operator splitting leads to significantly smaller systems of equations. This technique also allows the chemical reactions to be incorporated into transport models in a modular fashion.

If the original reactive transport equation, (2.11), is represented as:

$$\frac{\partial \mathbf{C}^{\mathbf{w}}}{\partial t} = F(\mathbf{C}^{\mathbf{w}}, \mathbf{X}) = F_{tr}(\mathbf{C}^{\mathbf{w}}) + F_{ch}(\mathbf{C}^{\mathbf{w}}, \mathbf{X}) \tag{3.9}$$

where $F_{tr}(\mathbf{C}^{\mathbf{w}})$ is the linear transport operator and $F_{ch}(\mathbf{C}^{\mathbf{w}}, \mathbf{X})$ represents the nonlinear reactions terms, then the solution of (3.9) can be denoted in conventional exponential notation as [*Rouhi and Wright*, 1995]:

$$\mathbf{C}^{\mathbf{w}}(\Delta t) = exp\{\Delta t\, F\} \cdot [\mathbf{C}^{\mathbf{w}}(0), \mathbf{X}(0)] \tag{3.10}$$

where $exp\{\Delta t\, F\}$ is the time advance operator.

The splitting methods exploit the fact that $exp\{\Delta t\, F_{tr}\}$ and $exp\{\Delta t\, F_{ch}\}$ can be calculated efficiently, using numerical techniques, and that the individual solutions can be used to estimate $exp\{\Delta t\, F\}$. For example, Strang operator splitting [*Strang*, 1968] can be represented as three sequential applications of operators:

$$exp\{\Delta t\, F\} = exp\{\Delta t/2\, F_{tr}\}\, exp\{\Delta t\, F_{ch}\}\, exp\{\Delta t/2\, F_{tr}\} \tag{3.11}$$

which is the simplest symmetric splitting method and formally has an error of order (Δt^2) [*Hundsdorfer and Verwer*, 1995; *Barry et al.*, 1996]. The algorithm given by (3.11) begins by solving a linear transport equation for each of the N_R mobile species for a time interval of $\Delta t/2$. The resulting concentration vector $\mathbf{C}^{\mathbf{w}}$ is then used as the initial condition for the nonlinear chemistry operator; the final application of the transport operator then advances the solution over $\Delta t/2$, resulting in $\mathbf{C}^{\mathbf{w}}(\Delta t)$. Because immobile species are not transported, their values $\mathbf{X}(\Delta t)$ are obtained directly after application of the second operator in (3.11). The more commonly-used "two-step" splitting method can be expressed as:

$$exp\{\Delta t\, F\} \;=\; exp\{\Delta t\, F_{tr}\}\, exp\{\Delta t\, F_{ch}\} \tag{3.12}$$

and has an error of order (Δt). Several sets of numerical experiments have been conducted using the above splitting schemes for linear first-order reactions [*Valocchi and Malmstead*, 1992] and two-species Monod reactions [*Morshed and Kaluarachchi*, 1995]. The results show that Strang splitting does yield solutions with smaller temporal errors than the standard two-step splitting.

Other approaches used with operator splitting include iteration, during a time step Δt, between the two time advance operators in (3.12) [*e.g. Zysset and Stauffer*, 1992; *Kinzelbach et al.*, 1991]. In this sequential iteration approach (SIA) each of the operators must contain a coupling term which accounts for the change caused by the other operator. *Steefel and MacQuarrie* [1996] have shown that the SIA can produce solutions which have an accuracy comparable to that obtained with a fully-coupled solution method.

3.2.1 Transport Equation Solution

The linear transport equations are solved by a control volume finite element technique using (3.1), with the primary variable being aqueous concentration. Coupling of transport in the drains and porous medium is achieved using superposition of elements as discussed previously for fluid flow. The discretized equations resulting from this process are:

$$\left[\bar{R}\,\frac{(C_l^{L+1} - C_l^{L})}{\Delta t}\right]_l v_l$$

$$
\begin{aligned}
&- \sum_{J \in n_I} \left[\varepsilon \left(\xi_{IJ}\right)^{L+1} + (1-\varepsilon)\left(\xi_{IJ}\right)^{L} \right] \Lambda_{IJ} \\
&+ \sum_{J \in n_I} q_{IJ} \left[\varepsilon \left(C_{IJ}\right)^{L+1} + (1-\varepsilon)\left(C_{IJ}\right)^{L} \right] \Omega_{IJ} \\
&+ \left[w \psi' \frac{\left({C'_I}^{L+1} - {C'_I}^{L} \right)}{\Delta t} \right]_M l_M \\
&- w \psi' \sum_{J \in n_M} \left[\varepsilon \left(\xi^*_{IJ}\right)^{L+1} + (1-\varepsilon)\left(\xi^*_{IJ}\right)^{L} \right] \Lambda^*_{IJ} \\
&+ w \psi' \sum_{J \in n_M} Q_{IJ} \left[\varepsilon \left(C'_{IJ}\right)^{L+1} + (1-\varepsilon)\left(C'_{IJ}\right)^{L} \right] \Omega^*_{IJ} \\
&+ \bar{C} \, Q'^{L+1}_M = 0
\end{aligned}
\tag{3.13}
$$

where $I = 1.....n$, $M = 1.....nd$, and L, v_I, n_I, M, l_M, nd, and n_M have been defined previously for (3.2); ε is the time weighting factor and $\bar{R}$ is a combined storage term:

$$\bar{R} = \theta_w + \theta_g H_n + \rho_b K_{dn} \tag{3.14}$$

As with (3.2), Υ_n does not appear explicitly in (3.13) because it is an internal flux between elements.

The remaining quantities in (3.13) are:

$$\xi_{IJ} = (C_J - C_I) \tag{3.15}$$

$$\xi^*_{IJ} = (C'_J - C'_I) \tag{3.16}$$

$$\Lambda_{IJ} = - \int_v \bar{D_{ij}} \frac{\partial N_I}{\partial x_i} \frac{\partial N_J}{\partial x_j} \, dv \tag{3.17}$$

$$\Lambda^*_{IJ} = - \int_v D_l \frac{\partial N_I}{\partial l} \frac{\partial N_J}{\partial l} \, dl \tag{3.18}$$

where $\bar{D_{ij}}$ is the combined dispersion coefficient:

$$\bar{D_{ij}} = \theta_w {D_{ij}}^w + \theta_g H_n {D_{ij}}^g \tag{3.19}$$

and the summation convention is assumed with respect to direction i and j when evaluating spatial derivatives, and

$$C_{IJ} = \frac{C_I + C_J}{2} \tag{3.20}$$

for central weighting of the advective term, or

$$C_{IJ} = C_I \text{ or } C_J \tag{3.21}$$

for upstream weighting of the advective term. For example $C_{IJ} = C_J$ if $\gamma_{IJ} > 0$. These options are also used for determining C'_{IJ}.

Solution of the matrix equations arising from (3.13) is also performed using an ILU-preconditioned CGSTAB algorithm [*VanderKwaak et al.*, 1995].

3.2.2 Kinetic Chemistry System Solution

The nonlinear system of equations defining the biogeochemical system at each node in the computation grid will usually be stiff due to the large range in the rate constants for the various chemical reactions. For stiff systems, the integration step size is restricted mainly by stability rather than by accuracy. This will be especially true when microbial and aqueous inorganic reactions are combined as shown in Section 2.6. Such stiff systems also arise in atmospheric chemistry models and some of the findings from that area of research are relevant to the present problem.

Sandu et al. [in press] presented a comprehensive numerical comparison between five explicit and four implicit solvers for a set of seven benchmark atmospheric chemistry problems from actual applications. Of the special-purpose explicit solvers, TWOSTEP [*Verwer*, 1994] was clearly the most efficient for a given accuracy. This solver is based on a Gauss-Seidel iteration scheme and thus works matrix (Jacobian) free. Of the implicit solvers, which use a Jacobian and some form of Newton iteration, VODE [*Brown et al.*, 1989] performed very efficiently on all of the benchmark problems; *Brown et al.* [1989] have also found that VODE is 2.0 to 2.7 times faster than the GEAR package [*Hindmarsh*, 1974], which is commonly used in subsurface reactive transport modelling [*e.g. Kinzelbach et al.*, 1991; *Miller and Rabideau*, 1993; *Zysset et al.*, 1994].

Based on its documented performance, the VODE algorithm was chosen as the ordinary differential equation (ODE) solver for the present model, although some preliminary testing was also performed with the TWOSTEP solver. *Brown et al.* [1989] give a detailed presentation of the VODE algorithm and only a brief description is given here. The method solves the system:

$$\frac{dy}{dt} = f(t,y) \tag{3.22}$$

by using several past values of the dependent variable vector y. The technique is one of the most efficient multistep methods for solving stiff systems [*Hindmarsh and Petzold*, 1995]. The general backward differentiation formula for advancing y is:

$$y_l = \sum_{i=1}^{k} \alpha_i \, y_{l-i} + \Delta t' \, \beta_o \, f_l \tag{3.23}$$

where l is the time step level, k is the number of backward steps considered, α_i are constants which depend on the time step sizes used over the last k steps, and β_o is a constant which depends on k. Equation (3.23) has order k, that is, global errors are order $(\Delta t')^k$; in the present study the maximum value of k in (3.23) was restricted to 3.

The nonlinear system at each time step is solved with Newton iteration where the Jacobian is treated as either full or banded. Methods which exploit the sparsity of the Jacobian may be advantageous for large (*i.e.* more than about 30 species) chemical systems [*Sandu et al.*, in press], but such methods have not been explored in this study. The Jacobian matrix may be generated either analytically or by numerical differentiation; however, analytic Jacobians are difficult to manually determine for complicated nonlinear chemical systems. In this study the MAPLE software [*Waterloo Maple Software*, 1994] is used to automatically generate the analytic Jacobian; thus it is easy to change the number of species or the chemical reactions and regenerate the Jacobian. Comparison of numerical and analytic Jacobians for chemical systems with up to 14 reactive species show that the total chemistry solve time is reduced by approximately 15% when the analytic Jacobian is employed.

In the operator splitting approach used here the time steps in (3.23) can be smaller than the transport time steps taken in (3.11) or (3.12). The only temporal discretization

requirement is that the final integration time reached by (3.23) correspond to the $L+1$ time level in (3.13).

3.3 Verification Examples

3.3.1 Variably-Saturated Groundwater and Drain Flow

The three-dimensional variably-saturated flow solution has been verified previously by *Therrien and Sudicky* [1996] for vertical drainage of a fractured tuff column. Additional problems were simulated as part of this work to verify important modifications to the model. Example 3 presented by *Clement et al.* [1994] was simulated to verify the algorithm for two-dimensional, transient water table mounding resulting from spatially nonuniform recharge. The results obtained with the present model agreed well with the numerical results of *Clement et al.* [1994] and the experimental data presented therein. This problem and the heterogeneous, dry initial condition example (test problem 2) of *Forsyth et al.* [1995] were used to test the variable-switching algorithm; when implemented, variable switching gave the same pressure head and saturation results but with a simulation time that was 20% less than using only pressure as the primary variable.

In order to verify the coupled groundwater and drain flow algorithm, the two-dimensional steady-state and transient flow problems presented by *Fipps et al.* [1986] are now solved. The original work of *Fipps et al.* [1986] identifies the soil as a sandy loam with a saturated hydraulic conductivity of 0.0536 m/hr; the values of the constants in the Brooks-Corey functions are reported for this soil ("Soil B") in the work of *Fipps and Skaggs* [1991].

The flow domain and boundary conditions are given in Figure 3.1. For the three-dimensional simulations the dimensions of the domain are 30.0 m, 30.0 m, and 3.0 m in the x-, y- and z-directions, respectively. The spatial discretization for the two verification problems is based on a seven-point finite difference operator using the modified influence coefficient approach, and nodal spacings equal to 1.0 m in the x-direction, 1.3 m in the

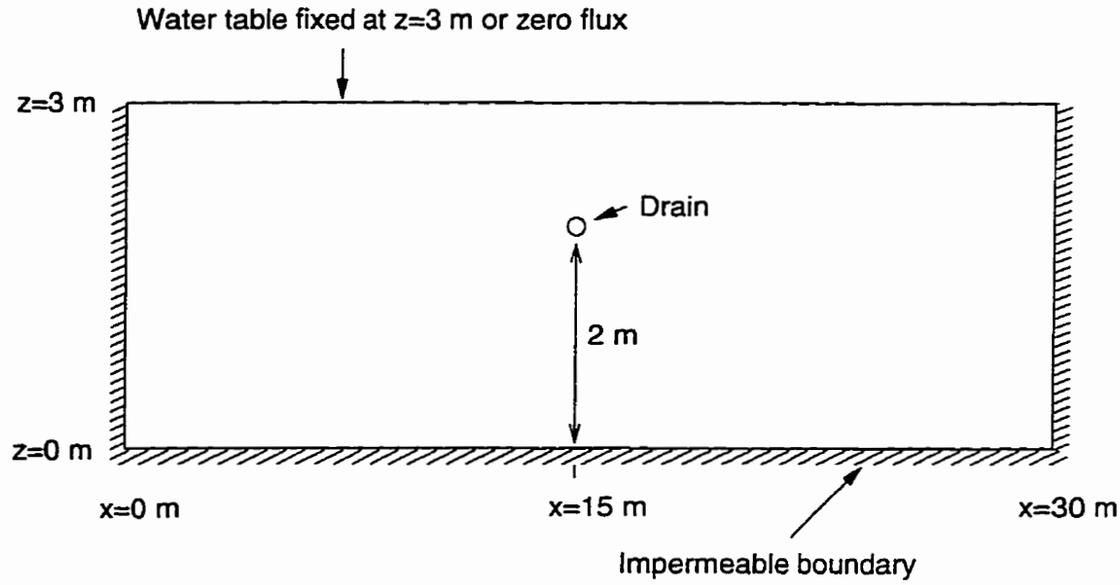

Figure 3.1: Flow domain and boundary conditions for the verification problems. The y-direction extends a distance of 30.0 *m* and the y= 0.0 *m* and y= 30.0 *m* faces of the domain are specified as impermeable boundaries. The drain extends from y= 1.0 *m* to y= 29.0 *m*.

y-direction, and 0.2 *m* in the z-direction. The grid is refined in the x- and z-directions; 8 additional nodes are located between x= 14.0 *m* and x= 16.0 *m* and 6 additional nodes are placed between z= 1.8 *m* and z= 2.2 *m*. This results in each x-z plane containing 858 nodes (20592 nodes for the entire grid), which is comparable in size to the two-dimensional triangular grids used by *Fipps et al.* [1986]. The single horizontal drain is assumed to extend from 1.0 *m* to 29.0 *m* in the y-direction, with the specified flow rate, Q', applied at the node located at x= 15.0 *m*, y= 1.0 *m* and z= 2.0 *m*. All the results are presented for the y= 15.0 *m* vertical plane.

The first problem involves steady-state flow with the water table fixed at the elevation of the ground surface. The drain flow rate is specified as 1.7584 m^3/hr. Two vertical profiles of pressure head for the simulation are shown in Figure 3.2, along with the analytical results of *Kirkham* [1949] as presented by *Fipps et al.* [1986]. It can be seen that there is good agreement between the two sets of results. The numerical solution was obtained in 11 Newton iterations with a total computational time of 48.9 sec. All CPU times reported are for computations performed on an IBM RS/6000 model 590 computer with 256 Mbytes of core memory.

For the second verification problem the steady-state solution obtained above is used as the initial condition; however, the top boundary condition is replaced by a zero-flux boundary which allows drainage to occur. For this problem the drain flow rate, Q', varies with time and this variation was interpolated from graphical data presented by *Fipps et al.* [1986]. The water table profile obtained after 15.0 *hr* of drainage is presented in Figure 3.3 along with the profile from one of the simulations presented by *Fipps et al.* [1986]. The results from *Fipps et al.* [1986] correspond to a simulation in which a resistance adjustment method was used to adjust the conductivities of the elements around a single node representing the drain. As can be seen from Figure 3.3 the results are in good agreement with those of *Fipps et al.* [1986], with the largest deviation occurring at approximately five to ten metres from the drain location. The maximum difference between the two solutions is less than one percent. The three-dimensional simulation required 26 time steps, 646 Newton iterations, and a total simulation time of 36.3 min.

Several illustrative examples using the drain flow algorithm are presented by *Mac-*

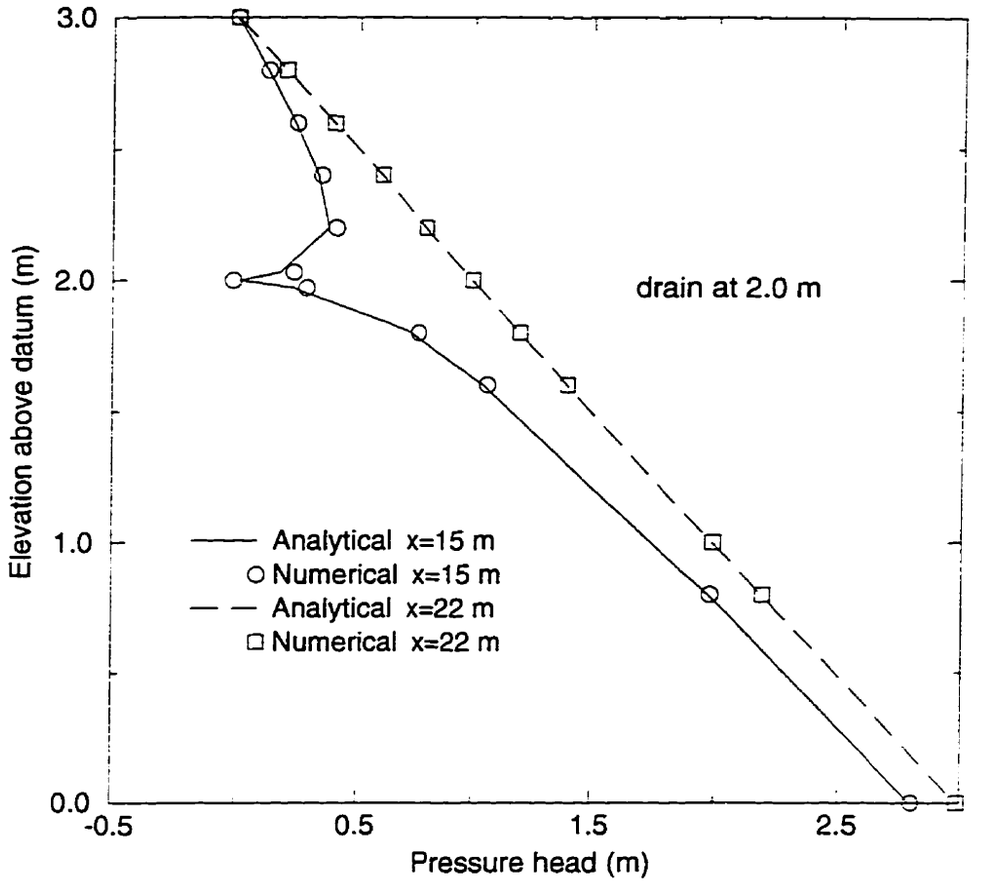

Figure 3.2: Comparison of numerical and analytical predictions for pressure head near a drain. The results are for steady state with the top boundary condition specified as zero pressure head.

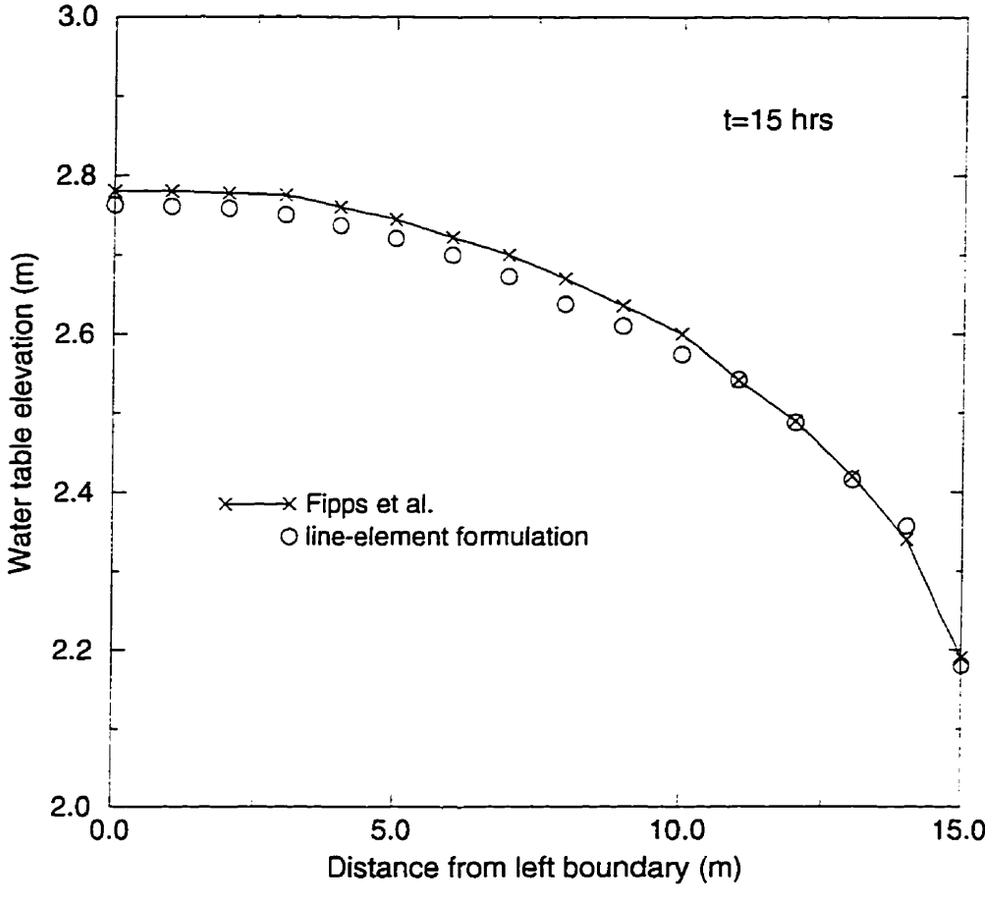

Figure 3.3: Comparison of the water table profile after 15.0 *hr* of drainage.

Quarrie and Sudicky [1996]. These examples show that very accurate mass balances are obtained for drain flow in both homogeneous and heterogeneous porous media.

3.3.2 Reactive Solute Transport

To verify the reactive transport solution, and to investigate several operator splitting schemes, two reactive transport problems are now presented and discussed.

Monod Kinetics

This verification problem involves two reacting solutes, an organic substrate and electron acceptor, and a dynamic biomass which interact via Monod kinetic expressions. Results from the coupled model presented by *MacQuarrie et al.* [1990] are used for accuracy comparisons; the model of *MacQuarrie et al.* [1990] was modified slightly in order to simulate reactive transport in a steady, but variably-saturated, one-dimensional flow field. This required minor modifications to the mass storage and dispersion terms. The electron acceptor is uniformly present at 1.0 mg/L at t= 0, when the substrate is introduced at x= 0.0 at a concentration of 1.0 mg/L. The nodal spacing is 0.4 m; this results in a maximum grid Peclet number (for the substrate) of 2.0. Other relevant model parameters are given in Table 3.1.

A comparison of the results from the two models is shown in Figure 3.4 for Strang splitting with a time step of 0.67 days. For this time step size the grid Courant number for a nonreactive solute is 0.95, while the maximum for the reactive species is 0.4 (for the electron acceptor). The agreement between the two models is very good. A significant amount of substrate and electron acceptor consumption occurs in the first 5.0 m of the domain, which results in a biomass increase in this region of about one order of magnitude.

A more quantitative comparison between the solution of *MacQuarrie et al.* [1990] and several operator splitting solutions is given in Table 3.2. Here the L_2 norm is presented for the difference in electron acceptor profiles at a time of 10 days; the electron

Parameter	Value
porosity, θ_S	0.4
water saturation (uniform), S_w	0.875
Darcy velocity, q_x	0.4 m^3/day
soil bulk density, ρ_b	1.35 g/cm^3
dispersivity, α_l	0.2 m
S distribution coefficient, K_{d1}	0.5 cm^3/g
E distribution coefficient, K_{d2}	0.0
S Henry's constant, H_1,	2.0
E Henry's constant, H_2,	10.0
S free-air diffusion coefficient, $D^o_{g_1}$	1.0 m^2/d
E free-air diffusion coefficient, $D^o_{g_2}$	5.0 m^2/d
initial biomass (uniform), X	3.5 x 10^{-4} mg/L
maximum specific substrate utilization rate, k_{max}	100.0 d^{-1}
S stoichiometric coefficient, r_1	1.0
E stoichiometric coefficient, r_2	3.0
S half-saturation constant, K_1	0.1 mg/L
E half-saturation constant, K_2	0.1 mg/L
biomass yield coefficient, Y	0.05
biomass decay coefficient, k^d	0.0
biomass inhibition coefficient, K_b	3.5 x 10^{-3} mg/L

Table 3.1: Transport and Monod parameters used for the reactive-transport verification problem (S = substrate; E = electron acceptor).

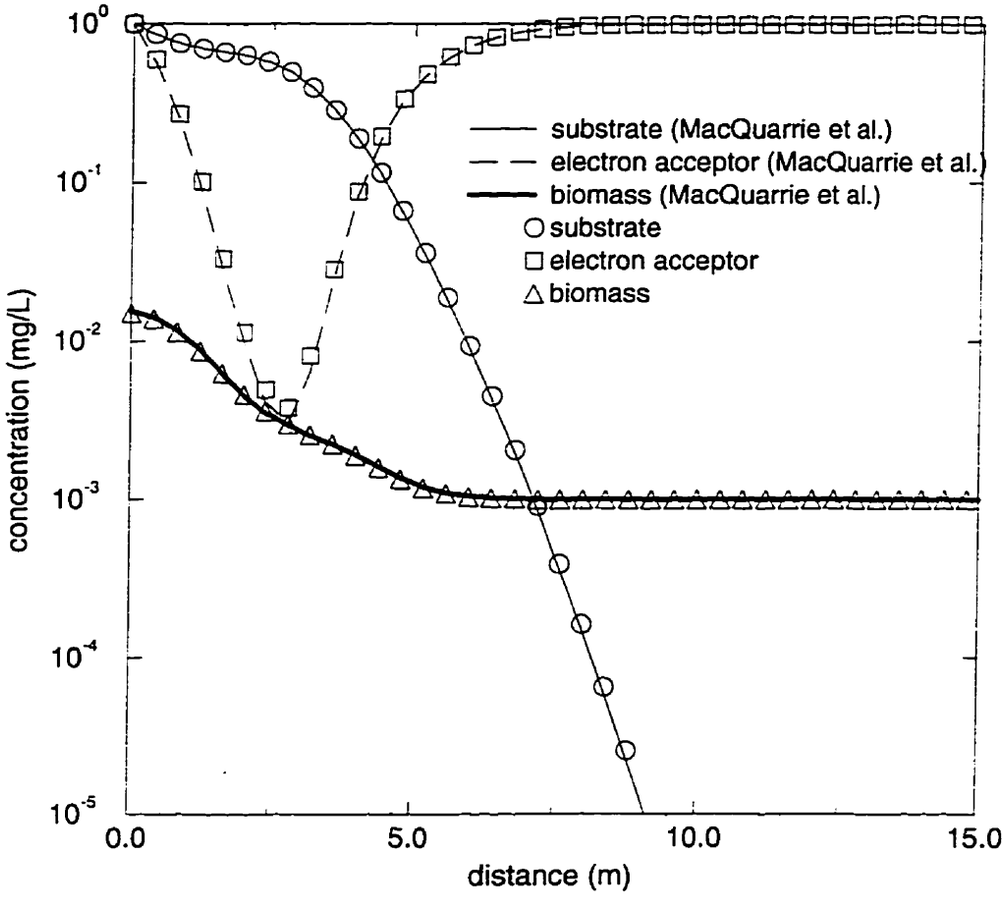

Figure 3.4: Reactive-transport verification results at a time of 10.0 days. Lines are results computed with the model of *MacQuarrie et al.* [1990]; symbols are results computed with Strang operator splitting and a time step of 0.67 days.

Splitting Method	Global Δt	L_2 norm for E	Normalized CPU Time	
			Transport	Chemistry
Strang	1.333	0.070	1.0	1.4
Strang	0.667	0.037	1.9	2.1
Strang	0.333	0.015	4.0	3.8
Normal	0.333	0.10	2.1	4.1
Iterative	0.333	0.011	7.1	13.1

Table 3.2: Accuracy and computing comparison for three types of operator splitting applied to the reactive-transport verification problem (E = electron acceptor).

acceptor always had the largest L_2 norm because of its higher reaction rate. Results are given in Table 3.2 for Strang splitting (*i.e.* (3.11)) with three different time steps, for normal splitting (*i.e.*(3.12)), and for the sequential iterative approach (SIA) as implemented by *Zysett et al.* [1994]. The Strang scheme quickly converges as the time step in (3.11) is reduced. It is interesting to note that for the smallest time step investigated, the iterative splitting scheme of *Zysett et al.* [1994] and the Strang scheme have the same level of accuracy; however, the iterative scheme requires more than twice the total CPU time. For the smallest time step, the CPU time requirements for the Strang splitting and normal splitting are about the same; however, the normal scheme has a error approximately one order of magnitude larger. These trends are consistent with previous numerical comparisons for more simplified reactions [*Valocchi and Malmstead*, 1992; *Zysett et al.*, 1994; *Kaluarachchi and Morshed*, 1995].

Using the VODE solver the solution of the chemical ODE system for this example problem took about 50 to 65% of the total CPU time. This relatively small proportion of the CPU time reflects the low number of species and the generally nonstiff chemistry. All

the simulations presented in Table 3.2 were repeated using the TWOSTEP solver which resulted in chemistry solve times which were less than the VODE solve times by a factor of two to three. *Zysett et al.* [1994] also noted a similar reduction in chemistry solve time when they substituted an explicit solver for the standard GEAR package.

Several additional one-dimensional reactive transport problems with Monod kinetics from *Kindred and Celia* [1989] and *Morshed and Kaluarachchi* [1995] have been simulated to verify the present code. Good agreement with the published solutions was obtained using Strang splitting. In addition, the two-dimensional aerobic biodegradation example of *MacQuarrie et al.* [1990] was simulated with the present model and excellent agreement was obtained for the spatial distribution of reactive species and the temporal variation of substrate mass.

Microbial and Abiotic Reversible Reactions

A comparison between the results obtained with Strang splitting and the sequential iterative approach is now given for a one-dimensional problem involving 13 reactive species. The problem is designed to represent the major reactions which occur as wastewater migrates vertically in the unsaturated zone, including ammonium and organic carbon oxidation and aqueous carbonate speciation as will be discussed in greater detail in Section 4.2. The reaction stoichiometry and kinetic data are provided in Appendix A and the reactions are coupled as discussed in Section 2.6.

The 1.0 metre vertical column is discretized with a nodal spacing of 0.05 m and the Darcy flux and water saturation are constant at 0.015 m^3/day and 0.5, respectively. For a time step of 0.5 days and a longitudinal dispersivity of 0.15 m, the maximum grid Peclet and Courant numbers are 0.33 and 0.75, respectively. The boundary and initial conditions are identical to those presented in Table 4.2, Section 4.2.1, except that the dissolved O_2 concentration is set to 6.0 mg/L at $x = 0.0$ in order to mimic a continuous supply of oxygen in the unsaturated zone.

A comparison of the results from the two operator splitting schemes is shown in Figures 3.5 and 3.6 at a simulation time of 50.0 days. The profiles of the various species

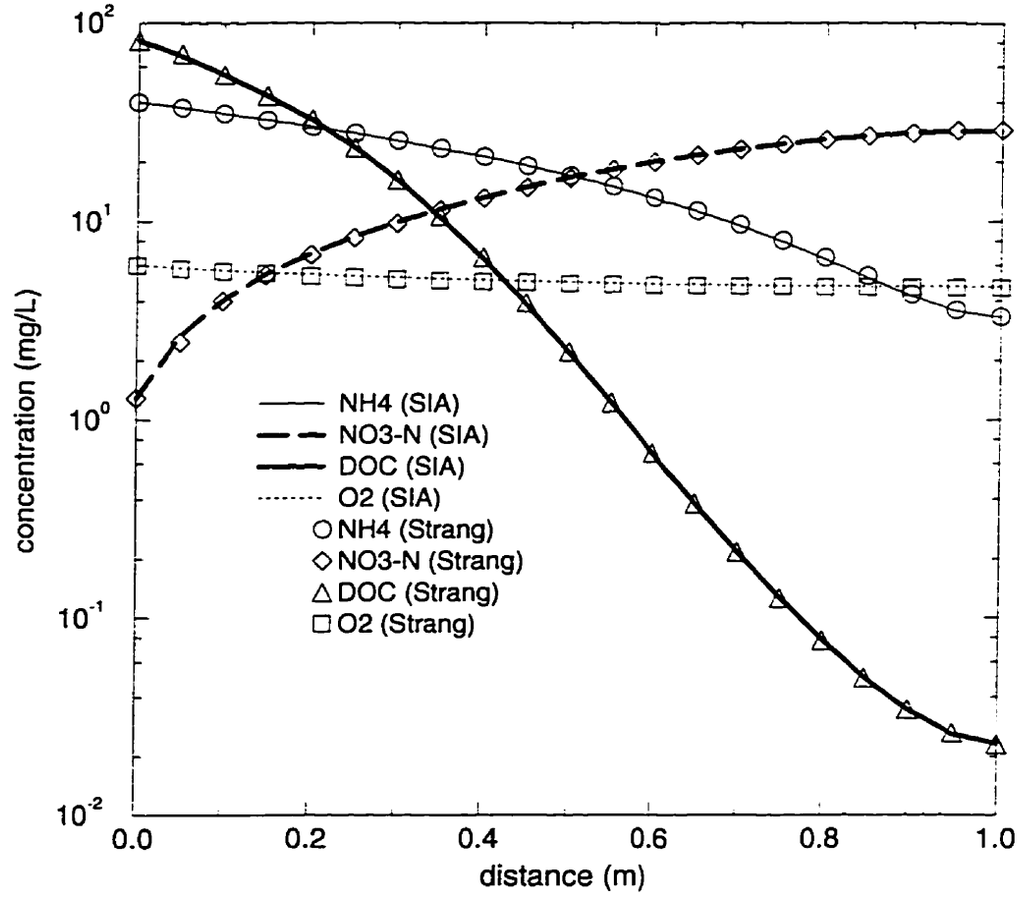

Figure 3.5: Strang and SIA results for wastewater chemistry test problem. Lines are results computed with the SIA and symbols are results computed with Strang operator splitting at a time of 50.0 days.

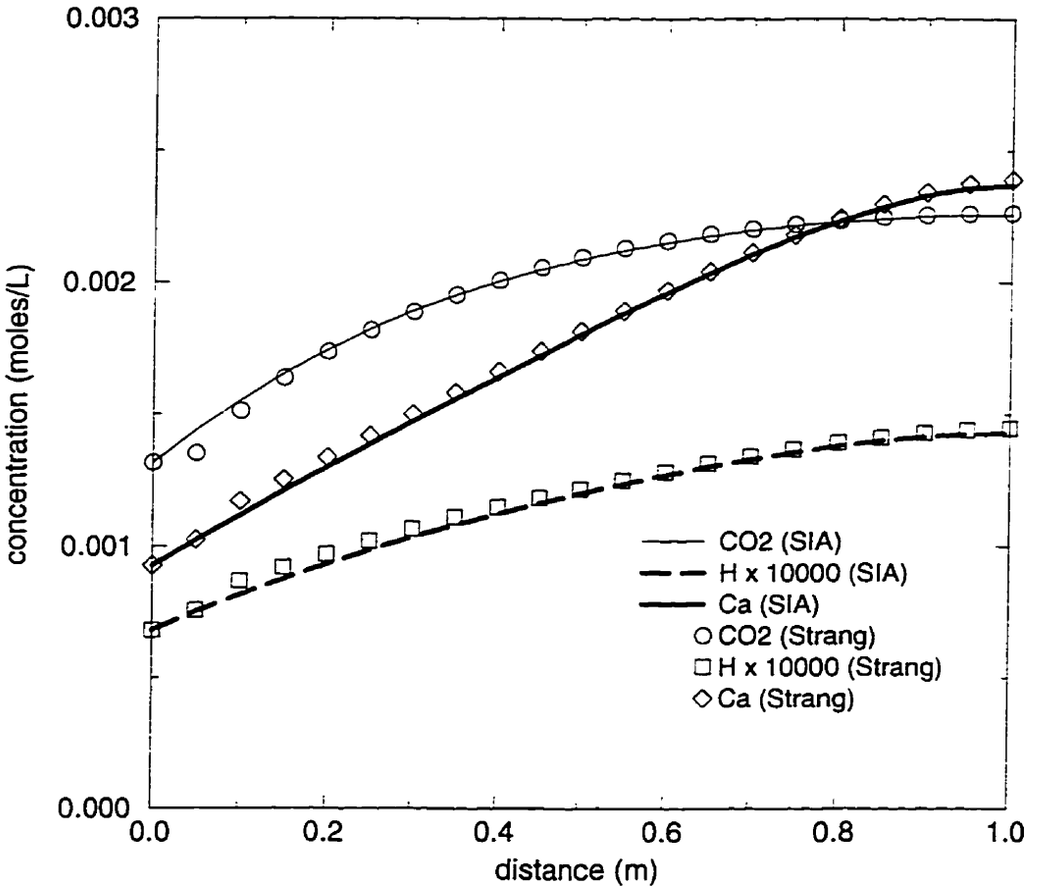

Figure 3.6: Strang and SIA results for wastewater chemistry test problem. Lines are results computed with the SIA and symbols are results computed with Strang operator splitting at a time of 50.0 days.

indicate that nitrification and oxidation of *DOC* are accompanied by production of CO_2 and $H+$, and that calcite dissolution is generating Ca^{2+}. The agreement between the two sets of results is very good. The SIA required 4.5 times more computation time that the Strang method and thus the Strang method is obviously the preferable approach.

The explicit TWOSTEP chemistry solver was also used on this example problem; however, the solver failed because of the increased stiffness of the system created by the addition of the fast reversible reactions. *Sandu et al.* [in press] have found that explicit solvers fail for more challenging problems (*i.e.* a large number of stiff eigenvalues) and noted that explicit methods do not mimic the conservation rules which exist for the original ODE system. Therefore it is apparent that implicit ODE algorithms will be the more robust solvers for general application to subsurface reactive transport.

Even with the implicit VODE algorithm, convergence problems (*e.g.* numerous failed Newton iterations and small time steps) have been noted for systems containing fast reversible reactions. To reduce the stiffness created by such reactions, the characteristic time scale [*Verwer*, 1994] of the fast reacting species can be increased. This is done by decreasing the forward and backward rate constants for the reactions involving these species while at the same time maintaining the correct equilibrium ratio of the rate constants. Thus the reactions are slowed down relative to the actual rate, but they are still kept sufficiently fast so that equilibrium can be achieved within a split-operator time step. For the previous example the characteristic time scale of the aqueous speciation reactions was increased by seven orders of magnitude, which resulted in a characteristic time scale which was still two orders of magnitude less than the transport time step of 0.5 days; this modification caused no change in the computed species concentrations but it reduced by a factor of 2.5 the number of time steps taken by the VODE solver. Testing of this approach on other problems has yielded similar results.

Chapter 4

Simulation of Nitrogen and Carbon Transport and Fate at the Cambridge, Ontario Field Site

In this chapter the reactive transport model based on Strang operator splitting is used to simulate wastewater-derived N and C transport and transformation at a field site near Cambridge, Ontario. The site has a conventional drain field of 100 m^2 which serves four occupants in a single family home. The Cambridge site has been extensively monitored and studied by researchers from the University of Waterloo [*Robertson et al.*, 1991; *Aravena et al.*, 1993; *Wilhelm et al.*, 1994a; *Shutter et al.*, 1994] and has been used to assess a conceptual biogeochemical model for wastewater evolution in sandy aquifers [*Wilhelm et al.*, 1996]. The physical setting and groundwater flow conditions at the site are described by *Robertson et al.* [1991] and *Shutter et al.* [1994]. *Robertson et al.* [1991] and *Wilhelm et al.* [1994a] provide detailed discussions of the observed wastewater composition and unsaturated and saturated zone geochemistry at the site.

One of the primary objectives of simulating the Cambridge field site is to apply the model in a predictive mode and compare the results to the field geochemical data for the major reactive species. This is accomplished by first calibrating the physical transport

portion of the model to a nonreactive solute plume, and then using the reactive transport model to predict the evolution of the N and C species. The biogeochemical kinetic parameters are obtained from the literature and thus are independent input data for the reactive transport simulation. No calibration was attempted with the kinetic parameters because this would defeat the objective of assessing the predictive ability of the model.

Because of the large width of the drain field (about 9 m) transverse to the main flow direction, and more frequent geochemical monitoring along the center line of the plume, the simulations presented here were conducted in two dimensions. Also, because the wastewater system at the site has been in operation year round since 1977, only steady-state flow simulations were performed.

4.1 Groundwater Flow and Nonreactive-Transport Simulations

The surficial unconfined aquifer at the Cambridge site consists of glaciolacustrine and outwash sands which are remarkably homogeneous in terms of hydraulic conductivity. A uniform isotropic saturated hydraulic conductivity of 20 m/day [*Shutter et al.*, 1994] is therefore applied to the entire domain. The *van Genuchten* [1980] parameters determined for the sands are given in Table 4.1.

Figure 4.1 shows the physical domain and boundary conditions used for the flow simulations. The aquifer is recharged at an average rate of 30 cm/yr, which has been determined using meterological data and previous nonreactive solute transport modelling at the site [*Shutter et al.*, 1994]. Using results from a bromide tracer test, *Robertson et al.* [1991] estimated that the drain field loading is about 200 cm/yr; however the wastewater flux is apparently higher towards the center of the drain field. When modelling flow from the drains it has been assumed that the largest flux occurs at the center drain, and that the flux decreases symmetrically towards the outer drains. This type of distribution is consistent with previous flow simulations [*Shutter et al.*, 1994]. The discharge rate, Q', from the outer drain to the center drain is specified as 4.38 x 10^{-3} m^3/day, 6.88 x 10^{-3}

Parameter	Value
Saturated moisture content, θ_S	0.40
Residual moisture content, θ_{res}	0.14
Air-entry pressure, ψ_{air}	-0.06 m
Fitting parameter, α	3.44 m^{-1}
Fitting parameter, β	3.99
Fitting parameter, γ	0.75

Table 4.1: Values of the *van Genuchten* parameters used for the $\psi - S_w$ and $k_{rw} - S_w$ relationships for the Cambridge site [*Shutter et al.*, 1994].

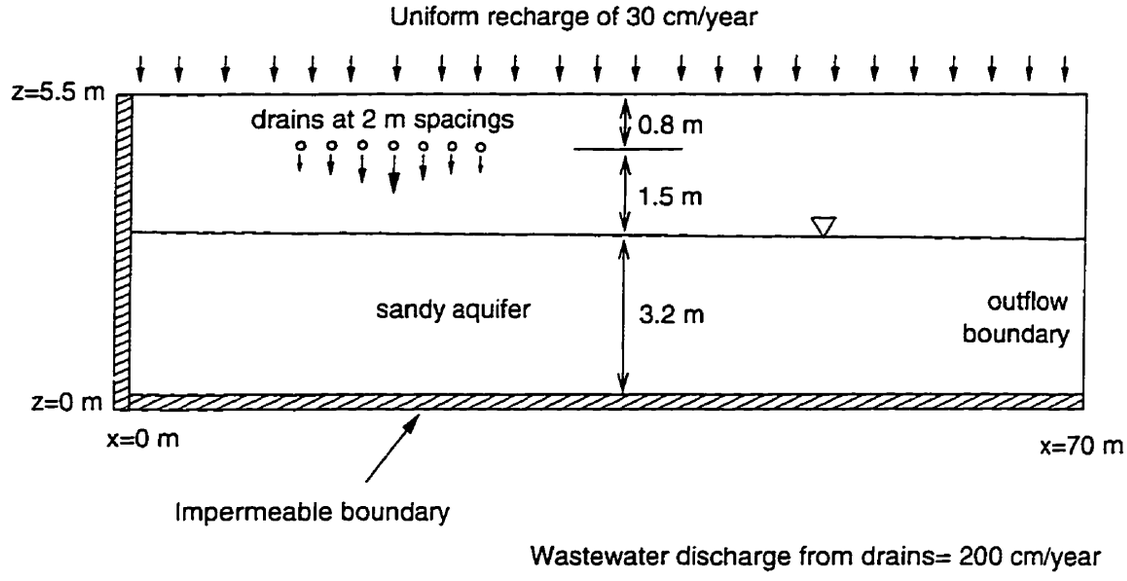

Figure 4.1: Physical domain for the Cambridge simulations.

m^3/day, 1.14 x 10^{-2} m^3/day, and 2.06 x 10^{-2} m^3/day, per unit width. In the model, the drains are located 0.80 *m* below the top boundary and are equally spaced at 2.0 *m* in the x-direction, which is consistent with the field layout.

The impermeable boundaries on the left and bottom of the domain shown in Figure 4.1 represent a flow divide and a relatively impermeable silt till, respectively. The right-hand boundary of the domain is treated as a specified head equal to 3.2 *m* over the interval z= 0.0 *m* to z= 3.2 *m*, and impermeable from 3.2 *m* to z= 5.5 *m*. The specified head of 3.2 *m* is the average saturated thickness of the aquifer.

The domain is discretized using three-dimensional hexahedral elements with grid refinement in the vicinity of the drains and capillary fringe. The grid contains a total of 182 nodes in the x-direction, 57 nodes in the z-direction, and 2 nodes in the y-direction (1.0 *m* thick section); element lengths as small as 0.1 *m* and 0.02 *m* are used in the x- and z-directions, respectively.

Simulation of the dissolved sodium plume at the site was performed to obtain dispersivity estimates. *Robertson et al.* [1991] and *Shutter et al.* [1994] present evidence and discuss why the sodium plume can be considered to behave conservatively at the Cambridge site. *Shutter et al.* [1994] have previously simulated the sodium plume using a two-dimensional finite element model and determined that appropriate values for α_l and α_t were 0.1 *m* and 0.001 *m*, respectively.

4.1.1 Results

The results of the steady state flow simulation give horizontal groundwater velocities in the saturated zone down gradient of the drain files of 28 to 32 *m/yr*; in the vadose zone beneath the drain field, the simulated vertical groundwater velocities range from about 27 *m/yr* to 73 *m/yr*. These values agree well with the field-determined horizontal velocities of 20 to 40 *m/yr* and vertical unsaturated zone velocity of 70 *m/yr* obtained by *Robertson et al.* [1991].

The simulated moisture profiles near the drain field are shown in Figure 4.2. The

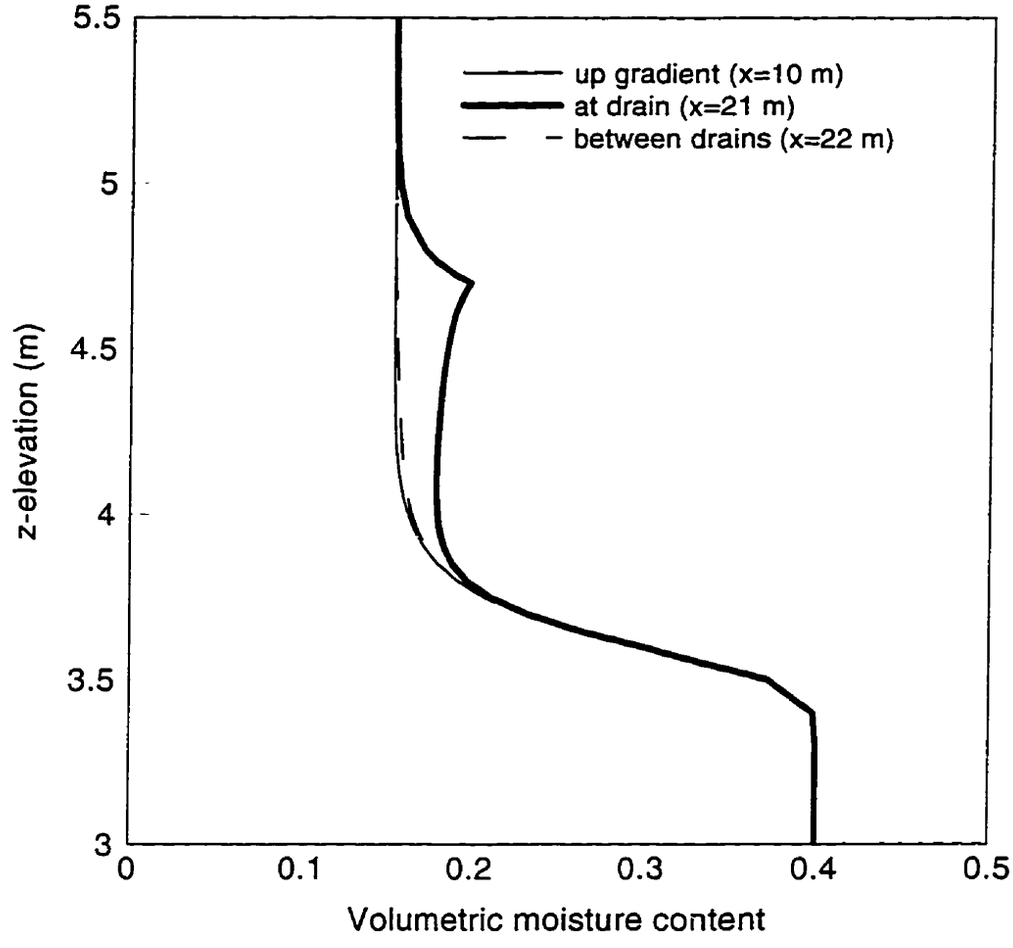

Figure 4.2: Simulated moisture profiles near drain field. A drain is located at x= 21 *m* and z= 4.7 *m*, and the ground surface is at z= 5.5 *m*.

results indicate that the increase in moisture content caused by the drain field is very localized and that water table mounding is insignificant. More importantly, from a biochemistry perspective, is that there is ample air space in the vicinity of the drain field to allow oxygen diffusion from the surface boundary. The simulated moisture profiles fall within the range of field moisture profiles from soil samples collected within the Cambridge drain field [*Shutter et al.*, 1994].

The nonreactive transport simulation was run with a time step of 0.25 days to a total time of 1100 days (three years). By this time the plume had reached essentially a steady state distribution within the model domain and thus the simulation was terminated. Maximum grid Peclet numbers were in the range of 4 to 6, while the maximum Courant number was less than 0.5. A Dirichlet boundary condition with a solute concentration of 90.0 mg/L was applied at all drains. This concentration is equal to the average sodium concentration in septic-tank effluent at the Cambridge site [*Wilhelm et al.*, 1994a]. The simulated sodium plume and the field plume are presented in Figure 4.3. For the numerical simulation the values for α_l and α_{tv} are 0.15 m and 0.004 m, respectively. There is very good agreement between the model and field plumes, particularly the longitudinal extent of transport of the 80 mg/L contour which reaches its steady-state limit about 12 m down gradient of the drain field. The upper portion of the simulated plume does not migrate as far below the water table as observed in the field; this could be a result of an underestimation of the annual recharge rate down gradient of the drain field. Despite this, the results shown in Figure 4.3 suggest that the dispersivities used are reasonable field-scale values for the relatively homogeneous Cambridge aquifer. These values of dispersivity are used for all subsequent reactive-transport simulations.

4.2 Biochemical System and Reactive-Transport Modelling

The N and C biochemical system at the Cambridge site is assumed to be adequately described by considering the transport and transformation of 13 reactive species. The

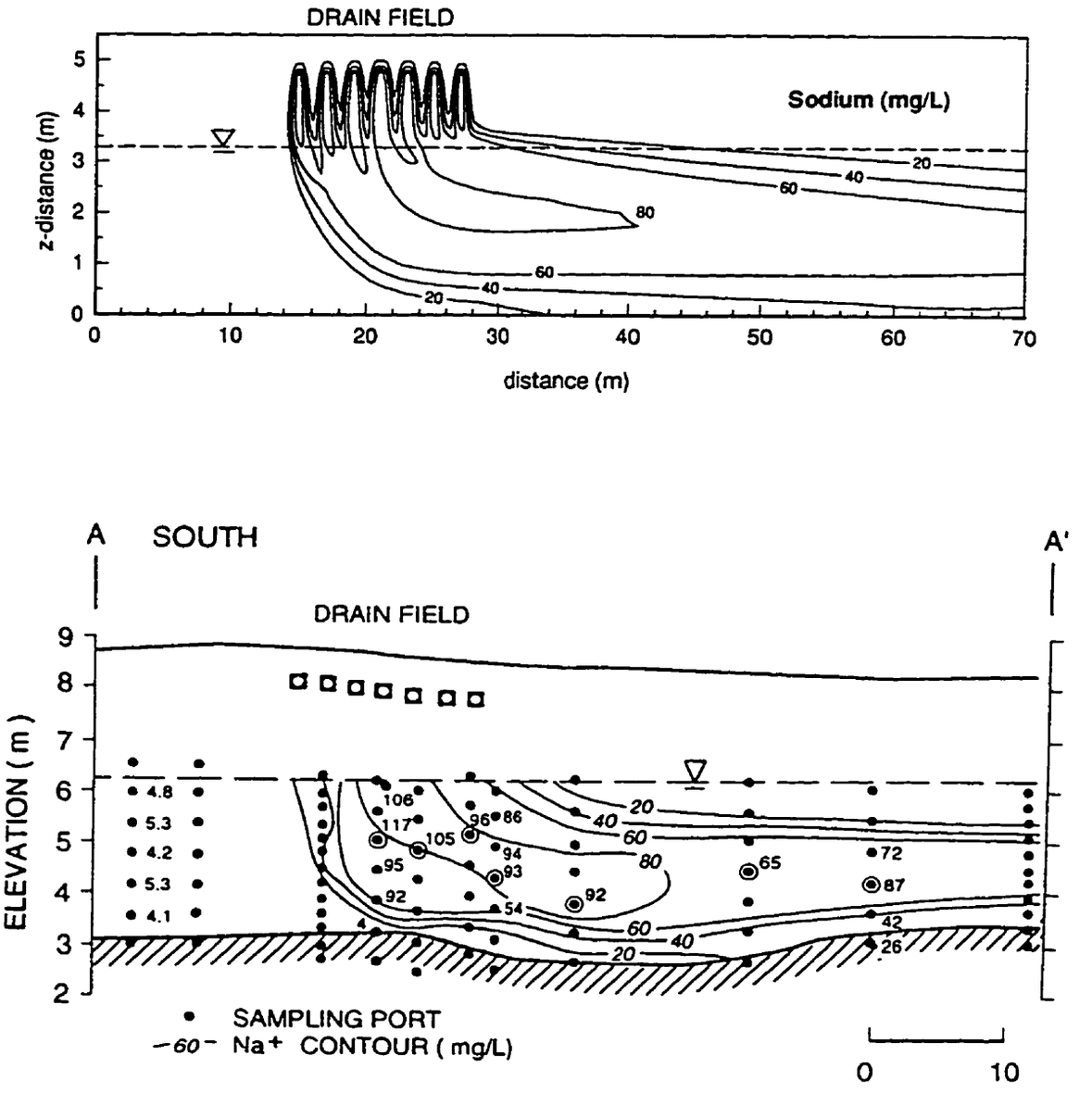

Figure 4.3: Sodium plumes from: a) model simulation at a time of 3.0 years, and b) field data of *Wilhelm et al.* [1996].

species and reactions are discussed below and are largely based on the conceptual biogeochemical model proposed by *Wilhelm et al.* [1994b]. Thus, a comparison of the reactive transport model results and the field results will provide additional evidence for evaluating the appropriateness of the conceptual model.

Nitrogen is assumed to enter the subsurface primarily as ammonium (NH_4^+) because of the reducing conditions in septic tanks [*Whelan and Titamnis*, 1982; *Whelan*, 1988; *Welskel and Howes*, 1992; *Wilhelm et al.*, 1994a]. Ammonium transport is influenced by cation exchange which is represented here as an equilibrium process using a constant partitioning coefficient. Although this is a simplification of the cation exchange process, *Ceazan et al.* [1989] have found that a linear isotherm approach successfully described ammonium exchange in a series of experiments conducted within a plume of sewage-contaminated groundwater, and during small-scale tracer injection tests. The aquifer sediments in the studies of *Ceazan et al.* [1989] consisted of glacial outwash with less than 0.1% clay, and thus are similar to the Cambridge sediments. Furthermore, field geochemical evidence presented by *Wilhelm et al.* [1994a] suggests that biologically-mediated reactions have a more significant effect on ammonium fate than does cation exchange.

Given sufficient dissolved oxygen, and a mediating population of nitrifying bacteria, ammonium is transformed to nitrate (NO_3^-) by nitrification. Nitrifying bacteria are ubiquitous in the shallow subsurface and are here assumed to be initially present at 0.1 *mg/L* aquifer - a value which *Leggett and Iskandar* [1981] suggest is representative of a low soil population of nitrifying bacteria. Nitrite is an intermediate species formed during nitrification; however, it is quite unstable and very rapidly converted to nitrate under aerobic conditions [*Behnke*, 1975]. Therefore in the present application nitrification is treated as an overall reaction [*Lasaga*, 1981] in which the intermediate species nitrite does not appear in the formulation.

Nitrate is modelled as a nonsorbing, nonvolatile solute which can be reduced to N_2 through the process of heterotrophic denitrification. This process requires labile organic carbon, which serves as the energy source for bacteria which are mostly faculative anaerobes [*Korom*, 1992]; it is well known that the presence of dissolved oxygen inhibits den-

itrification [*Henze et al.*, 1987; *Widdowson et al.*, 1988; *Korom*, 1992]. The end-product of denitrification, the gas N_2, is assumed to be nonreactive. Other possible reaction mechanisms for denitrification, such as the utilization of reduced sulfur compounds [*e.g. Frind et al.*, 1990], are not considered important in the shallow Cambridge aquifer and thus have not been included in the present biogeochemical model.

The primary source of dissolved organic carbon (*DOC*) is assumed to be the wastewater discharged via the septic system drains. Dissolved organic carbon is assumed to be nonvolatile, subject to sorption [*Jardine et al.*, 1992], and degraded aerobically by heterotrophic bacteria. The organic compounds which make up septic effluent *DOC* are not well characterized [*Wilhelm et al.*, 1994a], and are represented here with the simplified chemical formula CH_2O. More complex chemical formulas for *DOC* have been used, for example in models of reactive transport in estuaries [*Regnier et al.*, in press], but these yield stoichiometric relations which are similar to the ones employed here. The entire fraction of *DOC*, excluding any sorbed mass, is assumed to be labile and available to heterotrophic biomass. Although domestic wastewater usually contains a relatively nonlabile fraction the amount is generally less than 10% [*Wilhelm et al.*, 1994a] and is considered insignificant given the uncertainties in measuring and characterizing wastewater *DOC*. In the present model one heterotrophic biomass population performs both aerobic degradation of *DOC* and denitrification, which is consistent with, for example, models presented by *Widdowson et al.* [1988] and *Kinzelbach et al.* [1991]. The heterotrophic biomass is assumed to be initially present at 0.1 mg/L aquifer, which falls in the range typical for shallow aquifers [*Harvey and Widdowson*, 1992]. Other possible oxidation-reduction reactions involving *DOC* and, for example $Mn(IV)$- oxides, $Fe(III)$-oxides, or sulfates, are not considered in the present biogeochemical system. Such reactions will provide additional utilization of *DOC* in more reducing environments and may control metal mobility [*Robertson and Blowes*, 1995].

Nitrification and aerobic degradation produce species (*i.e.* H^+, $CO_{2(aq)}$) which may cause significant changes in the aqueous inorganic carbon chemistry. In this work a simplified inorganic chemistry system is considered, that is, $CO_{2(aq)}$ (or H_2CO_3), HCO_3^-, CO_3^{2-}, H^+, and OH^- are included. In poorly buffered sediments the addition of H^+

may cause decreases in wastewater plume pH, thus raising the possibility of increased metal mobility [*Robertson and Blowes*, 1995]. The dissolution of calcite ($CaCO_{3(s)}$) will effectively buffer added H^+; here it is assumed that calcite is the dominant buffering mineral in the aquifer sediments. This is based on the high carbonate content of the Cambridge sands, which contain about 21% by weight of $CaCO_3$ equivalent. The processes of calcite dissolution and precipitation are modelled using the empirical formulation and parameters presented by *Chou et al.* [1989]. Three independent but simultaneous kinetic reactions are considered; these cover a range of pH and CO_2 conditions and are formulated only in terms of species concentrations in the bulk solution. The reaction stoichometry and rate expressions are presented in Appendix A. The reaction rates depend on the reactive surface area of calcite per unit volume of aquifer; this is computed assuming spherical medium sand particles (1 *mm* in diameter). Because of the large fraction of carbonates in the Cambridge sediments, the reactive surface area was held constant for initial simulations, although this is not a requirement of the model in general. It should be noted that other formulations, including the concentration of surface species, may be required to model the dissolution-precipitation of more complex minerals.

The carbonate chemistry algorithm has been verified by comparing computed results to transient results presented by *Stumm and Morgan* [p.94, 1981], to results from a batch equilibrium model developed during this research, and to the transient results from a combined equilibrium-kinetic dissolution model under development at the University of Waterloo [*Mayer*, personal communication]. Good agreement was obtained for all comparisons.

Appendix A presents the complete biogeochemical system used to simulate the Cambridge wastewater plume. The various rate laws and kinetic parameters are not discussed in detail in the text. Monod parameters for nitrification were obtained primarily from *Leggett and Iskandar* [1981], who present a summary of parameters obtained by various investigators. Monod kinetic parameters for heterotrophic processes were selected following a review of several studies related to wastewater treatment modelling, and simulation of denitrification in groundwater [*Henze et al.*, 1987; *Widdowson et al.*, 1988; *Kinzelbach et al.*, 1991]. Kinetic parameters for aqueous inorganic carbon reactions were

obtained from the literature cited in Appendix A. Although microbially-mediated reactions are known to be influenced by temperature, methods to adjust Monod parameters for temperature effects are scarce; where possible, kinetic parameters were obtained or computed for a temperature of 12^oC. This temperature is considered to be representative of the average annual temperature in a shallow aquifer at this latitude; however, it is possible that the wastewater temperature near the drains may approach 20^oC.

Molecular diffusion coefficients in air and water for the various species were computed for a pressure of one atmosphere and a temperature of 12^oC using empirical correlation equations provided in *Reid et al.* [1977] or from data presented by *Shackelford and Daniel* [1991]. Values for the dimensionless Henry's constant for volatile species were computed using the idea gas law and the gas solubility in fresh water at a total pressure of one atmosphere [*Colt*, 1984].

Ideal conditions are assumed in the present application of the model because the ionic strength of the Cambridge wastewater plume is relatively low (approximately 0.01) and because additional species would have to be introduced into the biochemical system to accurately compute the ionic strength during a simulation. For other applications of the model to higher ionic strength plumes, the effect of ionic strength on the rates of kinetic reactions could easily be incorporated by using, for example, the Davies equation and the rate constant adjustment relationship given by *Stone and Morgan* [1990].

4.2.1 Initial and Boundary Conditions

To establish initial conditions for reactive solutes, the average background alkalinity and pH data presented by *Wilhelm et al.* [1994a; 1996] were used. These data were equilibrated with calcite, using the reaction module of the model, prior to running the transient reactive transport simulations. The calcite-equilibrated groundwater has a computed dissolved inorganic carbon (DIC) concentration of 47.0 mg/L, which compares well with the DIC concentration of 44 mg/L obtained by *Wilhelm et al.* [1994a] who used the PHREEQE geochemical code. The background concentration of DOC is assumed equal

to zero for the model simulation; this is equivalent to assuming that the observed background *DOC* (average concentration of 2.7 mg/L) is nonlabile. As well, no N is initially present in the model domain despite the fact that agricultural activities near the Cambridge site have caused the average nitrate-N concentration in background waters to be 28.1 mg/L [*Wilhelm et al.*, 1996]. Thus the model simulations depict the groundwater quality that would result from wastewater released above a pristine aquifer in which the water is initially in equilibrium with calcite. Dissolved oxygen concentrations in the groundwater outside the wastewater plume at the Cambridge site are typically 4 to 8 mg/L [*Wilhelm et al.*, 1994a] and a uniform value of 6.0 mg/L is used for initial conditions for model simulations.

The composition of wastewater at the drains was obtained from septic-tank effluent data presented by *Wilhelm et al.* [1994a; 1996]. It is assumed that the septic-tank effluent is completely devoid of dissolved oxygen and nitrogen gases. In order to obtain an approximate source concentration for *DOC*, the average chemical oxygen demand of the effluent (265 $mg\ O_2/L$) was converted to a molar equivalent of CH_2O; this results in a source concentration for *DOC* of 82.0 mg/L. It should be noted that the chemical oxygen demand measures the majority of the organic compounds in the wastewater, but that it does not measure reduced inorganic species such as NH_4^+ [*Sawyer and McCarty*, 1978]. The wastewater released from the drains is assumed to be in equilibrium with calcite which is in agreement with the findings of *Wilhelm et al.* [1996].

For the top surface boundary condition, the concentrations of dissolved oxygen and nitrogen are set to atmospheric levels. Because the current model does not consider root-zone generation of CO_2 the surface boundary condition for CO_2 is increased to background equilibrium groundwater levels of 5.3 x 10^{-4} $moles/L$, or 1.2% by volume. Thus, the top boundary conditions for the carbonate species are the same as the background carbonate concentrations. The assumption of atmospheric O_2 concentrations at ground surface is supported by unsaturated zone gas sampling performed by *Wilhelm et al.* [1994a] in November 1990. Although snow cover may be expected to restrict gas diffusion at the ground surface during the winter, *Solomon and Cerling* [1987] have shown that diffusion coefficients for CO_2 in snow pack are in the range of 0.02 cm^2/s to 0.10

Species	Initial Value	Source Value
NH_4^+ (mg/L)	0.0	40.0
NO_3^- (mg/L)	0.0	5.7
CH_2O (mg/L)	0.0	82.0
O_2 (mg/L)	6.0	0.0
CO_2 (mol/L)	5.3 x 10^{-4}	1.3 x 10^{-3}
N_2 (mg/L)	0.0	0.0
OH^- (mol/L)	7.6 x 10^{-8}	6.6 x 10^{-8}
CO_3^{2-} (mol/L)	2.2 x 10^{-6}	4.0 x 10^{-6}
H^+ (mol/L)	5.9 x 10^{-8}	6.8 x 10^{-8}
(pH)	7.23	7.17
HCO_3^- (mol/L)	3.4 x 10^{-3}	7.3 x 10^{-3}
Ca^{2+} (mol/L)	1.7 x 10^{-3}	9.3 x 10^{-4}
X_1 (mg/m^3 of porous media)	0.1	
X_2 (mg/m^3 of porous media)	0.1	

Table 4.2: Initial (background) conditions and wastewater source conditions used for Cambridge reactive-transport simulation. The source conditions are applied at the nodes corresponding to drains.

cm^2/s, and thus are much closer to diffusion coefficients in air than to saturated diffusion coefficients which are on the order of 10^{-5} cm^2/s.

The complete initial (background) and source wastewater chemistry data for the reactive-transport simulations are given in Table 4.2. The source conditions at the drain locations is assumed to be temporally constant.

4.2.2 Computational Considerations

The reactive transport simulation was run with a time step (Δt in 3.11) of 0.5 days to a total time of 1100 days. The simulation required 14 Mb of RAM and 63.6 hours of CPU

time on an IBM RS/6000 model 590 computer, with 61% of the total time being spent on solving the chemical system. To illustrate the significance of chemistry on the CPU time requirements, a shorter duration simulation was performed with the biochemical system simplified to include only NH_4^+, NO_3^-, *DOC*, O_2, and two biomass populations. The six species directly involved in the carbonate system and N_2 were excluded. For the reduced number of species a CPU time of 16.6 hours was required for a 550 day simulation and approximately 72% of this time was spent in solving the chemistry system. The results for the simulated species were in agreement with the results obtained with the full chemistry problem; however, for the full chemistry simulation 31.7 hours of CPU time were required to reach a simulation time of 550 days. Thus the number of reactive species significantly influences the computational requirements.

The complete 13-species problem was also simulated using the sequential iterative approach (SIA). As was determined for the one-dimensional problems presented earlier, the results for Strang splitting and the SIA were in very good agreement; however, the SIA required three times more CPU time than the Strang method.

4.2.3 Discussion of Results

The results for six of the major reactive species are shown in Figures 4.4 and 4.5. The plumes correspond to a simulation time of 1.5 years; in the unsaturated zone and in the saturated zone approximately 12 to 15 *m* down gradient of the drain field the species distributions have reached steady state by this time. From Figure 4.4, it is apparent that at steady state, nitrification and oxidation of *DOC* are complete after the wastewater has migrated less than 1.0 *m* in the unsaturated zone. The microbial transformation of NH_4^+ and *DOC* creates very steep geochemical gradients and effectively limits the vertical and horizontal extend of these species to the area directly below the drain positions. It should be noted, however, that for simulation times less than 100 days the fronts of the NH_4^+ plumes reached the capillary fringe. The plumes then began to recede as the microbial biomass in the unsaturated zone increased, which in turn caused the nitrification rates to increase. Corresponding to the nitrification of ammonium is the generation of nitrate,

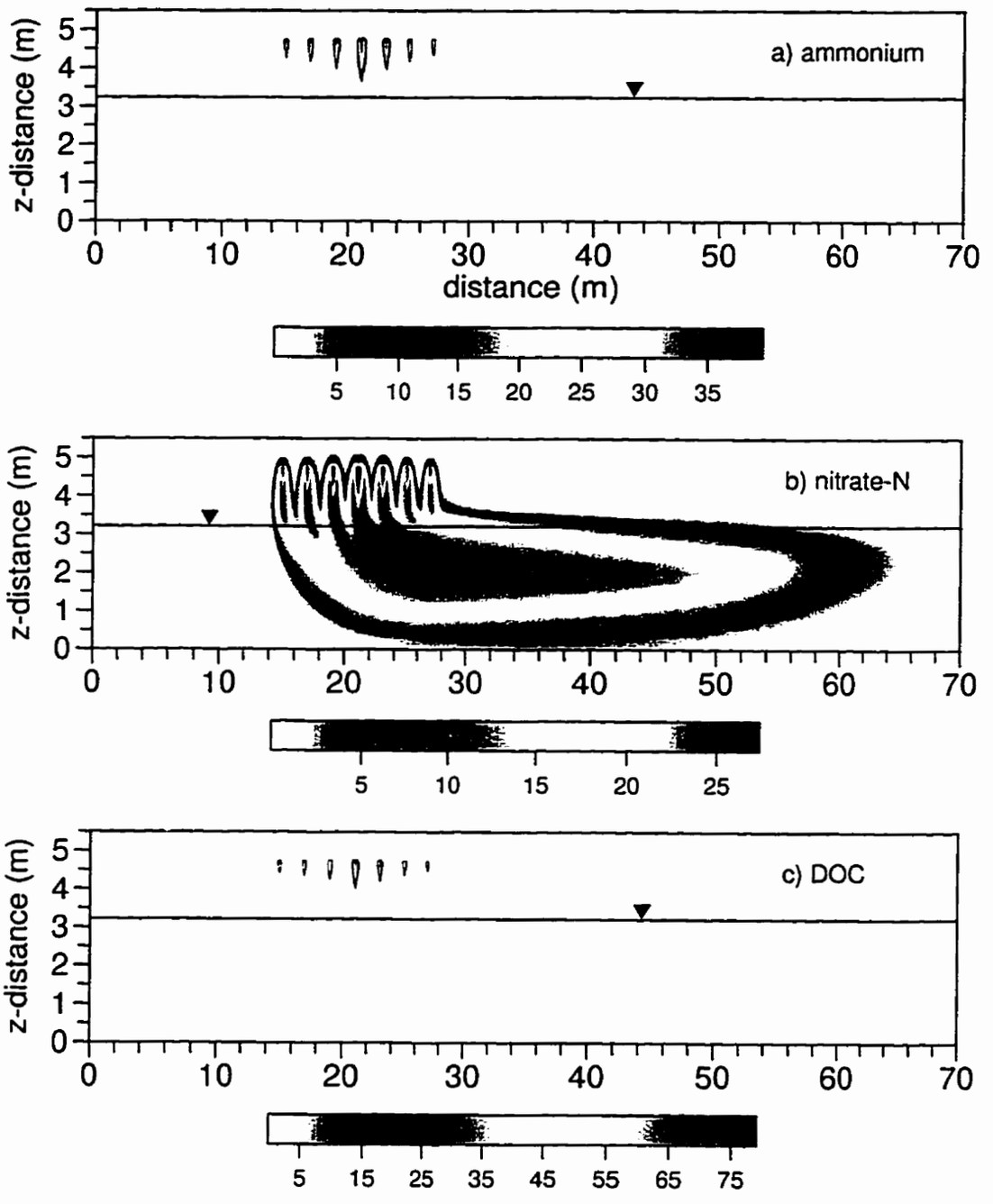

Figure 4.4: Simulated plumes at 1.5 years for: a) ammonium, b) nitrate (as N), and c) dissolved organic carbon. All concentrations are in mg/L.

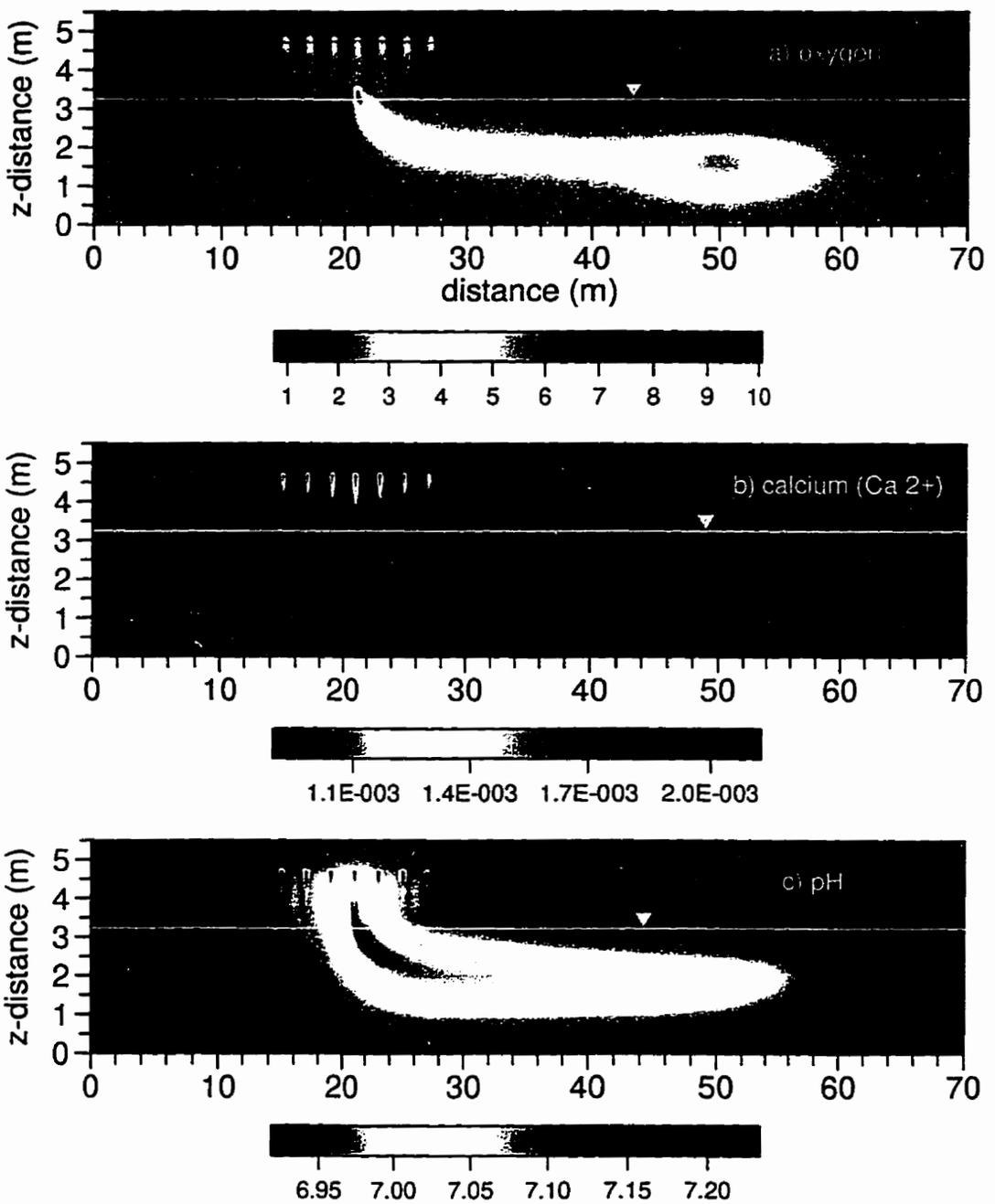

Figure 4.5: Simulated plumes at 1.5 years for: a) dissolved oxygen in mg/L, b) calcium in moles/L, and c) pH.

which forms an extensive plume in which the highest concentrations coincide with the edges of the NH_4^+ plumes. The nitrate distribution becomes reasonably homogeneous after the plume has migrated a short distance below the water table. Nitrification and *DOC* transformation both require dissolved oxygen and Figure 4.5 shows that O_2 is depleted relative to atmospheric levels in the unsaturated zone and further down gradient of the drain field. Immediately below the center drain, the dissolved oxygen concentration is as low as 1.0 mg/L. The low dissolved oxygen zone located between 46 m and 56 m is a transient feature which at later simulation times is advected out of the model domain. This low concentration zone is related to the fact that at early time the NH_4^+ plumes reach the capillary fringe and create temporary oxygen-depleted conditions at the water table.

An integrated temporal representation of the behaviour of the nitrogen species and *DOC* for the first 1000 days of the simulation is given in Figure 4.6. Ammonium and *DOC* mass in the system increase nearly linearly during the first 40 to 60 days of the simulation. Ammonium then begins to decrease as a result of increases in the nitrifying biomass. After 250 days both the ammonium and *DOC* mass remain essentially constant indicating that steady-state conditions have been achieved for these species. The generation of nitrate is delayed for the initial 20 or 30 days of the simulation which is again a result of the initially low nitrifying biomass. After this short lag time the nitrate mass increases in a linear manner much like the conservative tracer. After 750 days both the tracer and nitrate mass start to plateau and after 1100 days the mass of these species is constant, which indicates that steady-state distributions have been attained within the model domain. There is no net accumulation of N_2 during the simulation period which reveals that denitrification is not taking place; this is consistent with the complete oxidation of *DOC* in the unsaturated zone.

Three vertical profiles of the simulated oxygen concentration in the air phase are given in Figure 4.7. From this plot it is clear that oxygen consumption is occurring adjacent to the drains and that downward concentration gradients have developed. Away from the immediate vicinity of the drain field the oxygen concentration remains at atmospheric levels, which is in agreement with the unsaturated zone oxygen profiles presented by *Wilhelm et al.* [1994a; 1996] for locations away from the drain field. A field profile

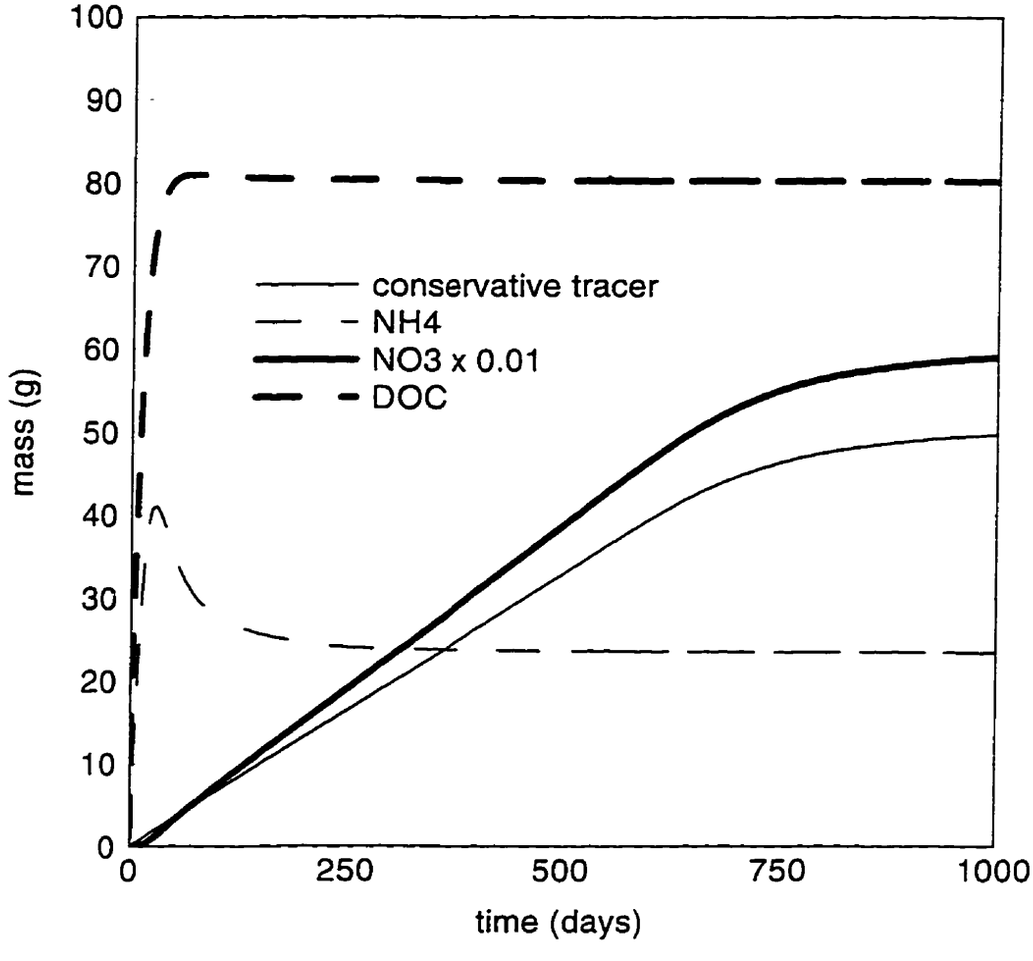

Figure 4.6: Total mass versus simulation time for several species.

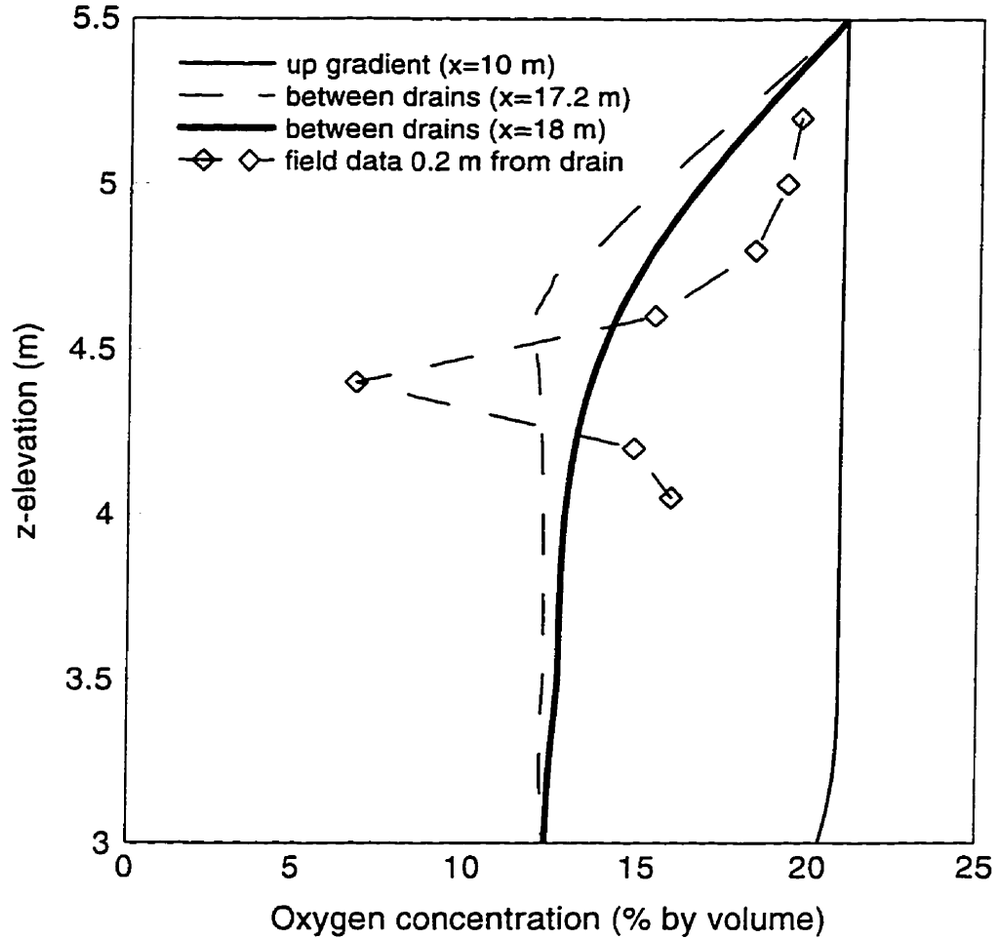

Figure 4.7: Profiles of oxygen concentration in the air phase. The boundary condition at z= 5.5 *m* is set to atmospheric content (21.0% by volume). Field data is from *Wilhelm et al.* [1994a].

located 0.2 *m* from a drain is also shown in Figure 4.7. Although the field profile is more erratic than the model profiles, the field data also clearly shows oxygen consumption near the drains. *Wilhelm et al.* [1994a] present other profiles located 0.2 *m* from a drain which indicate that oxygen concentrations at the depth of the drains may fluctuate from less than 10% to about 17% over a period of several days. Such transient conditions in soil gas in the shallow vadose zone may be due to short term atmospheric pressure changes which cause advective transport of atmospheric oxygen.

Two of the key carbonate species, calcium and pH, are shown in Figure 4.5. The calcium concentrations in the core of the plume are seen to be higher than either the wastewater or the background water concentrations. In the reactive transport model this can only be a result of calcite dissolution which is driven by the increased acidity in the vicinity of the drain field. As would be expected, the zones with the highest Ca^{2+} occur at the edges of the *DOC* and NH_4^+ plumes. The pH plume is about 0.2 to 0.3 pH units lower than the wastewater or background pH values. Thus, although H^+ and CO_2 are generated during the oxidation reactions (see Appendix A), calcite dissolution is apparently minimizing the pH drop. Careful inspection of the Ca^{2+} and pH plumes reveal that increased Ca^{2+} and decreased pH also occur above the drain locations in the unsaturated zone. This is caused by the air-phase diffusion of CO_2 from the area of the drains towards the surface boundary. Near the drains, the percentage of CO_2 in the soil air ranges from about 1.5 to 3.0%.

The results of the Cambridge simulation show that the most significant biogeochemical changes take place as the wastewater migrates from the drains to the shallow saturated zone. Recognizing the importance of reactions in the unsaturated zone, *Wilhelm et al.* [1994a] sampled septic-tank effluent and groundwater near the top of the saturated zone on five occasions between December 1987 and November 1990, which represents the most frequent sampling conducted at the Cambridge site. As noted previously, in the shallow water table zone and for 12 to 15 *m* down gradient of the drain field all reactive species reach steady state distributions by 1.5 years, which allows for a direct comparison of the model results at this time and the water table data presented by *Wilhelm et al.* [1994a; 1996]. Table 4.3 presents the model results and field data collected for water-

Species	Source Value for Simulation	Field Results	Model Results at Water Table
$NH_4^+ - N\ (mg/L)$	31.1	0.09	0.0
$NO_3^- - N\ (mg/L)$	1.3	26.7	20.3 to 26.0
$CH_2O\ (mg/L)$	82.0	3.3	0.0
$O_2\ (mg/L)$	0.0	≈ 5	1.0 to 5.5
pH	7.17	7.1	6.9 to 7.1
$HCO_3^-\ (mol/L)$	7.3×10^{-3}	5.6×10^{-3}	4.8 to 5.6×10^{-3}
$Ca^{2+}\ (mol/L)$	9.3×10^{-4}	2.3×10^{-3}	1.7 to 2.1×10^{-3}

Table 4.3: Comparison of model and field results for major reactive species. Field data is the average data for eight samples collected within 0.6 *m* of the water table. A range is given for the model results because the concentrations vary along the water table beneath the drain field.

table samples from piezometer points in the upper 0.6 *m* of the saturated zone directly beneath the drain field. A comparison indicates very good agreement between the two independent sets of data, with the possible exception of *DOC*. It should be noted that the low *DOC* concentrations observed in the field are considered to be indicative of relatively recalcitrant *DOC* [*Wilhelm et al.*, 1994a] which is currently not represented in the mathematical model. *Wilhelm et al.* [1994a] present saturated zone profiles of *DOC* which indicate that some aerobic oxidation may occur as which the *DOC* migrates down gradient; however, the influence of this on the *N* and *C* species appears to be of little importance. The behaviour of this fraction of the total *DOC* could be captured in the model by introducing a recalcitrant *DOC* species with much lower Monod rate constants.

The field and model results in Table 4.3 indicate that the reduced *N* in the wastewater is completely oxidized to NO_3^- in the unsaturated zone. Recent unsaturated zone monitoring at the Cambridge site [*Zanini*, 1996] suggests that nitrification is complete after a travel distance of about 0.5 *m*, which is in agreement with the numerical results. To follow the wastewater-derived NO_3^- further along the flow system *Wilhelm et al.* [1994a]

sampled seven piezometers positioned roughly along the central flow line of the effluent plume (the locations of these piezometers are shown by the circled dots in Figure 4.3b). This was considered more appropriate than attempting to map the two-dimensional distribution of NO_3^- because of the confounding influence of the background agricultural nitrate. *Robertson et al.* [1991] clearly demonstrate that NO_3^- concentrations within the core of the wastewater plume are approximately equal to background concentrations. Given the relatively weak transverse dispersion at the Cambridge site it is reasonable to consider that data collected along the central flow line of the plume is representative of wastewater nitrogen. Figure 4.8 presents the $NO_3^- - N$ field data along the plume center line and the model-predicted concentrations at seven corresponding locations. The model results are for a simulation time of three years, at which time the nitrate plume has reached steady state within the model domain. Although the model results appear somewhat lower than the field data in the central portion of the profile, the trends of both profiles are consistent and the average concentration for each profile differs by only 2.8 mg/L. Thus it is concluded that the model predictions very closely agree with the observed field data for both ammonium and nitrate.

The overall behaviour of the reactive species in the model simulations agrees well with the unsaturated and saturated zone geochemical reactions and transport processes described by *Wilhelm et al.* [1994a; 1996]. For example, nitrate remains in an oxidized state in the saturated zone because of the lack of labile *DOC* for denitrification. As well, oxidation of the wastewater *DOC* in the unsaturated zone generates CO_2 which then diffuses away from the drain locations, a process which *Wilhelm et al.* [1994a; 1996] had hypothesized should be taking place. The modelling results are also consistent with other field studies of denitrification in nitrogen-enriched sandy aquifers, where denitrification is carbon limited and organic carbon that might support denitrification is consumed by unsaturated zone processes [*Harman et al.*, 1996; *DeSimone and Howes*, 1996]. At the Cambridge site *Wilhelm et al.* [1994a; 1996] also noted that Ca^{2+} increased relative to the effluent because of calcium carbonate dissolution, and that only a small decrease in pH occurred. These changes are also well represented by the reactive transport model.

The favorable comparison between the simulation results and the field data suggests

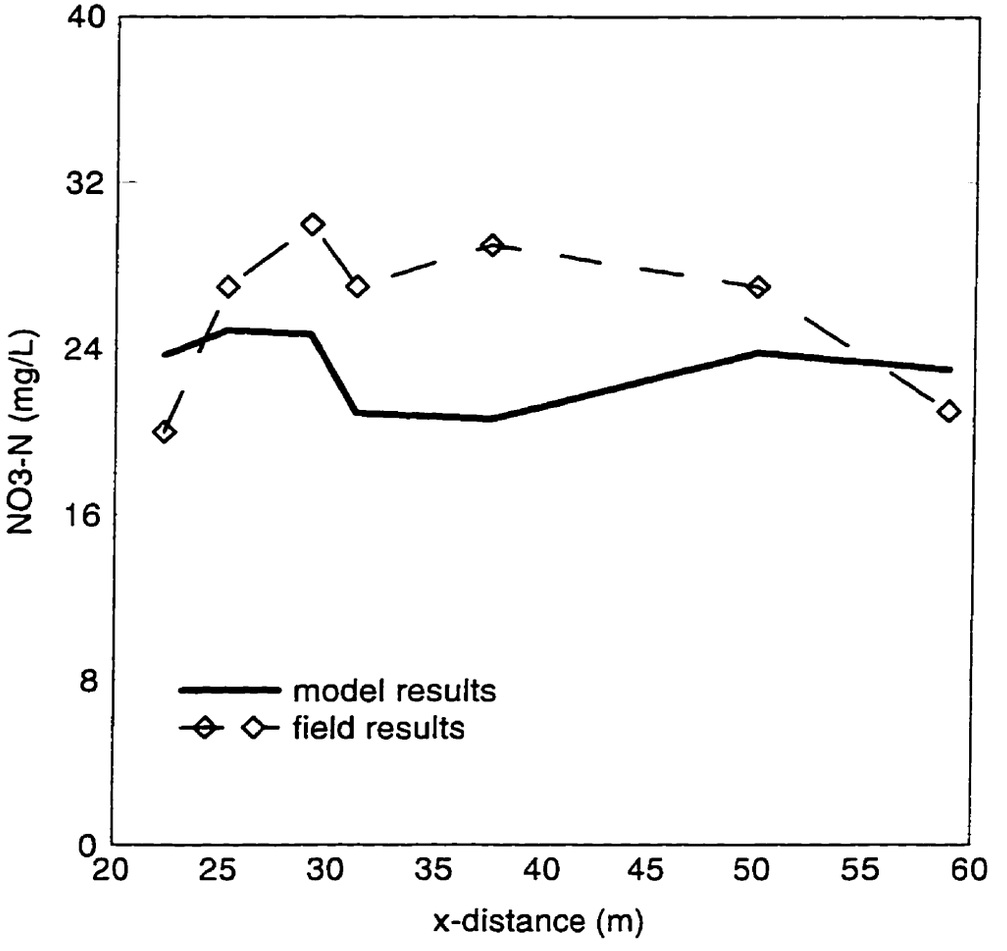

Figure 4.8: Longitudinal profiles of nitrate-*N* along the plume center line. Field data is from *Wilhelm et al.* [1994a] and the piezometer locations are shown in Figure 4.3b.

that the major physical and biochemical processes have been correctly captured in the reactive transport model. This gives justification for using the model to explore some of the key factors which may influence wastewater evolution in sandy aquifers.

Chapter 5

Analysis of Factors Affecting Wastewater Plume Evolution

In this chapter the reactive transport model is employed to conduct an analysis of several factors which are considered to have an important influence on wastewater plumes in shallow aquifers. Because current concepts about the evolution of wastewater plumes in sandy aquifers are based on case studies, it is often difficult to ascertain which physical and biochemical parameters are most important in controlling the observed distributions of species. For example, one may have a good understanding of an existing plume at a site where the water table is located one metre below the drain field, but how would the distribution of species in the plume differ if the water table was only 0.5 m below the drain field? Such questions can be answered very efficiently using a numerical model that incorporates the salient physical and biochemical processes.

In order to impose a reasonable limit on the number of simulations performed, only selected parameters are investigated in the present analysis. The parameters are ones which have been postulated in the scientific or regulatory literature as being significant and include: distance to the water table, wastewater loading rate, soil moisture characteristics, calcium carbonate content of the aquifer, the composition of the wastewater, and seasonal use. The approach to the analysis is to vary these parameters from their

base-case values, where the base case is taken as the Cambridge, Ontario simulation described in Chapter 4. The information obtained from these simulations will provide further insight into the processes occurring when wastewater is introduced into shallow sandy aquifers.

Although the model requires numerous biogeochemical rate parameters, these parameters are not investigated in the present sensitivity analysis. The kinetic parameters having the most uncertainty are those in the multiple-Monod expressions; the sensitivity of reactive transport simulations to these parameters have been investigated in detail by *Chen et al.* [1992] and *Essaid et al.* [1995].

5.1 Distance to the Water Table

Many geographic areas have inadequate subsurface wastewater treatment which is often attributed to high water tables [*e.g. Cogger et al.*, 1988]. As shown in the previous chapter, biochemical reactions in the unsaturated zone are very important in controlling a) the chemical species which reach the water table, and b) the type of reactions which occur in the down gradient saturated zone. Although this is generally recognized, different jurisdictions may have widely differing criteria for the minimum distance between the drain field and the seasonally high water table. *Cogger et al* [1988] note that this minimum distance varied from 0.30 *m* to 0.90 *m* for two Atlantic coast states with similar soil conditions.

In the simulation performed here, the water table (*i.e.* zero pressure head) is maintained near 0.5 *m* below the Cambridge drain field by setting the right-hand boundary condition in Figure 4.1 as a specified head equal to 4.2 *m* over the interval z= 0.0 *m* to z= 4.2 *m*. All other physical and biochemical parameters are the same as used in the simulation presented in Chapter 4. The simulated moisture profiles near the drain field for the base case and the high water table case are shown in Figure 5.1. Although the drains are still located in the unsaturated zone, clearly the unsaturated distance below the drain field (located at z= 4.7 *m*) is significantly reduced.

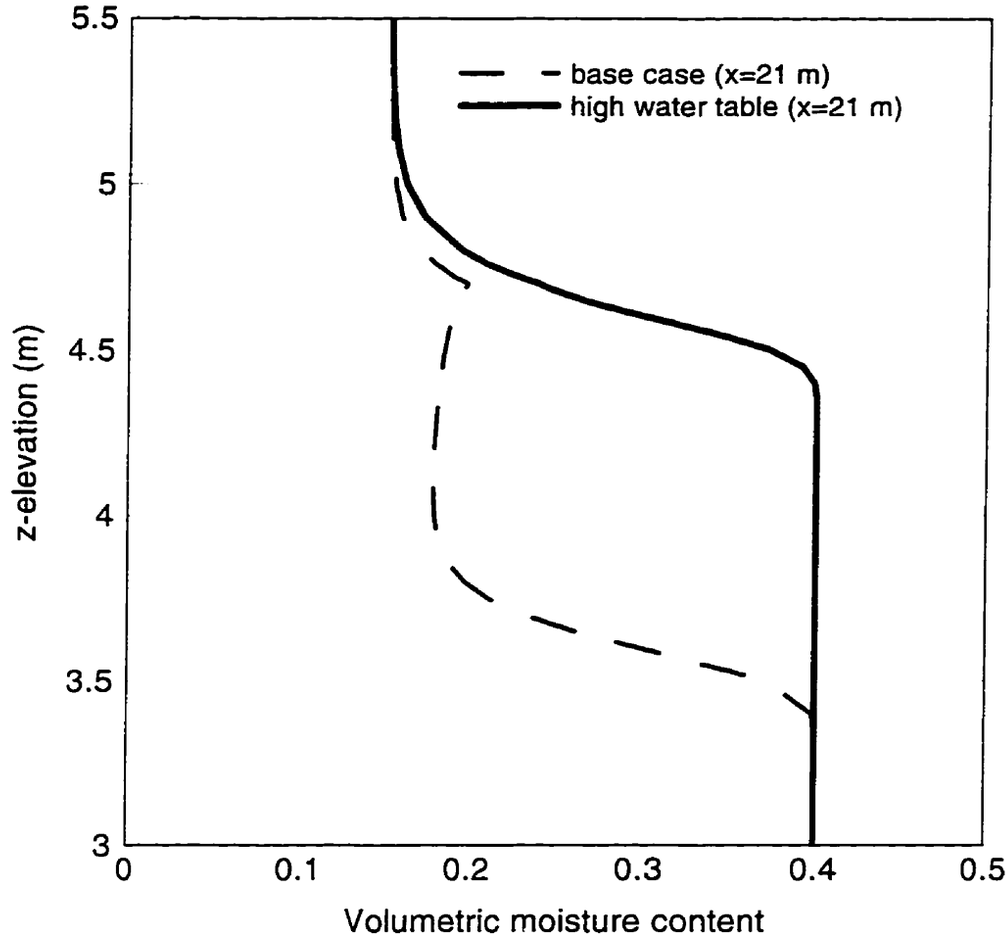

Figure 5.1: Comparison of moisture profiles in drain field for the base case and the high water table case. In both cases a drain is located at x= 21 *m* and z= 4.7 *m*.

The results obtained for six of the major reactive species are shown in Figures 5.2 and 5.3. The plumes correspond to a simulation time of 1.5 years and can be compared directly with the plumes shown in Figures 4.4 and 4.5. The most striking difference between the results is for ammonium, nitrate, and dissolved oxygen. With the higher water table the residence time in the unsaturated zone is reduced and nitrification is incomplete; this results in a plume of NH_4^+ below the water table and a significantly smaller NO_3^- plume with lower concentrations. Figure 5.2 shows that *DOC* is not completely oxidized by the time the wastewater reaches the water table and that incomplete ammonium oxidation results in anoxic conditions ($O_2 < 0.1\ mg/L$) below the drain field. The anoxic plume expands with time due to advection and dispersion. It is also important to note that calcium and pH evolve differently than in the base case. For example, Figure 5.3 shows that Ca^{2+} in the central portion of the plume is less than the background concentration because of the limited calcite dissolution. The temporal behaviour of the nitrogen species and *DOC* mass is given in Figure 5.4. These reactive species behave quite differently than for the base case (Figure 4.6); ammonium and *DOC* mass continue to increase for the duration of the simulation due to the limited oxidation of these species and the total nitrate mass in the domain at 500 days is 3.5 times less than that of the base case.

Although there is significant potential for denitrification because of the large anoxic plume, the process is limited by the lack of *DOC* below the water table. Denitrification is spatially restricted to the fringes of the *DOC* plume emanating from the central drain (Figure 5.2); in this very localized area the dissolved N_2 concentrations are about 2 mg/L above the atmospheric equilibrium concentration. The model biogeochemical system does not include *DOC* oxidation by $Mn(IV)$- or $Fe(III)$-oxide coatings which are common in many aquifers; however, if such reactions were included they would only serve to attenuate *DOC* more rapidly than shown in Figure 5.2c.

The results obtained here support the main findings of a field study by *Cogger et al.* [1988], who observed a correlation between water table depth and the predominant nitrogen species in dune sands. They found high concentrations of NH_4^+ and little NO_3^- in groundwater beneath a distribution field which was located 0.3 to 0.6 m above the water table. Similar to observed in this work, anoxic groundwater conditions prevailed

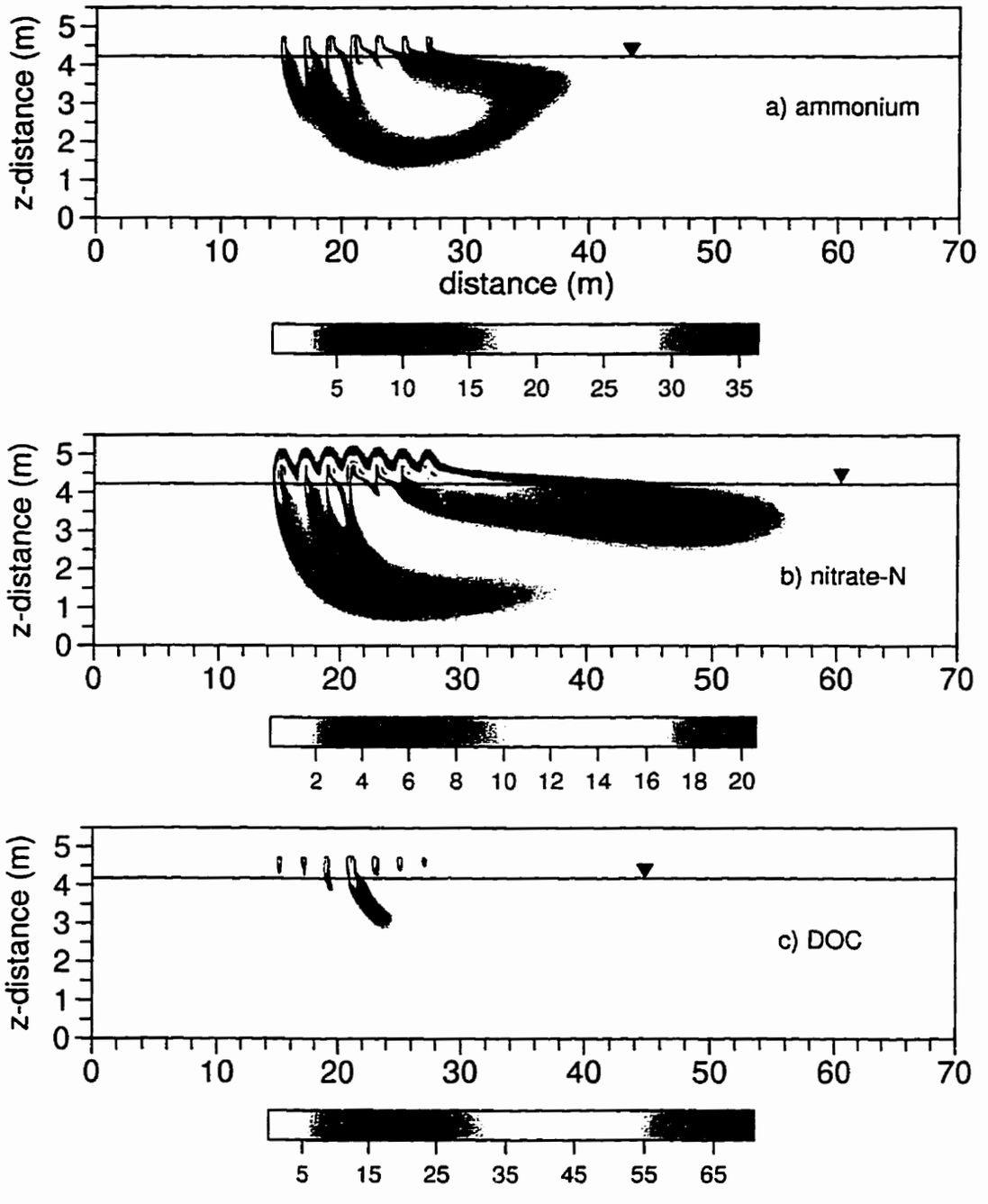

Figure 5.2: Simulated plumes for the high water table case at 1.5 years for: a) ammonium, b) nitrate (as N), and c) dissolved organic carbon. All concentrations are in mg/L.

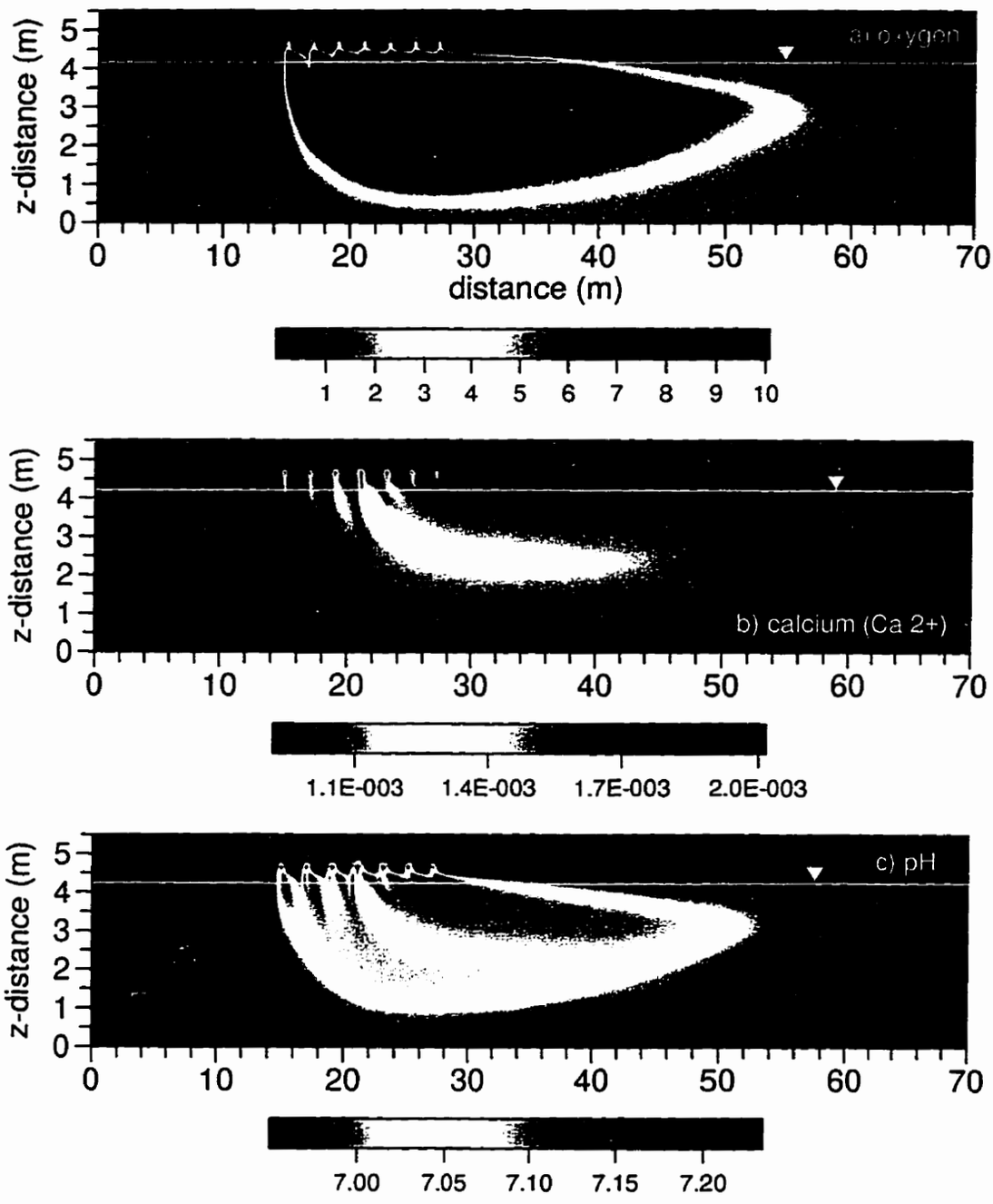

Figure 5.3: Simulated plumes for the high water table case at 1.5 years for: a) dissolved oxygen in mg/L, b) calcium in moles/L, and c) pH.

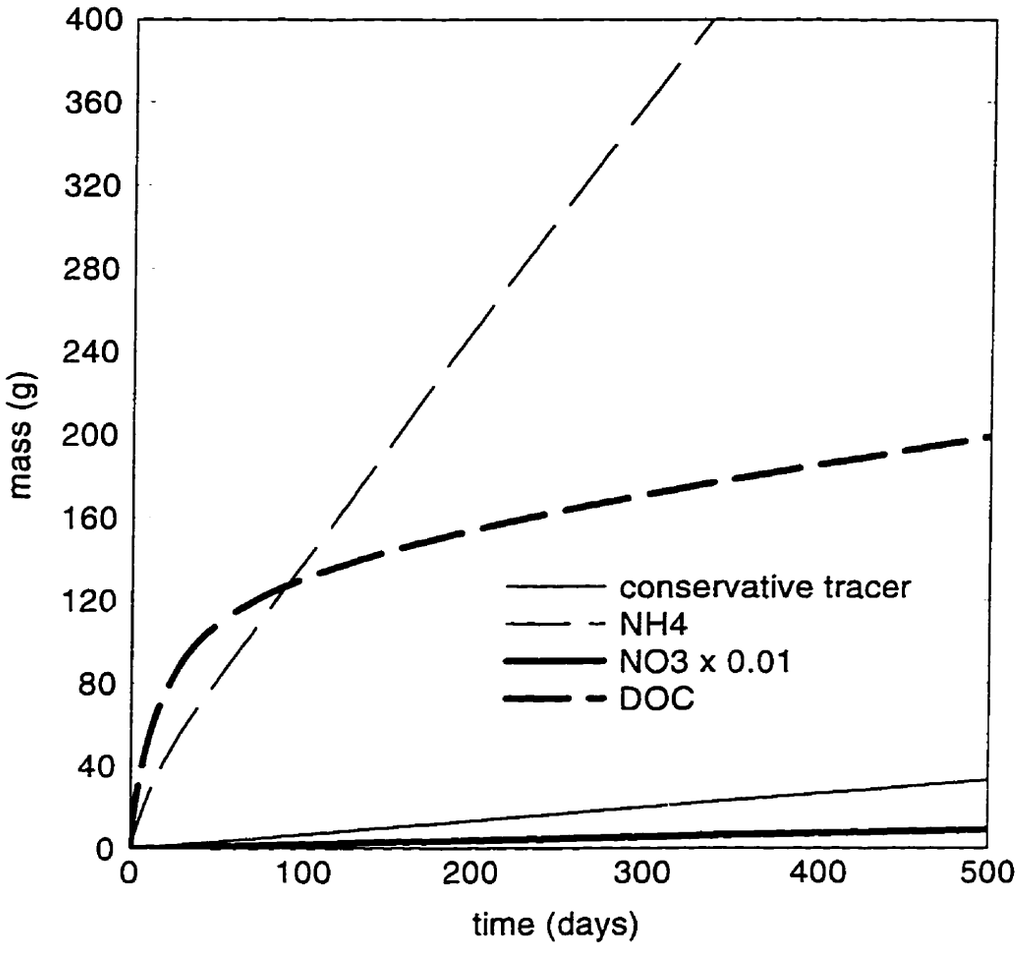

Figure 5.4: Total mass versus time for several species for the high water table case.

below the field throughout the year. Conversely, beneath an adjacent distribution field located 0.6 to 0.9 m above the water table, essentially complete nitrification occurred throughout the year of investigation. The simulation results and the findings of *Cogger et al.* [1988] suggest that in fine to medium sand aquifers complete oxidation of ammonium and *DOC* requires about one metre of travel in the unsaturated zone.

5.2 Wastewater Loading Rate

The wastewater loading rate to the subsurface is usually controlled by regulating the drain field area. For example, some jurisdictions specify the required length of drain as a function of the number of occupants or the daily wastewater flow. Soil moisture characteristics are rarely considered when determining appropriate wastewater loading rates.

A simulation was conducted in which the Cambridge simulation drain inflow rates (*i.e.* Q' in equation 2.2) were doubled, which increased the drain field loading to 400 cm/yr. This simulation can also be considered to represent a 50% reduction in the length of the distribution field normal to the modelled section. As shown in Figure 5.5, doubling the loading rate causes only minor increases in the volumetric moisture content in the immediate vicinity of the drains. Transport velocities are increased to between 36 m/yr and 120 m/yr in the unsaturated zone beneath the drain field. As shown in Figure 5.6 the increased velocities result in incomplete nitrification below the center of the drain field, although *DOC* is completely oxidized before reaching the water table (results not shown). The resulting nitrate plume is similar to the base case plume except that it has migrated further down gradient at 1.5 years because of the increased velocities. The size of the anoxic groundwater plume shown in Figure 5.6 has increased relative to the base case due to the increased oxygen demand at the water table; however, denitrification is again limited due to the lack of labile *DOC* in the saturated zone. The calcium concentrations and pH in the core of the plume are similar to the Cambridge base case.

Overall, the biochemical changes caused by increasing the wastewater loading rate

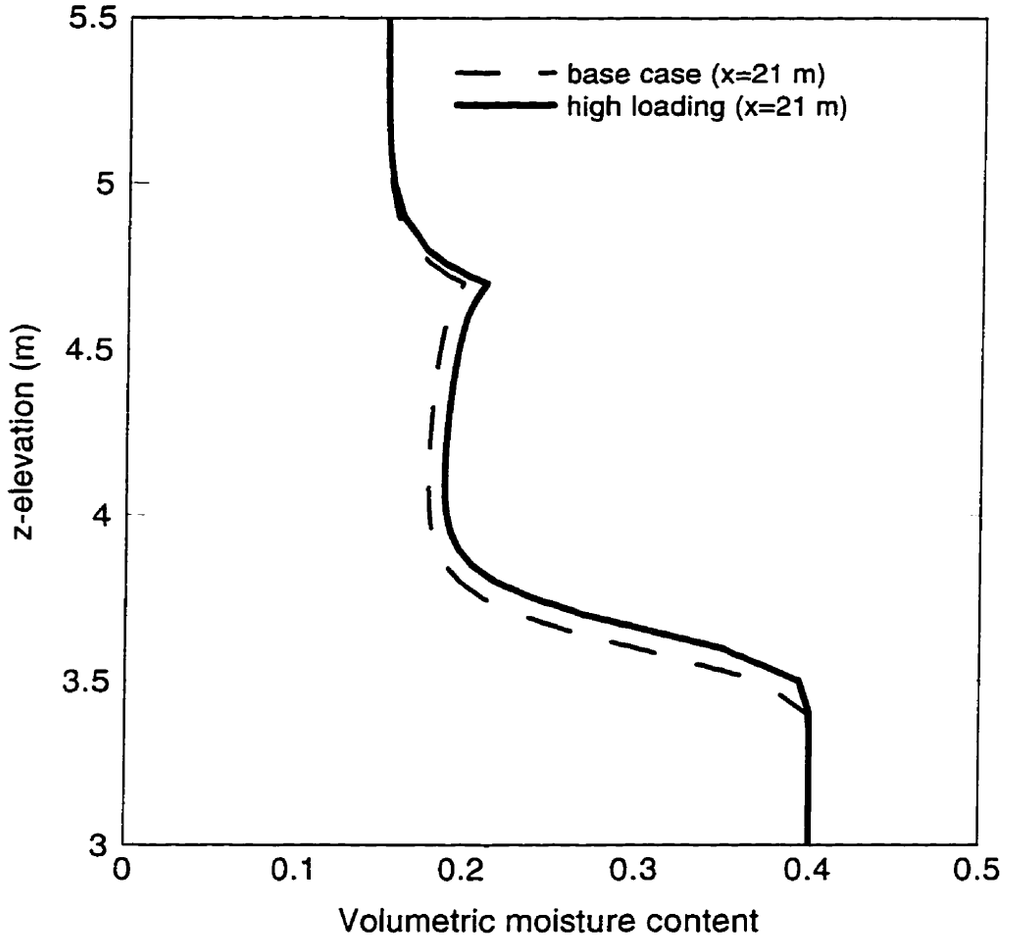

Figure 5.5: Comparison of moisture profiles in drain field for the base case and the high wastewater loading case. In both cases a drain is located at x= 21 *m* and z= 4.7 *m*.

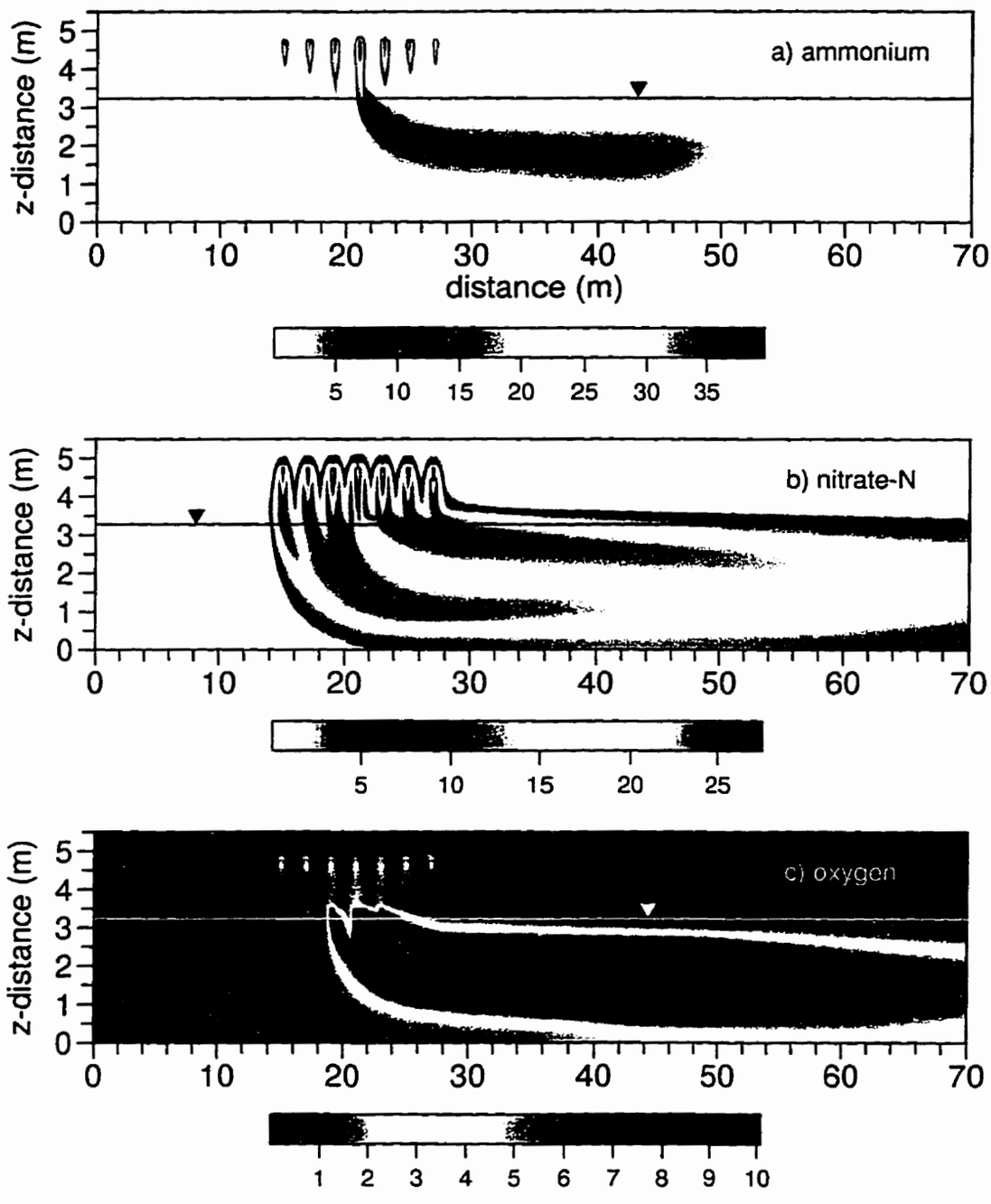

Figure 5.6: Simulated plumes for the increased loading case at 1.5 years for: a) ammonium, b) nitrate (as N), and c) dissolved oxygen. All concentrations are in mg/L.

Parameter	Value
Saturated moisture content, θ_S	0.422
Residual moisture content, θ_{res}	0.026
Air-entry pressure, ψ_{air}	-0.08 m
Fitting parameter, α	7.7 m^{-1}
Fitting parameter, β	9.74
Fitting parameter, γ	0.897

Table 5.1: Values of the *van Genuchten* parameters used for the $\psi - S_w$ and $k_{rw} - S_w$ relationships for the coarse sand simulation [*Akindunni et al.*, 1991].

are relatively minor due principally to the high conductivity of the Cambridge sands. The sands can accommodate the increased specific discharge from the drains with only a minor reduction in the volumetric air content in the unsaturated zone. *Cogger et al.* [1988] also found that, provided 0.6 to 0.9 m vertical separation was maintained between the drain field and the water table, increasing the loading rates in sandy soils up to 1500 cm/yr did not reduce nitrification in the unsaturated zone.

5.3 Soil Texture

It was hypothesized that wastewater plumes in relatively coarse textured sands would be similar to those resulting from high wastewater loading rates in fine to medium sands, such as at Cambridge. To investigate this, a simulation was conducted using the "coarse sand" properties given by *Akindunni et al.* [1991]. The coarse sand is assigned a saturated hydraulic conductivity of 112 m/day and the *van Genuchten* [1980] parameters given in Table 5.1.

The moisture profiles for the base case and the coarse sand simulation are shown in Figure 5.7. Although the wastewater loading rates are the same for both cases, the vertical velocities are much higher in the coarse sand because of the significantly lower

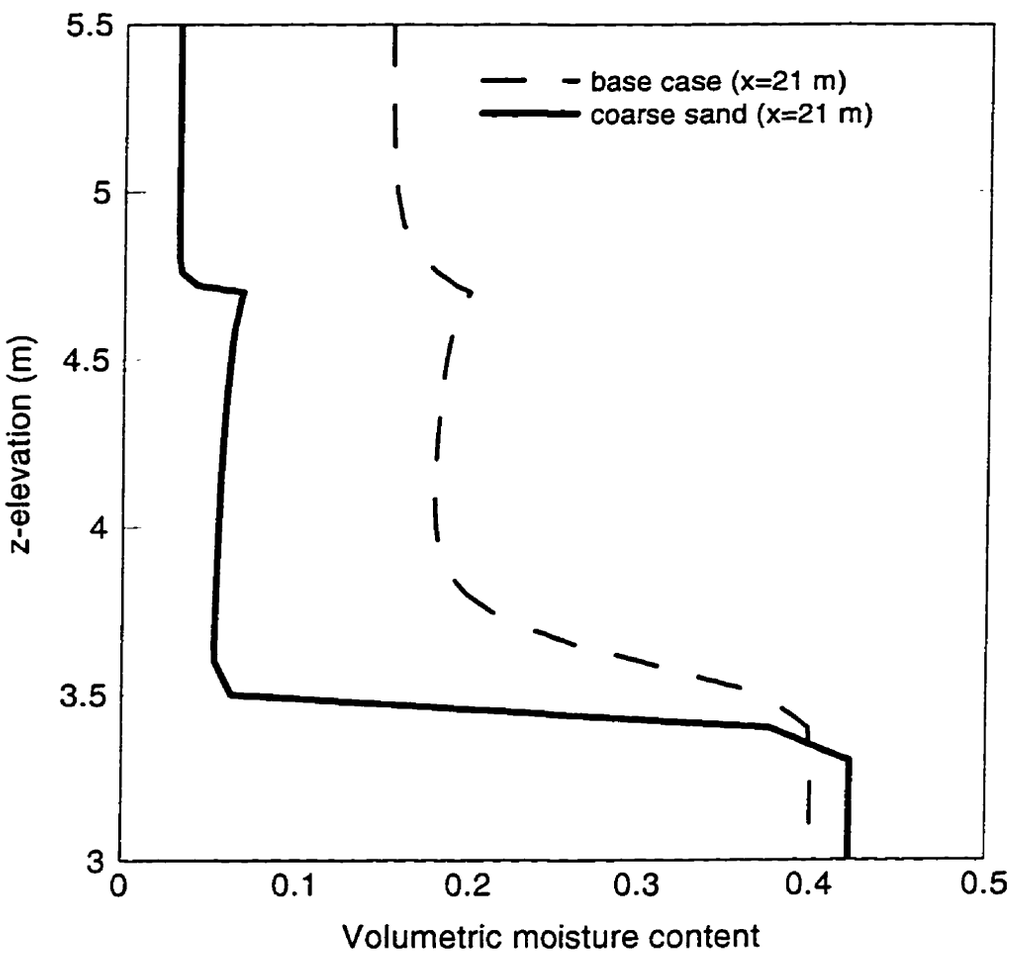

Figure 5.7: Comparison of moisture profiles in drain field for the base case and the coarse sand case. In both cases a drain is located at x= 21 *m* and z= 4.7 *m*.

moisture content. This has essentially the same effect as a high loading rate in a fine to medium sand as can be see by comparing Figures 5.6 and 5.8. Dissolved organic carbon (not shown) is once again completely oxidized before reaching the water table.

5.4 Carbonate Content of Aquifer and Wastewater Composition

As discussed previously, the oxidation of *DOC* and NH_4^+ produces acid. Previous studies of the geochemistry of septic system plumes in shallow aquifers have lead to the conclusion that this acidity will be effectively buffered by mineral dissolution in carbonate-rich settings [*Whelan*, 1988; *Robertson and Blowes*, 1995; *Wilhelm et al.*, 1996]. In poorly buffered sediments, *Robertson and Blowes* [1995] have found that wastewater oxidation can cause reducing conditions and pH decreases which in turn contribute to enhanced mobility of *Fe*, *Mn*, and trace metals. The liberation of trace metals such as *Cr*, *Zn*, and *Al* will be a concern in areas where groundwater discharges to sensitive aquatic ecosystems.

The influence of aquifer carbonate content is first investigated by simulating the Cambridge site with the assumption that the aquifer sediments contain no calcite ($CaCO_3$). This is a limiting case because the aquifer sediments are being represented as completely inert with respect to aqueous carbonate reactions. It should be noted that this a rather hypothetical situation because in natural systems pH reductions can obviously be buffered by other reactions. For example, dissolution of primary or secondary aluminum minerals may be an important pH-buffering mechanism in carbonate-deficient sediments and can serve to maintain pH in the vicinity of 4.0 to 4.5 [*Appelo and Postma*, 1994].

Because it is assumed that calcite is not present, the background initial groundwater cannot be in equilibrium with $CaCO_3$ and the initial conditions are varied from those given in Table 4.2; instead, as shown in Table 5.2, the background chemistry is specified to agree with that observed by *Robertson and Blowes* [1995] at the Killarney, Ontario site.

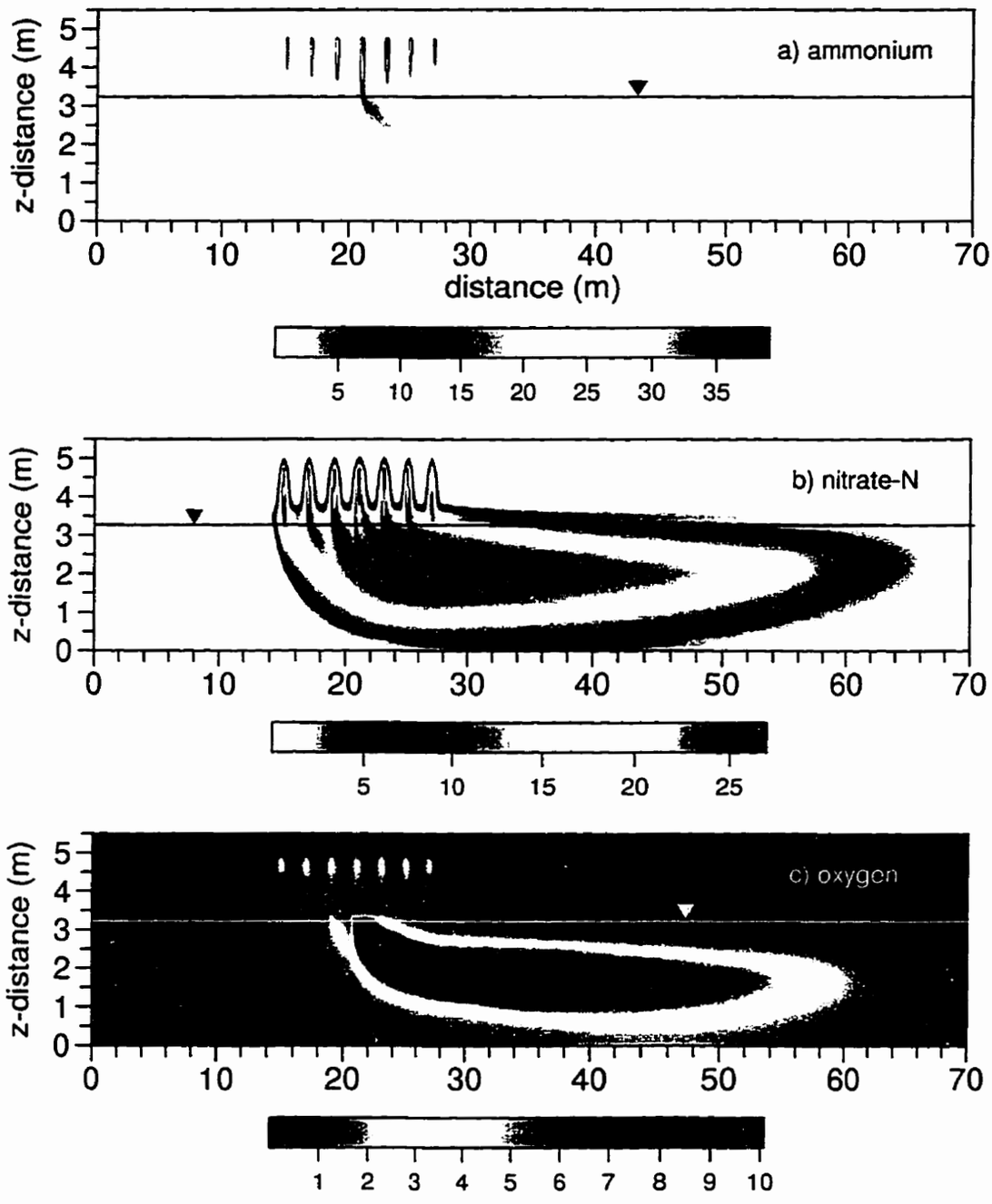

Figure 5.8: Simulated plumes for the coarse sand case at 1.5 years for: a) ammonium, b) nitrate (as N), and c) dissolved oxygen. All concentrations are in mg/L.

Species	Initial Value	Source Value
NH_4^+ (mg/L)	0.0	40.0
NO_3^- (mg/L)	0.0	5.7
CH_2O (mg/L)	0.0	82.0
O_2 (mg/L)	6.0	0.0
CO_2 (mol/L)	5.5×10^{-4}	1.3×10^{-3}
N_2 (mg/L)	0.0	0.0
OH^- (mol/L)	1.41×10^{-9}	6.6×10^{-8}
CO_3^{2-} (mol/L)	7.75×10^{-10}	4.0×10^{-6}
H^+ (mol/L)	3.17×10^{-6}	6.8×10^{-8}
(pH)	5.50	7.17
HCO_3^- (mol/L)	6.6×10^{-5}	7.3×10^{-3}
Ca^{2+} (mol/L)	1.0×10^{-4}	9.3×10^{-4}
X_1 (mg/m^3 of porous media)	0.1	
X_2 (mg/m^3 of porous media)	0.1	

Table 5.2: Initial (background) conditions and wastewater source conditions used for the no calcite reactive-transport simulation.

The distributions of O_2, Ca^{2+}, and pH are shown in Figure 5.9. It should be first noted that the amount of oxidation taking place is the same as the base case, as evidenced by the dissolved oxygen plume and the fact that the NH_4^+, $NO_3^- - N$, and DOC plumes are identical to those shown in Figure 4.4. As well, Figure 5.9 shows that Ca^{2+} from the drain field is being transported as a conservative tracer due to the assumption of an inert aquifer matrix. The most notable observation is that although the pH decreases as the wastewater migrates away from the drain field, the pH in the core of the plume is not depressed to the low levels (*i.e.* 4.4 to 5.0) observed by *Robertson and Blowes* [1995]. The reason for this is that the Cambridge wastewater contains sufficient alkalinity to buffer most of the acidity and prevent a major decrease in the plume pH. This illustrates that it is not sufficient to consider solely the carbonate content of the sediments when attempting to assess whether low-pH conditions will develop.

As shown in previous simulations, the CO_2 generated by DOC oxidation in the unsaturated zone will partition into the air phase and diffuse away from the drain field. This physical loss of CO_2 from solution will also assist in buffering pH decreases. The importance of this process was assessed by repeating the no-calcite simulation and treating CO_2 as a nonvolatile species with a Henry's law coefficient of zero. Thus all CO_2 produced by oxidation remains in solution. The simulation results for this case (not shown) reveal that the pH in the plume core is approximately 0.6 pH units less than shown in Figure 5.9. Therefore, the loss of CO_2 from solution provides only a minor amount of buffering.

Table 5.2 indicates that the Cambridge wastewater contains NH_4^+ at a concentration of 40 mg/L (or 31 mg/L as $NH_4^+ - N$) which is not atypical; however, comparisons of septic tank effluent chemistry presented by *Whelan and Titaminis* [1982] and *Harmen et al.* [1996] clearly show significant variability in $NH_4^+ - N$ data. A reasonable range for $NH_4^+ - N$ in septic tank effluent appears to be from 30 mg/L to 120 mg/L which implies that the acid producing potential may be several times greater than for the Cambridge effluent. To demonstrate this, the wastewater NH_4^+ concentration was doubled and the simulation with no calcite in the aquifer was repeated. Figure 5.10 shows the results for three reactive species for the case of increased NH_4^+. The increased oxygen demand has

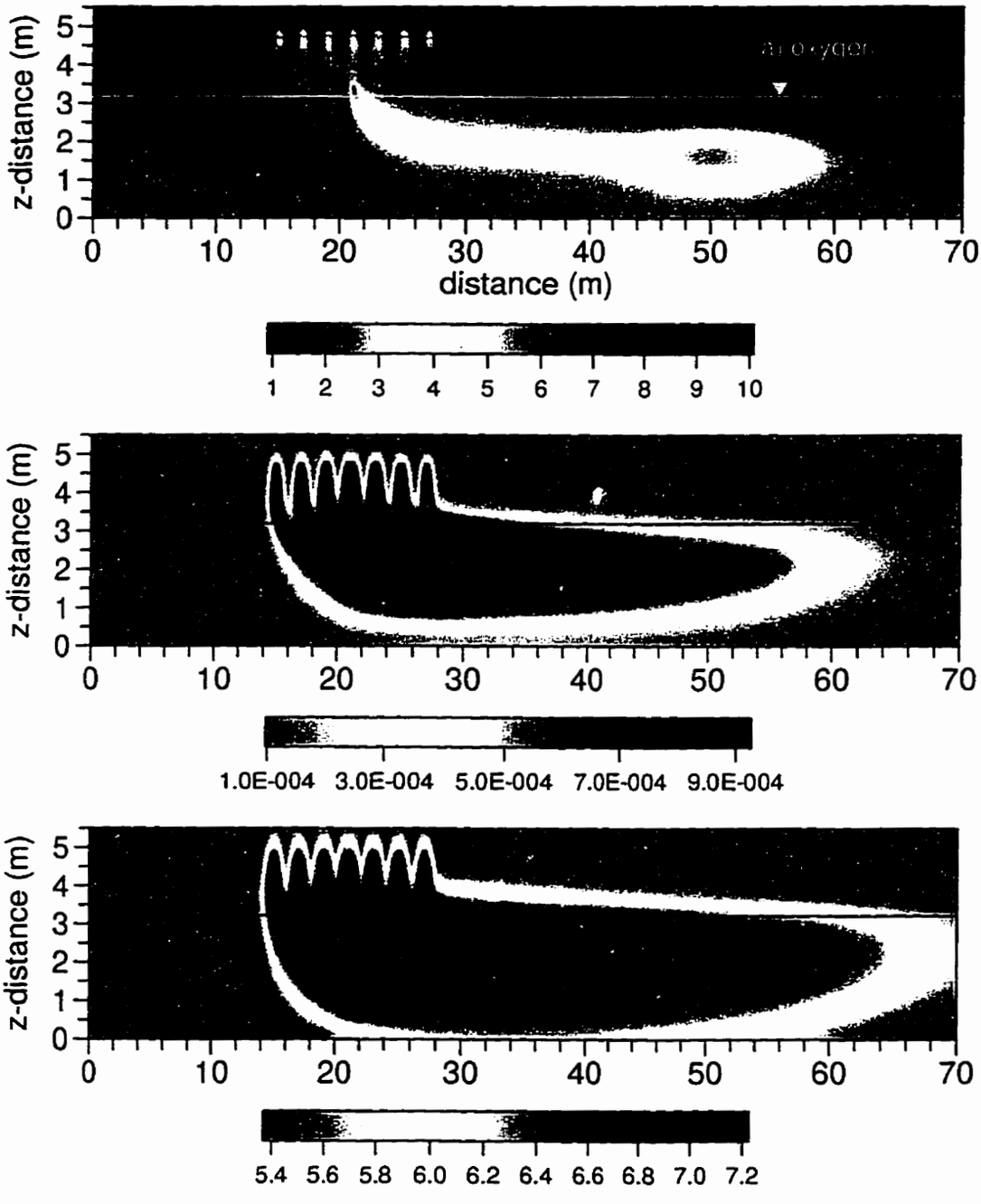

Figure 5.9: Simulated plumes for the case with no calcite at 1.5 years for: a) oxygen in mg/L , b) calcium in moles/L, and c) pH.

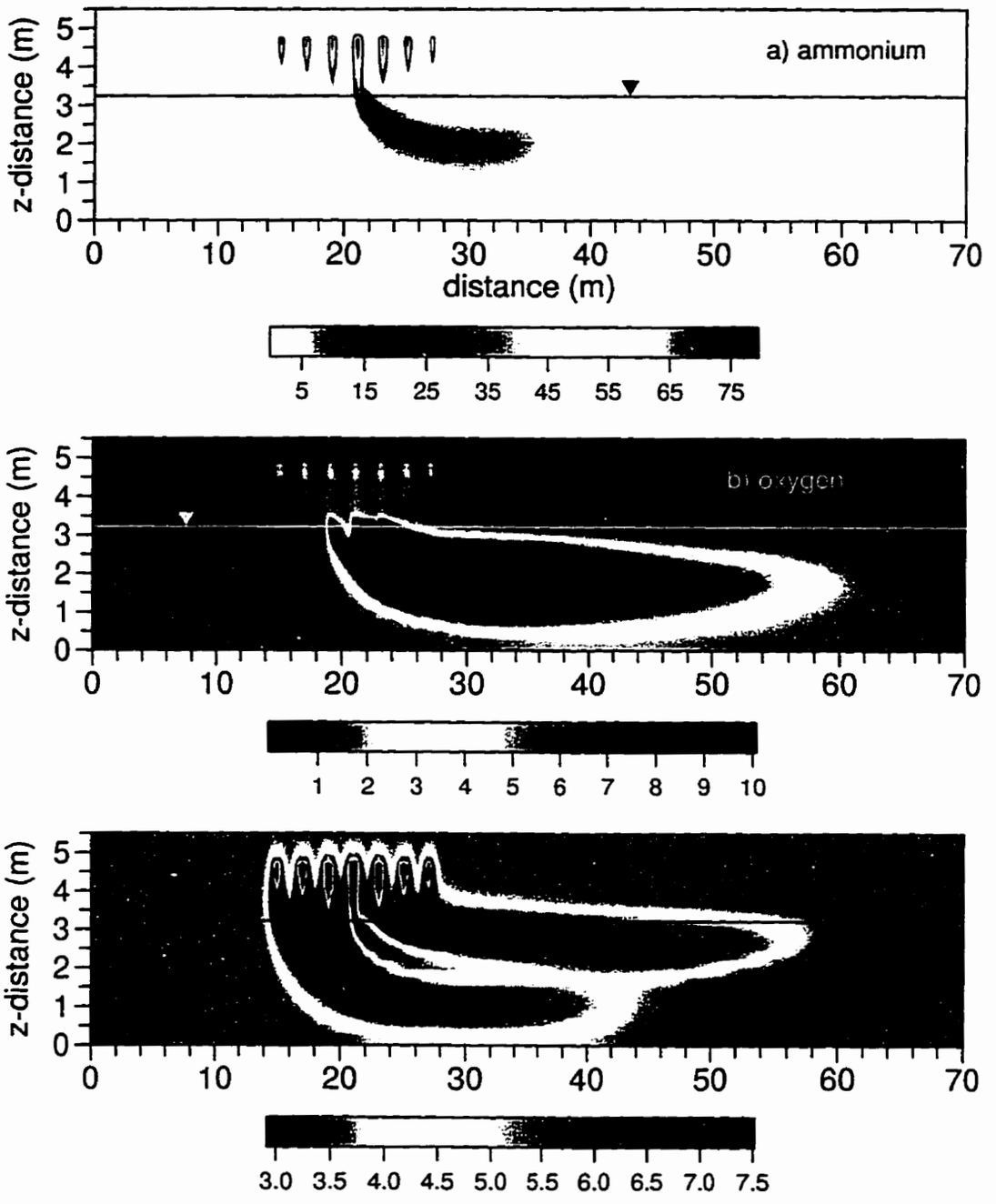

Figure 5.10: Simulated plumes for the case with increased ammonium and no calcite at 1.5 years for: a) ammonium in mg/L, b) dissolved oxygen in mg/L, and c) pH.

resulted in NH_4^+ migration to the water table, although *DOC* is again completely oxidized in the unsaturated zone. This causes anoxic conditions to develop below the drain field and a large pH drop in portions of the plume. As mentioned above, pH decreases may be buffered by reactions not currently considered in the biogeochemical model and thus the pH values of 3.0 to 4.0 in Figure 5.10 may not be observed in the field; however, the simulation does clearly illustrate the potential for significant pH changes. Below the center drain, the oxidation of NH_4^+ is not complete and the NH_4^+ concentration at the water table is about 30 mg/L; in this small region the pH remains at about six. Thus it is clearly demonstrated that the creation of low pH conditions will require sediments with a low carbonate content, as well as sufficiently high wastewater NH_4^+ concentrations. In addition to these two factors there must be sufficient transport time and oxygen supply in the unsaturated zone to allow for complete oxidation of the ammonium.

It is also important to consider the nature of the acid-producing reactions. As an example, the base case simulation was repeated with the wastewater *DOC* (*i.e.* CH_2O) doubled to 164 mg/L; all other parameters were as given in Table 5.2. Despite this increase in the oxygen demand of the wastewater, *DOC* is again completely aerobically degraded in the unsaturated zone and the NH_4^+, $NO_3^- - N$, and *DOC* plumes at 1.5 years are very similar to those shown in Figure 4.4. The O_2, Ca^{2+}, and pH distributions are essentially the same as those given in Figure 5.9; this illustrates that doubling *DOC* does not lead to the low pH values obtained when NH_4^+ is doubled. This is a direct consequence of the stoichiometries of the organic matter aerobic degradation reactions (reactions 1 and 4 in Appendix A) and the nitrification reactions (reaction 2 in Appendix A); nitrification of one mole of NH_4^+ produces twice as much H^+ as the oxidation of one mole of CH_2O.

5.5 Seasonal Loading Pattern

The evolution of wastewater plumes in shallow aquifers can be expected to be different than shown previously if the loading to the drain field is seasonally variable. This is il-

lustrated here by performing a one year transient flow and reactive transport simulation. All parameters used for the simulation are the same as for the Cambridge base case except that the nitrifying and heterotrophic biomass are allowed to decay. The decay rate constants k_1^d and k_2^d (see equation (2.17) and Appendix A) are both set to 0.05 $1/day$ [*Leggett and Iskandar*, 1981; *Henze et al.*, 1987]. Including decay will result in a reduction in biomass in the absence of required nutrients; however, the biomass is not allowed to decrease to less that the initial background concentrations. The simulation represents a six month (180 day) wastewater loading period followed by a six month (180 day) "resting" period in which no effluent is introduced into the subsurface. The recharge rate at the top boundary is held constant at 30 cm/yr for the entire simulation.

Figure 5.11 and 5.12 show the ammonium (NH_4^+) and nitrate-N plumes at the end of the loading period and at two subsequent times. The dissolved ammonium concentrations rapidly decline following cessation of wastewater loading, and after six months the maximum concentration has dropped by one order of magnitude to about 3.4 mg/L. This could be interpreted as a removal of the nitrate source; however, Figure 5.12 shows that maximum nitrate-N concentrations initially increase during the nonloading period and, in the core of the saturated zone plume, the concentrations remain relatively constant at approximately 25 mg/L. This persistence of the nitrate plume can be explained by the fact that a significant amount of NH_4^+ mass is sorbed due to cation exchange during the loading period. For example, at 180 days the maximum dissolved NH_4^+ concentration at z= 4.5 m is temporally constant at 35 mg/L (27 mg/L expressed as N). Based on a $K_{d_{NH_4}}$ of 0.34 cm^3/g [*Ceazan et al.*,1989] and a θ_w of 0.17, the sorbed mass in equilibrium with this concentration is equivalent to an aqueous concentration of about 73 mg/L expressed as N. After wastewater loading ceases, ammonium-free recharge water causes the sorbed mass to partition back to the aqueous phase where it is oxidized to nitrate. Dissolved oxygen results (not shown) indicate atmospheric oxygen concentrations exist in the unsaturated zone beneath the drain field at 240 days. Thus, the nitrate-N concentrations locally rise to approximately 70 mg/L in the unsaturated zone immediately below the central drain as can be seen in Figure 5.12. This causes nitrate-N concentrations above the drinking water limit of 10 mg/L to persist for the entire six months follow-

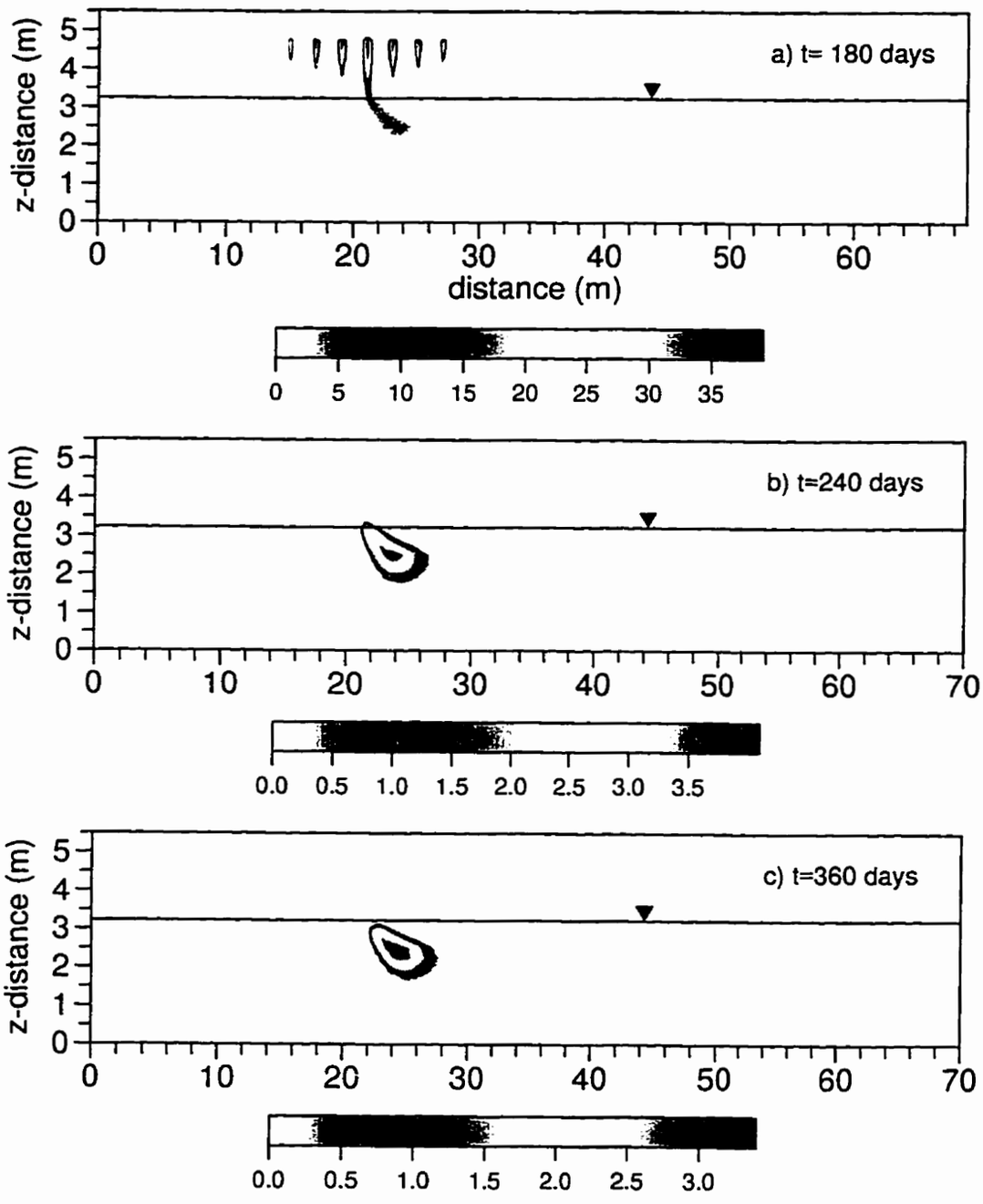

Figure 5.11: Simulated ammonium plumes for the seasonal loading case. Note that the colour bar is different for each time and that concentrations are in mg/L.

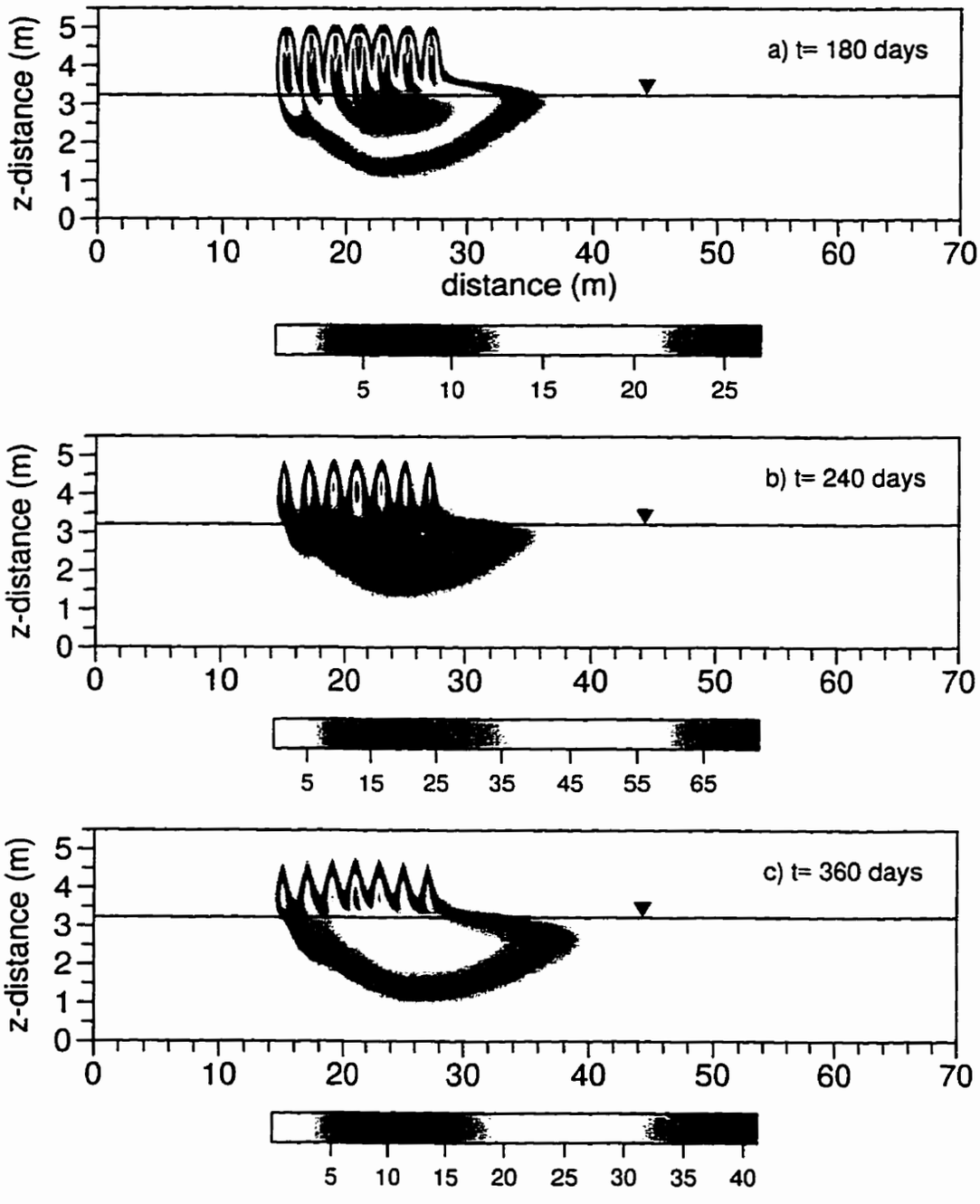

Figure 5.12: Simulated nitrate-N plumes for the seasonal loading case. Note that the colour bar is different for each time and that concentrations are in mg/L.

ing cessation of wastewater release. The increase in nitrate mass between 180 days and 240 days can also be seen in Figure 5.13. During this time interval most the of the ammonium mass in the system is oxidized and after 240 days the total nitrate mass in the system remains essentially constant. It is also noted that *DOC* is rapidly degraded in the unsaturated zone following 180 days and thus, as in most of the previous simulations, there is no wastewater-derived *DOC* available for denitrification.

The preceding examples serve to illustrate that the evolution of wastewater plumes in sandy aquifers will depend on many factors, and that the interaction between physical flow and transport and the biogeochemical reactions must be accounted for in order to predict the influence of any of these factors. For example, without a model such as the one developed here, it is not possible to predict the relative importance of wastewater chemistry versus wastewater application rate for a given set of hydrogeological conditions. Here it has been demonstrated that increasing the loading rate to 400 cm/yr in a fine to medium grain sand aquifer has only a minor influence in the unsaturated zone moisture content, and thus the supply of O_2 remains sufficient to allow for oxidation of wastewater N and C.

For most of the scenarios simulated here the impacts of septic systems include the generation of plumes which have nitrate concentrations above drinking water limits, which are anaerobic, and which may also have low-pH values. Thus, it can be expected that shallow groundwater quality will be impacted to some degree by the release of wastewater in unconfined sandy aquifers. While it will not be practical to simulate the impact for each onsite wastewater system in a given area or jurisdiction, the use of tools such as the simulation model developed here will provide more predictive capability than is currently available for aquifers in which nitrate or trace metals are of particular concern.

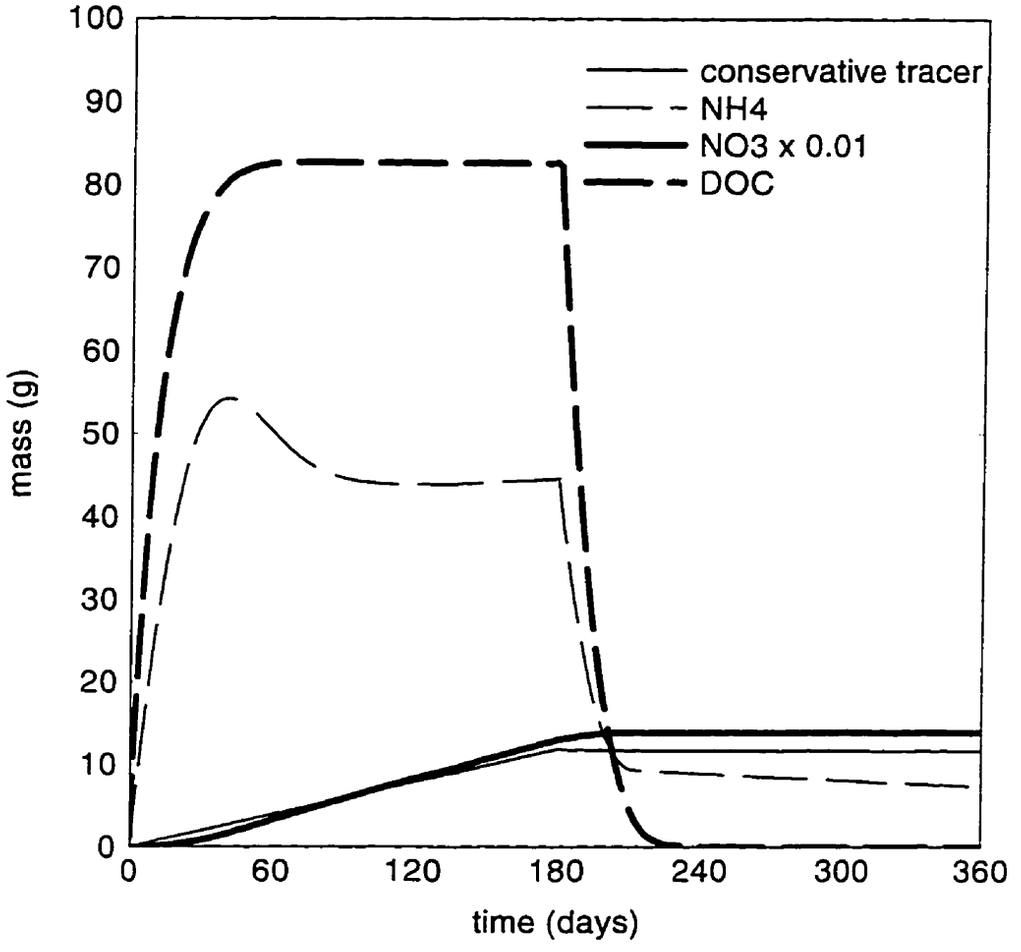

Figure 5.13: Total mass versus time for several species for the seasonal loading case.

Chapter 6

Numerical Investigation of a Fine-Grained Denitrification Layer

Nitrate is a mobile solute which may be stable in many shallow groundwater flow systems. These characteristics make NO_3^- a contaminant of concern with respect to drinking water quality and surface water eutrophication. The most widely recognized process that acts as a sink for nitrate in groundwater is heterotrophic denitrification, in which subsurface bacteria in an anaerobic environment use NO_3^- as an electron acceptor to oxidize dissolved organic matter. The denitrification pathway terminates with molecular nitrogen (N_2) which resists further chemical change [*Krom*, 1992]. Although sulfide- or pyrite-based denitrification may occur in aquifers containing sediments of marine or lacustrine origin [*Postma et al.*, 1991] these pathways are not important in many sandy aquifers of glacial origin [*e.g. Smith et al.*, 1991; *Wilhelm et al.*, 1994a; *DeSimone and Howes*, 1996]. Studies of wastewater-derived nitrate have usually found that conditions are not favorable for heterotrophic denitrification. The reaction is inhibited by molecular oxygen (O_2) in aerobic aquifers and in anaerobic conditions the lack of labile organic carbon often limits the denitrification rate [*e.g. Wilhelm et al.*, 1994a; *DeSimone and Howes*, 1996]. The previously presented numerical simulation results support these field observations; it is shown in Chapter 5 that for situations where nitrification ($NH_4^+ \rightarrow NO_3^-$) is

complete, the labile dissolved organic carbon (*DOC*) from the drain distribution field is also completely oxidized and therefore unavailable for subsequent denitrification. Thus wastewater-derived *DOC* will not be sufficient to support heterotrophic denitrification.

Valiela et al. [1997] have recently suggested that the addition of labile carbon sources to septic distribution fields to enhance denitrification may be a key to reducing nitrogen loading to eutrophication-stressed coastal watersheds. *Robertson and Cherry* [1995] have performed field trials where *in situ* denitrification of septic system nitrate was promoted by installing horizontal porous layers of fine-grained material in the vadose zone below septic drains. The porous layers remained tension saturated and were supplemented with solid organic carbon such as wood chips or sawdust which supplied labile *DOC*. This passive, low cost method was shown to effectively reduce NO_3^- concentrations for the particular configurations investigated. One of the possible adverse side effects of the horizontal denitrification layer which was identified was excess *DOC* leaching; however, the down-gradient impact of this could not determined from the small-scale field trials. The experiments involved installations of porous layers at relatively small distances (*i.e.* 0.2 to 0.4 *m*) above the water table, and in several cases incorporated enclosures to ensure flow of wastewater through the denitrification layer. It is unclear what effect these factors had on the observed performance of the layers.

The objective of this chapter is to perform a numerical investigation of the physical and biochemical processes taking place when a porous denitrification layer, such as proposed by *Robertson and Cherry* [1995], is placed below a drain field in a shallow sandy aquifer. The current understanding of how such a porous layer will function is extended by conducting simulations of field-scale installations, and by determining the importance of the position of the porous layer relative to the drain field and water table. The influence of wastewater composition and carbonate content of the sediments are also investigated. The simulation results assist in identifying down-gradient impacts of the denitrification layer and additional factors which require further experimental investigation.

6.1 Numerical Modeling Approach

The simulations are performed using the flow and reactive transport model presented in Chapters 2 and 3. The domain is two dimensional and the scenario is based on the Cambridge configuration shown in Figure 4.1; however, to reduce computation time and because the focus is on transport and reactions close to the drains and fine-grained layer, the horizontal extent of the domain is reduced to 40.0 m. A uniform distribution of wastewater is considered a desirable feature of distribution fields and because the configuration investigated here would be installed in conjunction with new drain fields, it is assumed that the loading of 200 cm/yr is equally distributed among the drains. This results in an individual drain discharge rate of 9.42 x 10^{-3} m^3/d, per unit width. The aquifer is again assigned a saturated hydraulic conductivity of 20 m/d and the soil moisture properties given in Table 4.1. The initial condition for flow is static equilibrium (*i.e.* gravity drainage) with the water table at z= 3.2 m, and the boundary conditions are shown in Figure 4.1. For the reactive species, the initial groundwater and wastewater chemistry is given in Table 4.2.

Robertson and Cherry [1995] identified high water saturations (*i.e.* $S_w \approx 1.0$) as a requirement of the denitrification layers. This will prevent the diffusion of atmospheric oxygen into the layer and thus conditions will be anaerobic. The properties of the fine-grained materials investigated by *Robertson and Cherry* [1995] were similar to those of the Touchet silt given in *Akindunni et al.* [1991], and these properties are used for the present simulations. The silt has a saturated hydraulic conductivity of 0.5 m/d and the *van Genuchten* [1980] parameters given in Table 6.1.

The denitrification layer must act as a source of labile *DOC*. *Carmichael* [1994] and *Robertson and Cherry* [1995] present data showing the release of *DOC* from denitrification layers amended with wood chips or sawdust is a kinetic process, indicating that the effluent *DOC* is a function of residence time in the layer. *Robertson and Cherry* [1995] also show that the *DOC* in water exiting saturated denitrification layers is initially on the order of 150 mg/L to 250 mg/L and that after one year these concentrations are generally less than 100 mg/L. Based on the *DOC* adsorption studies of *Jardine et al.* [1992],

Parameter	Value
Saturated moisture content, θ_S	0.485
Residual moisture content, θ_{res}	0.18
Air-entry pressure, ψ_{air}	-1.65 m
Fitting parameter, α	0.4 m^{-1}
Fitting parameter, β	7.05
Fitting parameter, γ	0.86

Table 6.1: Values of the *van Genuchten* parameters used for the $\psi - S_w$ and $k_{rw} - S_w$ relationships for Touchet silt [*Akindunni et al.*, 1991].

a kinetic dissolution model is used to simulate the release of *DOC* from wood chips or sawdust. The model has the following form:

$$\frac{d\overline{DOC}}{dt} = \alpha_d \left(\overline{K_d}\, DOC - \overline{DOC}\right) \tag{6.1}$$

where $\overline{DOC}$ is the mass of solid organic carbon per unit mass of solids ($M/M\ solids$), α_d is a first-order mass transfer coefficient ($1/T$), $\overline{K_d}$ is a linear distribution coefficient for the layer ($L^3\ water/M\ solids$), and *DOC* is the dissolved organic carbon concentration ($M/L^3\ water$). *Robertson and Cherry* [1995] suggest that a denitrification layer containing 2% by mass of solid organic carbon is appropriate for the typical design life of a domestic septic system and this initial $\overline{DOC}$ concentration is used here. The distribution coefficient and mass transfer coefficient were obtained by using the reactive transport model to generate *DOC* breakthrough curves for a range of residence times in saturated carbon-supplemented layers. The effluent concentrations were then compared with the data of *Robertson and Cherry* [1995]; this calibration process did not include other reactions, such as denitrification, and thus the early time *DOC* data was used as a basis for assessing the coefficients in (6.1). Reasonable agreement with observed *DOC* concentrations is obtained by using $\overline{K_d}$= 50.0 and α_d= 2.0 x 10^{-4} $1/d$ which produce the *DOC* effluent curve in Figure 6.1. It must be emphasized that very little data exist to verify this relationship; however, *Robertson and Cherry* [1995] indicate that *DOC* concentra-

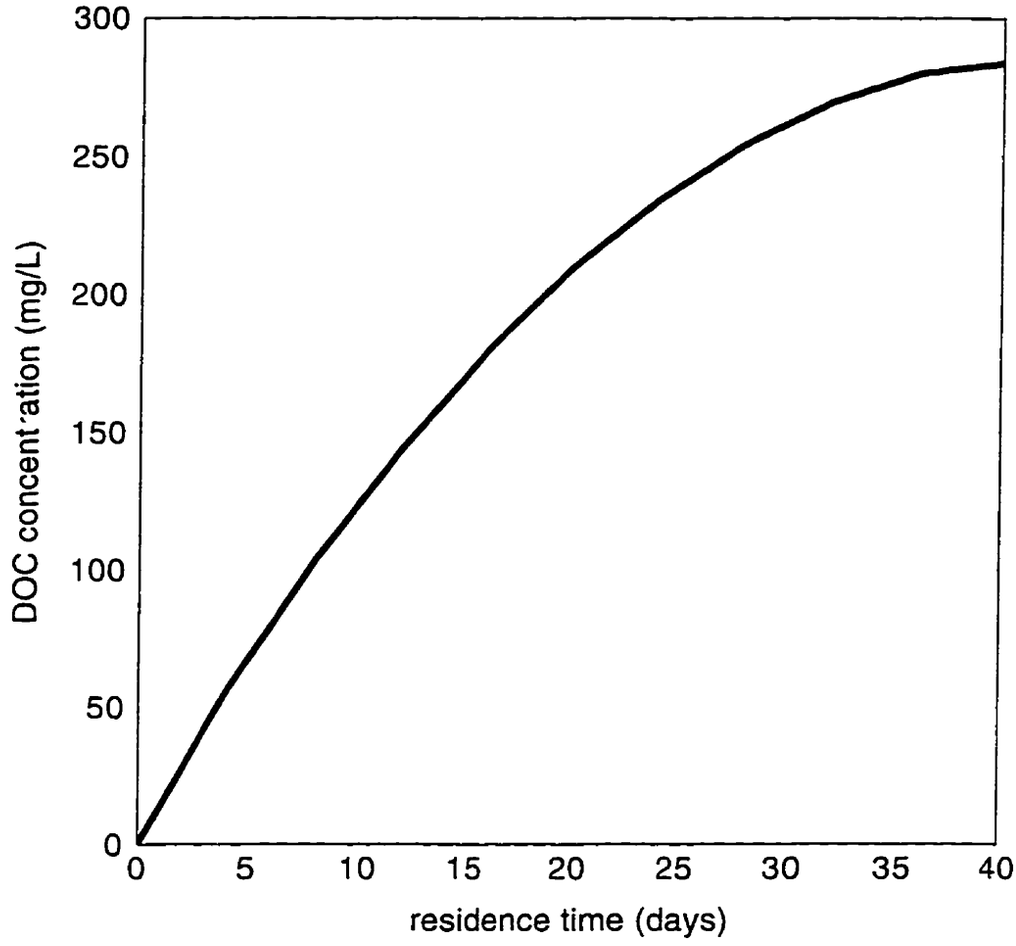

Figure 6.1: Comparison of effluent *DOC* concentration versus residence time in carbon supplemented layer.

tions of 150 mg/L are typical of a layer residence time on the order of 10 to 15 days, and that for a 40 day residence time concentrations will approach 250 mg/L. Further experimental work would be necessary to more accurately formulate the mathematical representation of DOC release from wood waste materials. The DOC leached from the denitrification layer is represented chemically as CH_2O and is assumed to possess the same Monod kinetic parameters as wastewater DOC. Appendix A presents the complete biogeochemical reaction system and associated rate parameters used to simulate the evolution of wastewater species. The addition of (6.1) to this reaction system was straight forward because of the modular structure of the reactive transport model.

6.2 Field Scale Installation above a Shallow Water Table

The first simulation presented is one in which the bottom of a 0.25 m thick denitrification layer is installed 0.5 m above the water table. This configuration is similar to the field trials discussed by *Robertson and Cherry* [1995] and would be typical for areas where the water table is approximately two metres below ground surface. The arrangement allows the wastewater to migrate 0.75 m in the unsaturated zone before reaching the denitrification layer, which previous simulations have shown to be adequate for nitrification of 40 mg/L of ammonium. The fine-grained layer extends horizontally from x= 14.0 m to x= 28 m, with drains spaced at 2.0 m intervals from x= 15.0 m to x= 27.0 m. A minimum drain spacing of 2.0 m is typically required by local septic system regulations. The simulation assumes temporally constant wastewater release from the drains and thus is representative of year-round use of the septic system.

Steady-state flow conditions are reached after 30 days and Figure 6.2 shows several steady-state saturation profiles. The fine-grained zone is at full saturation because the minimum pressure head within the layer is -0.72 m, which is greater than the air-entry pressure in Table 6.1. At this pressure head, the hydraulic conductivity of the fine-grained layer is approximately 150 times greater than that of the surrounding unsaturated sand and all wastewater flow passes through the layer. Saturations in the sand immediately

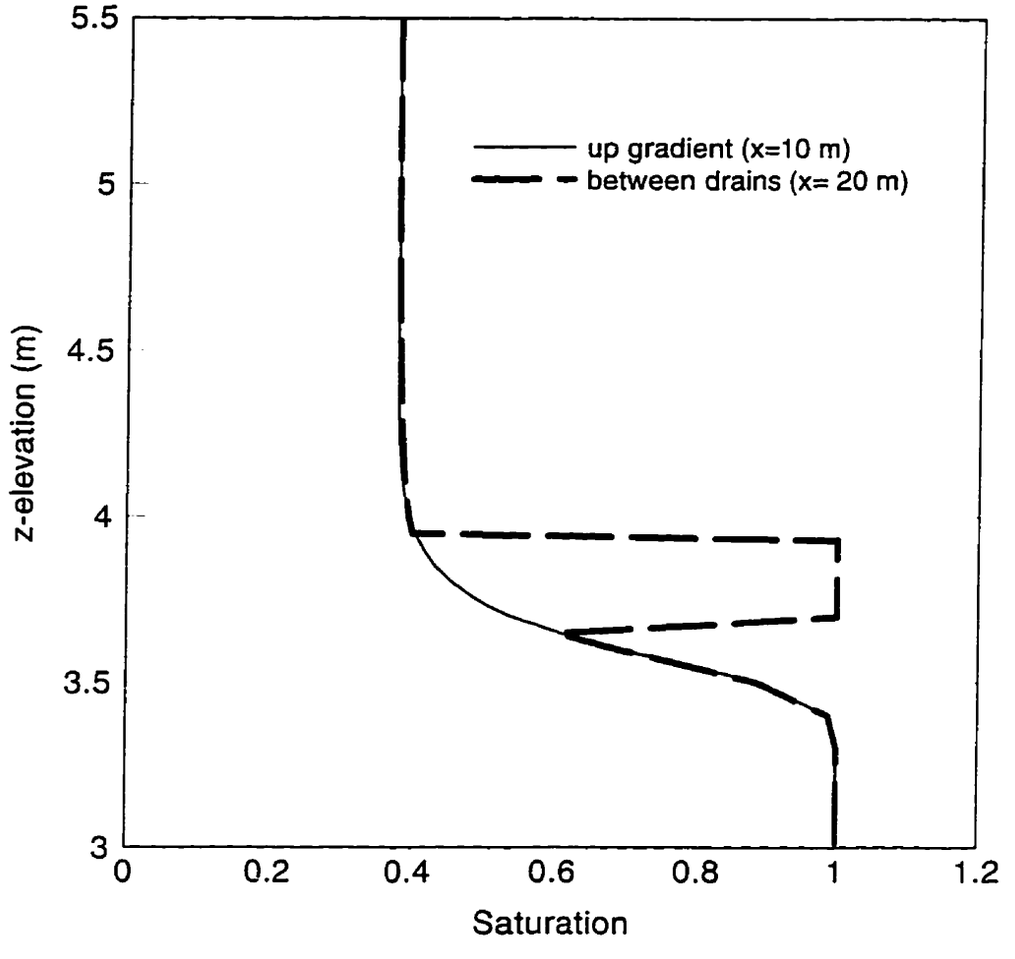

Figure 6.2: Profiles of water saturation with a denitrification layer located between x= 14.0 *m* and x= 28.0 *m*, and z= 3.70 *m* and z= 3.95 *m*.

below the layer are not increased above the up-gradient values; however, saturations are greater than 0.6 and this will restrict atmospheric O_2 diffusion below the layer. Because of the localized release of wastewater above the layer, vertical velocities within the fine-grained zone vary horizontally and range from 0.007 m/d to 0.02 m/d, resulting in residence times of 12.5 to 34 days.

The results obtained for six of the major reactive species are shown in Figures 6.3 and 6.4. The plumes correspond to a simulation time of one year when ammonium and nitrate have essentially reached steady-state distributions. The majority of the ammonium mass released from the drains is oxidized before reaching the fine-grained layer (indicated by the rectangle Figures 6.3 and 6.4); however, concentrations less than 1.0 mg/L are present in the saturated zone. At simulation times less than 60 days, the low nitrifying biomass in the domain causes the nitrification rate to be less than it is at one year and NH_4^+ concentrations of up to 5 mg/L migrate to the water table. Nitrate is abruptly attenuated in the denitrification layer and no $NO_3^- - N$ concentrations in excess of 0.2 mg/L reach the water table. The attenuation is due entirely to heterotrophic denitrification (reaction 3 in Appendix A), as nitrate is not influenced by partitioning or other geochemical processes. Figure 6.4b indicates the localized zones of denitrification in which molecular nitrogen concentrations rise to 19 mg/L, which is about 3 mg/L above the atmospheric equilibrium value. Dissolved N_2 concentrations of up 21 mg/L have been measured in anaerobic wastewater plumes and are considered a key piece of evidence to confirm denitrification [*DeSimone and Howes*, 1996]; however, given the very discrete pockets of elevated N_2 shown in Figure 6.4b it would be difficult to use field measurements of N_2 to confirm denitrification in the present scenario.

Figure 6.3c shows that significant concentrations of *DOC* from the wastewater do not reach the denitrification layer and that concentrations of up to 220 mg/L are generated within the layer. The highest *DOC* concentrations occur between the drain locations where little nitrate is available for denitrification. It is also noted that very little *DOC* is migrating from the edges of the fined-grained zone which indicates that aerobic degradation of *DOC* is occurring around the perimeter of the layer. The migration of *DOC* in the capillary fringe and shallow saturated zone is significantly retarded relative to the low-

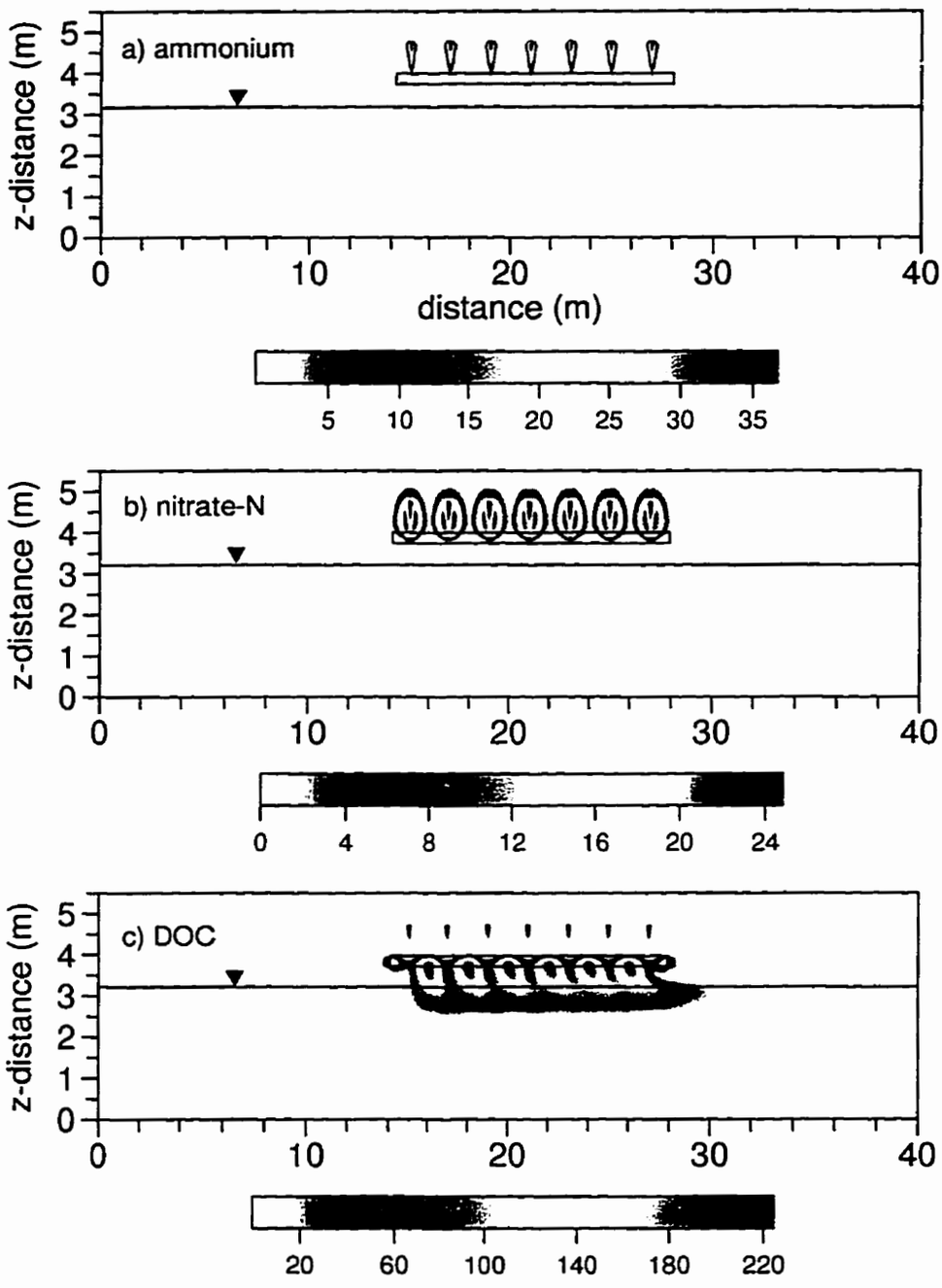

Figure 6.3: Simulated plumes at one year for a horizontal denitrification layer for: a) ammonium, b) nitrate-N, and c) dissolved organic carbon. All concentrations in mg/L.

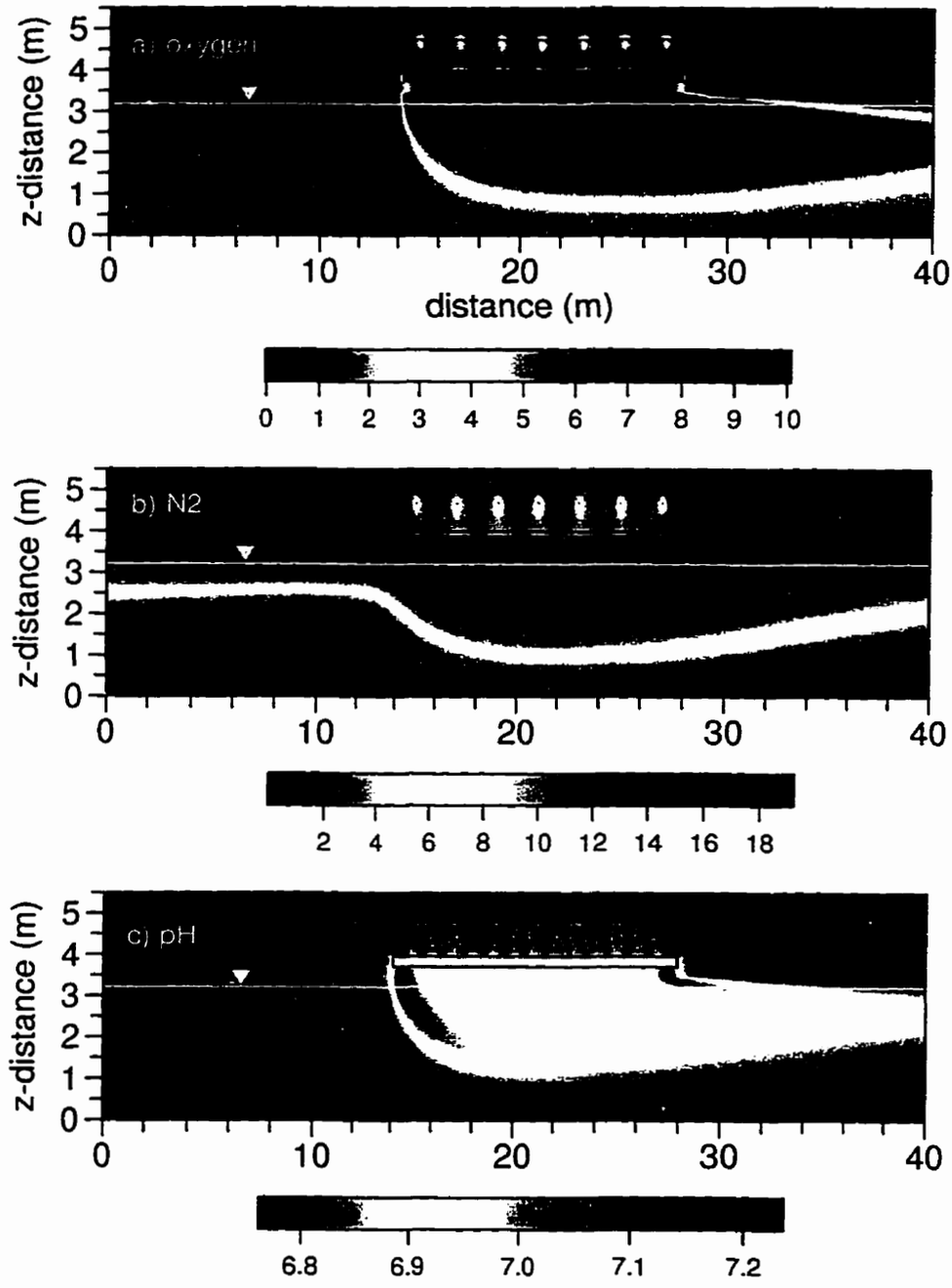

Figure 6.4: Simulated plumes at one year for a horizontal denitrification layer for: a) dissolved oxygen in mg/L, b) molecular nitrogen in mg/L, and c) pH.

O_2 and pH plumes shown in Figure 6.4. The retardation factor for *DOC* in the aquifer material is approximately 6.0 and this is the primary cause of the attenuation of *DOC* observed in Figure 6.3c.

The combination of high *DOC* and low air-filled porosity in the fine-grained layer and underlying sand result in an anaerobic zone within the denitrification layer and in the saturated zone down gradient of the drain field. This low-O_2 plume expands with time due to advection and dispersion. Because dispersion is a relatively weak process in shallow sandy aquifers the anaerobic plume will persist for a significant distance down gradient and thus potentially influence other geochemical processes. For example, the migration of an anoxic plume through an initially aerobic aquifer will promote reductive dissolution of $Fe(III)$- and $Mn(IV)$-bearing minerals [*Appelo and Postma*, 1994], resulting in the release of $Fe(II)$ and $Mn(II)$ and associated adsorbed metals or other contaminants. It is also important to note that the development of a anoxic plume may also lead to enhanced mobility of wastewater-derived phosphorous [*Zanini*, 1996], an important limiting nutrient in many inland water bodies.

Figure 6.4 shows that only a minor pH reduction occurs as the wastewater migrates from the drain field to the water table, with the simulated pH decrease of 0.2 being comparable to the reductions observed by *Robertson and Cherry* [1995]. The zone of decreased pH also correlates with a region of elevated Ca^{2+} concentrations (up to 2.4 x 10^{-3} moles/L). The elevated Ca^{2+} indicates calcite dissolution; however as shown in Chapter 5, the acidity produced by oxidation of the Cambridge wastewater is buffered to a large extent by alkalinity originally present in the wastewater. When the present scenario is modeled using the initial conditions in Table 5.2 and the assumption that no calcite is available for dissolution, the pH of water in and below the denitrification layer is in the range of 6.6 to 6.9 which is a minor decrease relative to the plume pH with calcite dissolution. It should be noted that the denitrification process (reaction 3 in Appendix A) leads to an increase in alkalinity which also assists in buffering pH changes. As shown in Figure 6.5 for the simulation which ignores calcite dissolution, the alkalinity is initially high in the vicinity of the drain (x= 4.70 *m*) and quickly decreases with depth. When the denitrification zone (x= 3.70 *m* to x= 3.95 *m*) is encountered, the alkalinity of the

solution increases and this effectively maintains a constant pH within the denitrification layer. Although *Robertson and Cherry* [1995] did not monitor alkalinity in the detail presented here, *Smith et al.* [1991] present field data from a noncalcarious aquifer which supports the denitrification-related alkalinity increases shown in Figure 6.5.

After one year of use the solid organic carbon concentration within the denitrification layer decreases to a minimum of 1.87% by mass. At this rate of decline the denitrification layer would release *DOC* for 15 years, which is slightly less than the 20 year design life estimated by *Robertson and Cherry* [1995]. The initial $\overline{DOC}$ concentration would have to be increased to approximately 3% by mass to have *DOC* release for 20 years.

The importance of the initial wastewater composition was investigated by increasing the NH_4^+ concentration to 80 mg/L. It has been shown in Chapter 5 that such a change to the Cambridge wastewater chemistry will cause a low-pH plume to develop in an aquifer which is devoid of pH-buffering minerals, such as carbonates or aluminosilicates. As well, the increased N content of the wastewater will result in more NO_3^- being produced which in turn will consume more *DOC* within the denitrification layer. To ensure that nitrification is complete before the wastewater reaches the fine-grained layer, the distance between the drain field and the layer is increased to 1.25 m; however, the distance from the bottom of the denitrification layer to the water table is maintained at 0.5 m. The initial groundwater and wastewater chemistry is again given in Table 5.2, with the exception that NH_4^+ is increased to 80 mg/L. The results for *DOC*, HCO_3^-, and pH are given in Figure 6.6 for a simulation time of 180 days. Ammonium and nitrate results are not shown because, as expected, nitrification and denitrification are complete before the wastewater reaches the water table. Because of the higher nitrogen loading from the drain field, more *DOC* is consumed and the *DOC* concentrations exiting the denitrification zone are reduced to a maximum of 180 mg/L. These amounts are still sufficient, however, to create an anaerobic plume beneath and down gradient of the drain field (not shown). Thus, the increased ammonium content of the wastewater does not alleviate this impact. Figure 6.6c shows that low pH conditions are restricted to the unsaturated zone above the denitrification layer; heterotrophic denitrification within the layer produces enough HCO_3^- to provide significant buffering of the acidity and the pH of water entering the

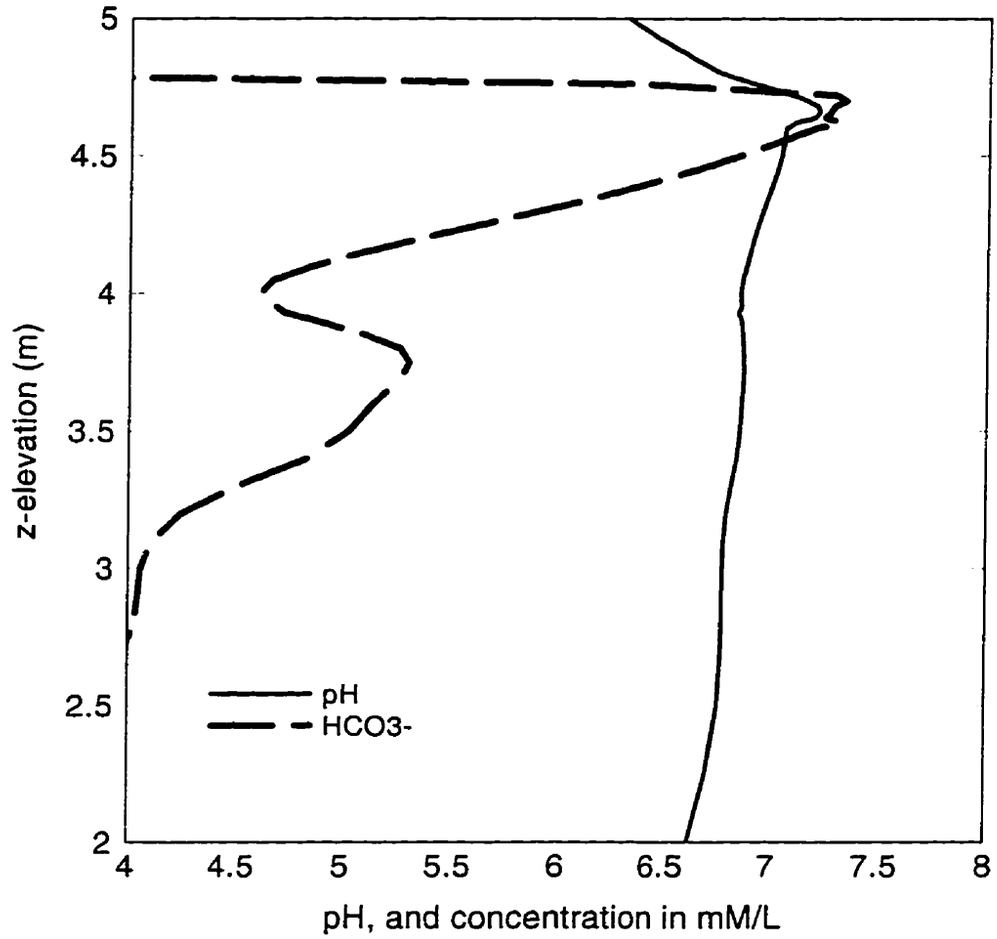

Figure 6.5: Profiles of alkalinity (*i.e.* HCO_3^-) and pH for a simulation which assumes no calcite dissolution. The profiles correspond with the location of a drain and the denitrification layer extends vertically from z= 3.70 *m* to z= 3.95 *m*.

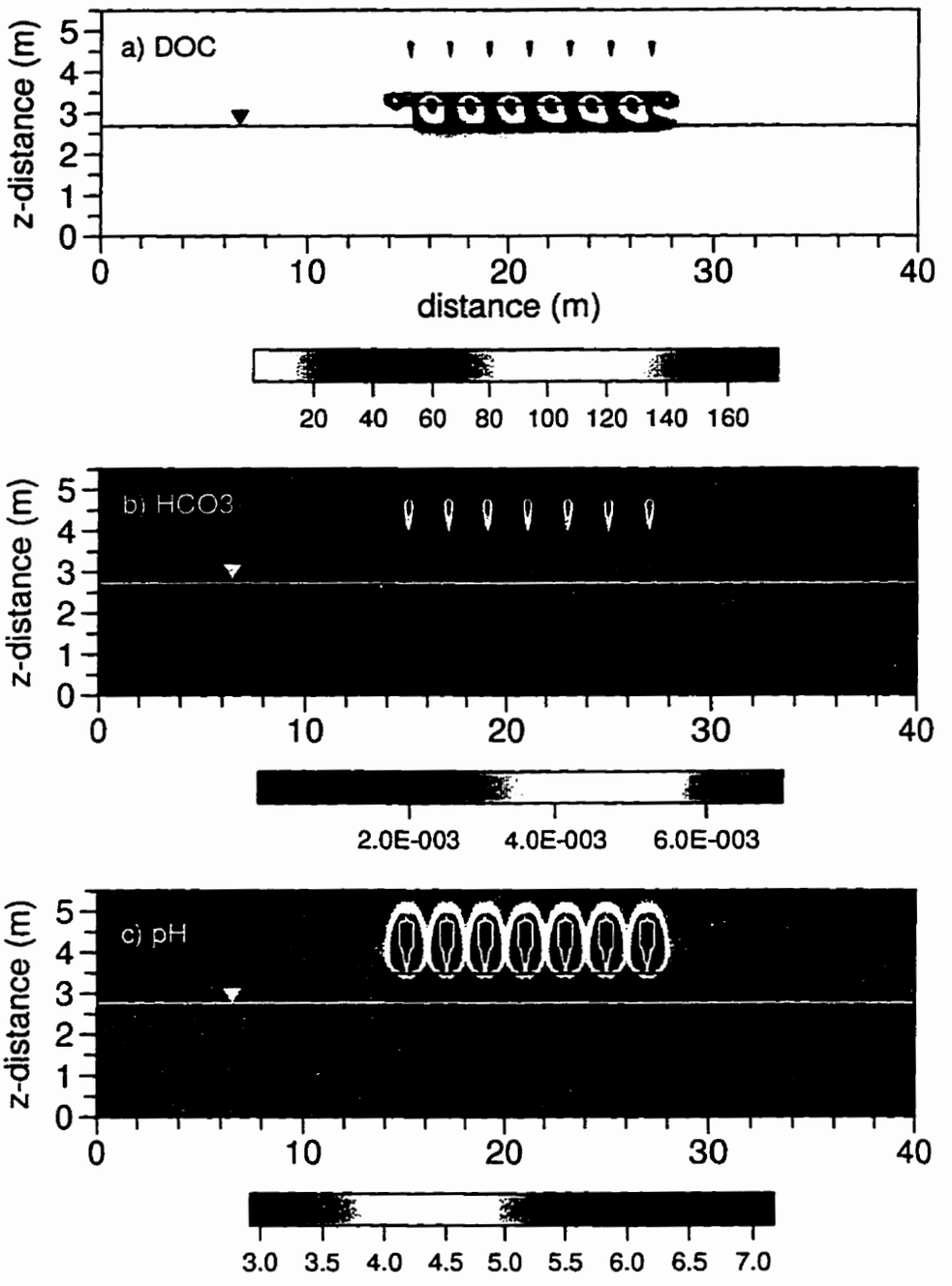

Figure 6.6: Simulated plumes at 180 days for increased ammonium and no calcite for a) dissolved organic carbon in mg/L, b) bicarbonate in moles/L, and c) pH.

aquifer is increased to between 6.0 and 6.5. This finding is in contrast with the results presented in Chapter 5 for a similar simulation without the denitrification zone (Figure 5.10); there it is shown that in the absence of the denitrification layer and any carbonate minerals, water of pH 3.0 to 3.5 migrates down gradient and into the saturated zone. Although the pH in noncalcarious sediments may be buffered by other mineral phases currently not considered in the model and may only decrease to values near 4.5 [*Appelo and Postma*, 1994; *Robertson and Blowes*, 1995], the results in Figure 6.6c clearly show that the denitrification reaction has the ability to raise the pH from even lower values to near neutral ones.

The simulation results indicate, as was also shown by *Robertson and Cherry* [1995], that a fine-grained zone positioned between septic drain fields and the water table will be a viable method to create an anaerobic region above the water table. Because wastewater *DOC* is oxidized prior to reaching the anaerobic zone, it will be necessary to add a *DOC* releasing material to the layer in order to remove nitrate by denitrification. Using the aforementioned kinetic dissolution model to represent *DOC* release from wood chips indicates that enough excess *DOC* may be leached from the denitrification zone to create anaerobic conditions, which may have geochemical implications further down gradient. The concentrations of *DOC* exiting the denitrification layer are predicted to be as high as 220 mg/L after one year. After one year of operation in the field trials of *Robertson and Cherry* [1995] *DOC* concentrations leaving the denitrification layers were less than 86 mg/L. The lower *DOC* concentrations found in the field may be explained, in part, because samples were collected in lysimeters located in the denitrification layer directly below wastewater drains. Careful inspection of Figure 6.3c and Figure 6.6a indicates that the lowest *DOC* concentrations (ranging from 40 to 80 mg/L) occur at the locations directly below the drains. For the 2.0 m drain spacing, approximately six metres of the 14.0 m wide denitrification zone intercepts low-nitrate concentration water and thus much of the *DOC* released from the layer is not consumed by denitrification. Furthermore, because the sand beneath the fine-grained zone is at a high moisture content, diffusion of atmospheric O_2 is limited and aerobic degradation is ineffective at reducing *DOC* concentrations.

6.3 Installation above a Deep Water Table

If the distance between the denitrification layer and the water table is increased it might be expected than much of the excess *DOC* will be consumed by aerobic biodegradation below the denitrification layer. Thus, the formation of an anaerobic plume may not occur in areas with a deep water table. This was investigated by maintaining the water table 1.7 m below the bottom of the fine-grained layer. The original Cambridge wastewater and groundwater chemistry as given in Table 4.2 were used and it was assumed that calcite was present in the aquifer.

Figure 6.7 shows that the fined-grained layer is again at full saturation because the pressure heads within the layer do not fall below the air-entry value. This, combined with the release of *DOC*, creates an anaerobic zone in which nitrate from the wastewater is removed by denitrification. Figure 6.8 shows the distributions of *DOC*, O_2 and pH at a simulation time of one year. Although *DOC* concentrations of up to 210 mg/L are generated within the denitrification layer, the leached *DOC* is aerobically degraded prior to reaching the water table. Thus, given a sufficiently thick unsaturated zone below the denitrification layer, *DOC* will not reach groundwater; however, Figure 6.8b shows that aerobic degradation of the excess *DOC* consumes sufficient oxygen to create anaerobic conditions below the central part of the drain field. The anaerobic zone is smaller than for the shallow water table case presented above and would impact a smaller portion of the down-gradient aquifer. Obviously, whether anaerobic conditions develop below the denitrification zone depends on the *DOC* loading from the layer (in terms of oxygen demand) and the thickness of unsaturated zone. For the present drain field configuration, additional simulations have been performed which show that the distance between the bottom of the fine-grained layer and the water table must be at least 3.7 m in order to obtain minimum dissolved oxygen concentrations of about 4 mg/L at the water table. Such distances will only be available in areas where the water table is approximately five to six metres below ground surface. Because many areas do not have this thickness of unsaturated zone, anaerobic conditions will be a common side effect of such alternative drain field designs.

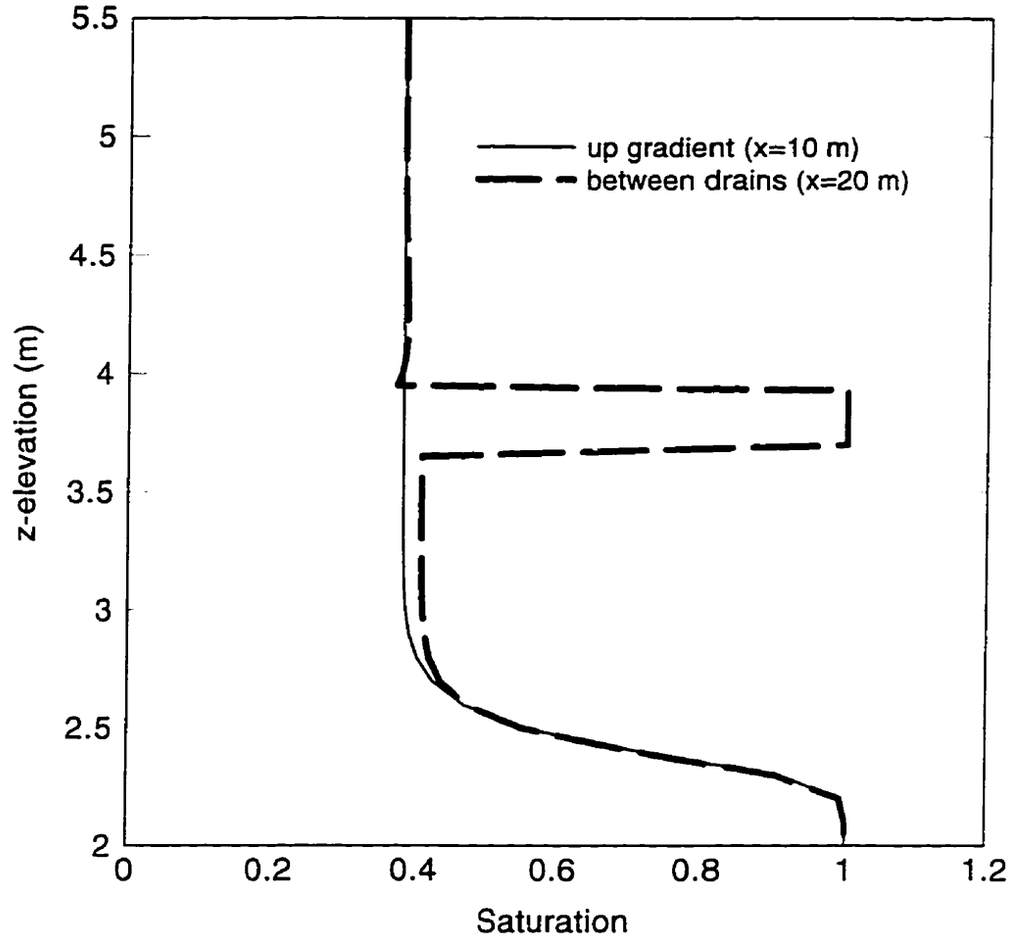

Figure 6.7: Profiles of water saturation for deep water table case with denitrification layer positioned between x= 14.0 *m* and x= 28.0 *m*. The layer extends vertically from z= 3.70 *m* to z= 3.95 *m*.

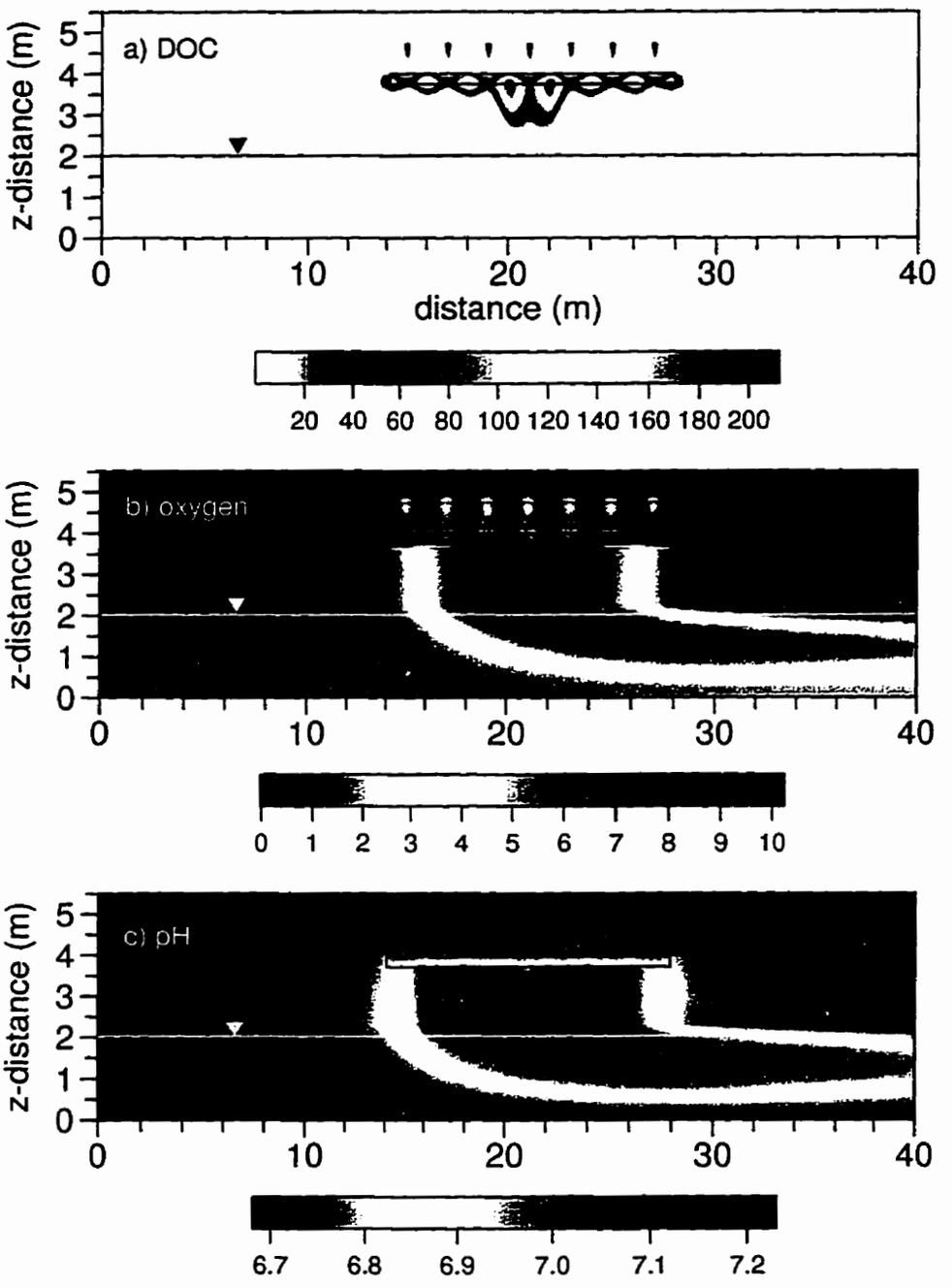

Figure 6.8: Simulated plumes for a deep water table at one year for: a) dissolved organic carbon, b) dissolved oxygen, and c) pH. DOC and oxygen concentrations in mg/L.

The increased amount of *DOC* oxidation in the deeper water table situation results in somewhat increased acid production. Figure 6.8c shows that the pH of the water in the vicinity of the drain field is about 0.2 pH units lower than for the shallower water table case. When the deep water table simulation was repeated with the assumption of no calcite dissolution, it was found that the pH below the drain field fell in the range of 6.3 to 6.7. Thus, it is again found that essentially neutral pH values are maintained in the plume core for sediments with no buffering capacity.

6.4 Influence of Drain Spacing

In the previous simulations it was shown that much of the excess *DOC* from the denitrification layer resulted because areas of the layer did not intercept water containing nitrate. This is related to the narrow width of the ammonium plumes, and associated nitrate plumes, which migrate from the drain field. At a horizontal spacing of 2.0 *m* only about 50% of the fine-grained layer experiences denitrification. To obtain a more uniform distribution of denitrification within the layer, the drain spacing above the layer was reduced to 1.0 *m* and the simulations were repeated for the shallow and deep water table scenarios. The drains are located between x= 17 *m* and x= 23 *m* and the denitrification layer extends from x= 16 *m* to x= 24 *m*. The wastewater flow rate from each drain is the same as in previous simulations.

Figure 6.9 shows the distributions of NH_4^+, NO_3^--N, and *DOC* at a simulation time of one year which can be compared directly with Figure 6.3. Compared to the case of a 2.0 *m* drain spacing, the nitrification rate is reduced and NH_4^+ concentrations of about 5 mg/L occur in the saturated zone below the denitrification layer. The oxygen distribution at one year (not shown) indicates concentrations in the region between the drains and the fine-grained layer are in the range of 2 to 3 mg/L, where previously the concentrations were 4 to 6 mg/L (Figure 6.4). Because the position of the saturated-zone ammonium plume corresponds with the anaerobic plume (results not shown), the ammonium is not oxidized down gradient of the denitrification layer. As found previously, *DOC* from

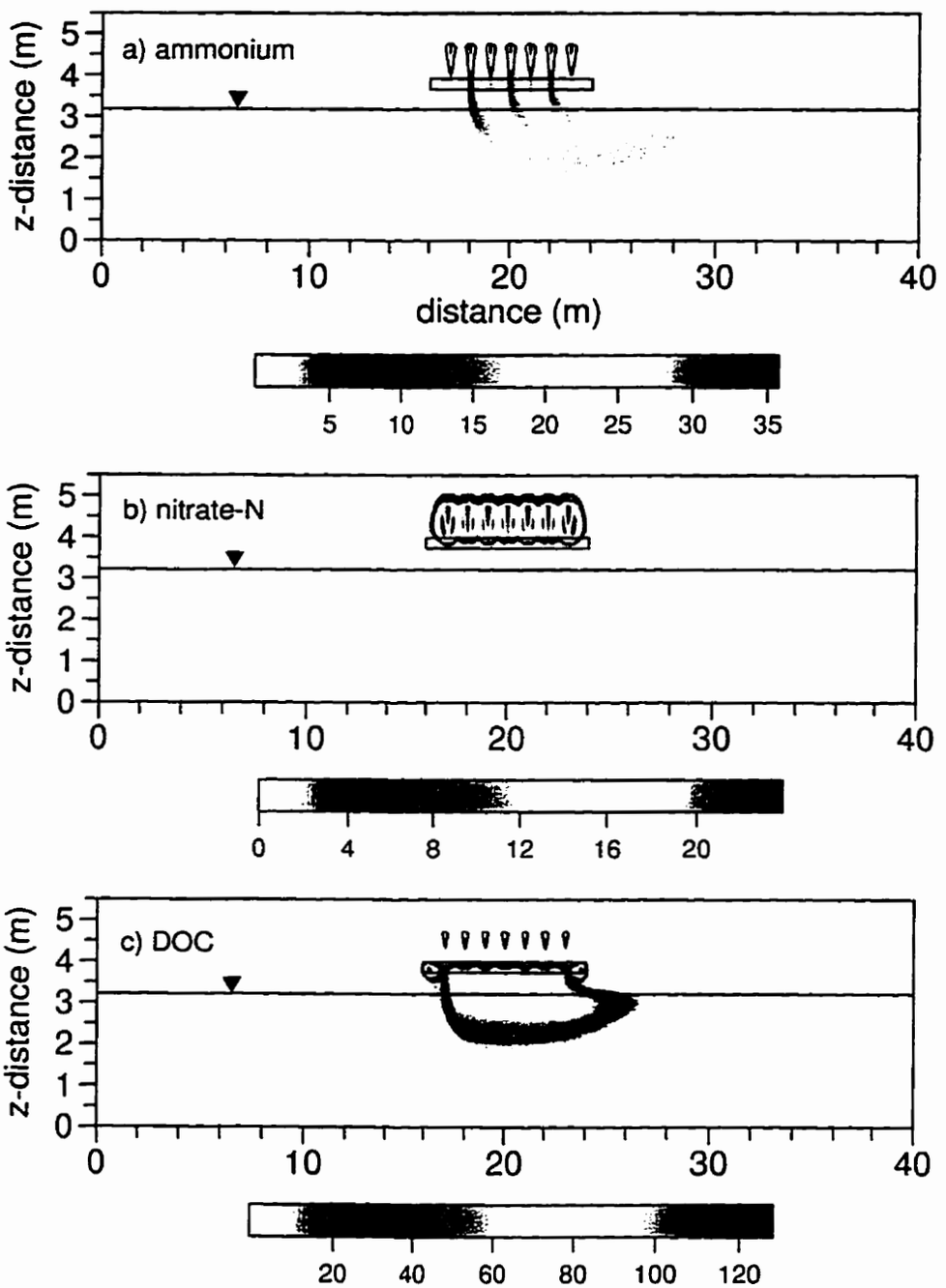

Figure 6.9: Simulated plumes at one year for a shallow water table and a drain spacing of 1.0 metres for: a) ammonium, b) nitrate-N, and c) dissolved organic carbon. All concentrations in mg/L.

the wastewater is completely oxidized and nitrate is again removed by denitrification. Importantly, Figure 6.9c shows that maximum *DOC* concentrations migrating from the layer are reduced to approximately 80 mg/L; however, because the denitrification layer is relatively close to the water table, this amount of *DOC* exceeds the supply of oxygen and an anaerobic plume develops which is similar to the plume shown in Figure 6.4a.

For the deeper water table case the results for *DOC*, dissolved oxygen, and nitrate-N are given in Figure 6.10 which can be compared with the results of Figure 6.8. It is seen that *DOC* migration from the denitrification zone is effectively arrested by aerobic biodegradation below the layer. Because the *DOC* concentrations are not as high as was found for the case of a 2.0 m drain spacing, the oxygen demand is reduced and dissolved oxygen concentrations remain between 4 and 6 mg/L below the denitrification layer. Under these aerobic conditions the ammonium which migrates through the layer is oxidized to nitrate; however, the maximum nitrate-N concentration at the water table is only 1 mg/L. Complete nitrification below the drains could be assured by increasing the distance between the drains and the denitrification layer. Relative to the background chemistry given in Table 4.2, the Ca^{2+} and HCO_3^- concentrations in the plume entering the saturated zone are increased by 5 x 10^{-4} and 4 x 10^{-3} $moles/L$, respectively. The pH of the saturated-zone plume is depressed about 0.4 pH units relative to the background water. These represent relatively small changes in chemistry and suggest that the down-gradient impact of the septic system is likely to be minimal.

For the specific conditions simulated, this final scenario should be considered near optimal from the perspective of minimizing the groundwater quality impacts on the shallow aquifer. The closer drain spacing helps ensure a more uniform nitrate loading to the fined-grained layer and also has the added benefit of requiring less land area and less carbon-supplemented material.

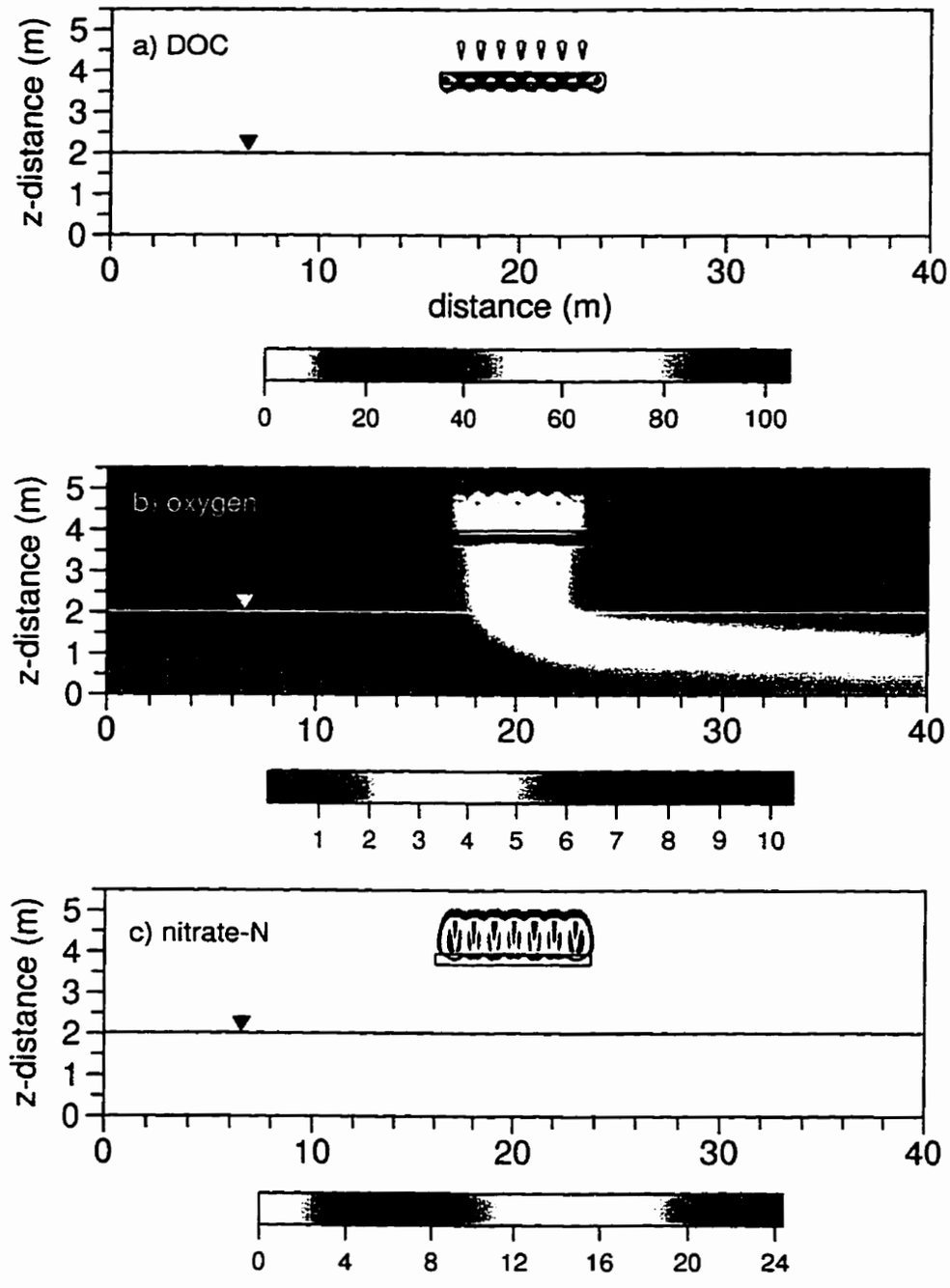

Figure 6.10: Simulated plumes at one year for a deep water table and a drain spacing of 1.0 metres for: a) dissolved organic carbon, b) dissolved oxygen, and c) nitrate-N. All concentrations in mg/L.

Chapter 7

Summary and Conclusions

The objectives of this thesis were to develop and apply a mechanistic flow and reactive transport model which couples the most relevant physical and biochemical processes involved in wastewater plume evolution in shallow aquifers. The model was used to elucidate the behaviour of nitrogen and carbon species in unconfined sands and to study the performance of an alternative septic drain field design. Although release of effluent into the shallow subsurface is one of the most common means of disposing of domestic wastewater, this is the first time multicomponent reactive transport simulations have been performed to investigate the groundwater quality impacts from such systems.

A primary consideration in the development of the model was the use of accurate and efficient numerical methods. Flow in porous media and subsurface drains is coupled using a superposition method which can also be used with other three-dimensional, variably saturated flow simulators which employ Newton linearization. The coupling method was shown to accurately represent flow to or from individual drains, a feature which is important in the present application. Because of the significant computational requirements involved in field-scale simulations of reactive transport, Strang operator splitting was investigated as a solution technique. Based on a series of reactive transport problems involving Monod and first- and second-order kinetic reactions, it is concluded that Strang splitting is both accurate and efficient for simulating the major nitrogen and

carbon species in wastewater. Solution times using Strang splitting are two to four times less than with sequential iterative approaches. An additional advantage of such an operator splitting method is the associated modular structure of the model, which allows for easy modifications to the reactive transport problem. The fully kinetic formulation which is used to solve the reaction system does not require an assumption of chemical equilibrium, and avoids iteration between disconnected equilibrium and kinetic reaction solutions. The kinetic reactions are solved using some well-tested ordinary differential equation solvers; from the investigations performed here it is apparent that implicit solution techniques, such as used in VODE, will be more robust that specialized explicit solvers such as the TWOSTEP algorithm. The implication is that implicit solvers will be required to solve chemical systems involving microbially-mediated and aqueous inorganic reactions, which are common in groundwater reactive transport problems. Even with the use of implicit chemistry solvers however, convergence performance is improved by scaling the reaction rates of the fast reversible reactions. Such scaling of the reaction rates does not affect the computed solution but can reduce the number of Newton iterations required for convergence.

The model was compared with geochemical data collected at a well-studied field site near Cambridge, Ontario. The site has a drain field of 100 m^2 which releases wastewater into a shallow unconfined sandy aquifer. The model was first calibrated to a conservative solute distribution to obtain physical transport parameters, and then used to predict the fate of the major N and C species. A comparison showed very good agreement between the model predictions for major reactive species and the concentrations observed in the shallow saturated zone. For example, NH_4^+ and DOC are completely oxidized in the unsaturated zone which results in increased Ca^{2+} concentrations because of calcium carbonate dissolution. A comparison of field and simulated profiles of NO_3^- along the saturated-zone plume also show very good agreement. The modelling results are also consistent with other field studies of denitrification in nitrogen-enriched sandy aquifers, where denitrification is carbon limited and organic carbon that might support denitrification is consumed by unsaturated zone processes. At the Cambridge site only a small decrease in pH is predicted by the model, which is again consistent with the field obser-

vations. Although the comparison does not constitute a complete model validation, the good agreement between model simulations and field observations is encouraging and it is concluded that the model correctly captures the major processes affecting wastewater-derived nitrogen and carbon.

Using the Cambridge site as a base case, the model was used to examine the sensitivity of the reactive species distributions to several key physical and chemical factors. It was shown that when the distance between the drain field and the water table is reduced to 0.5 m, nitrification is incomplete and that a much smaller $NO_3^- - N$ plume develops. Increasing the wastewater loading rate had a relatively minor effect on the the evolution of reactive species because of the high hydraulic conductivity of the sand aquifer. For a simulation that had no carbonate or other buffering minerals present in the aquifer it was discovered that the pH did not fall to the low values commonly associated with septic plumes in noncalcarious sediments. Only by doubling the ammonium content of the wastewater was it possible to generate plumes with pH in the range of 3 to 4, which illustrates the importance of having knowledge about the wastewater chemistry. By simulating a seasonal loading scenario it was revealed that ammonium sorbed during the loading period was subsequently released and oxidized to nitrate during the resting period. Thus nitrate concentrations above the drinking water limit persisted near the drain field for the entire six month interval following cessation of wastewater loading. It is concluded that the evolution of wastewater plumes in sandy aquifers will depend on many factors, and that the interaction between physical flow and transport and the biogeochemical reactions must be accounted for in order to predict the influence of any of these factors. This has important implications for the current regulation-driven approach for siting and designing onsite wastewater disposal systems. In sensitive areas where nitrate or trace metals may be of concern it is suggested that a more scientific approach, using tools such as the model developed here, should be given consideration.

The model was next used to investigate an alternative septic drain field design which incorporates a denitrification layer supplemented with solid organic carbon in the form of wood chips or sawdust. The layer is shown to be very effective in removing nitrate by heterotrophic denitrification and thus reducing nitrogen loading to shallow aquifers. For

noncalcarious sediments the modelling investigation indicates an additional side effect of such a denitrification layer: the heterotrophic denitrification reaction provides sufficient buffering capacity to prevent the migration of low-pH plumes into the saturated zone. Using the typical regulatory requirement of a 2.0 *m* drain spacing, it is shown that the movement of excess *DOC* from the denitrification layer is significant enough to create anaerobic conditions in aquifers where the water table is less than five to six metres below ground surface. This anaerobic zone will be transported down gradient, and may or may not contain *DOC* depending on the thickness of the unsaturated zone below the denitrification layer. The creation of an anaerobic plume may lead to other geochemical impacts which are not directly assessed in this work. If the drain spacing is reduced to 1.0 *m* then the *DOC* concentrations leached from the layer are significantly reduced and anaerobic conditions do not develop for a water table depth of only 3.5 *m* below ground surface. This alteration to the drain field design would minimize the down gradient impacts of the septic system in areas with a relatively shallow water table.

Several aspects of this work warrant further investigation. Even though the Strang splitting technique is shown to be efficient, it may be possible to improve the performance of the model by investigating two additional numerical techniques. The first is the use of flux-corrected or flux-limited transport algorithms, and the second is the formulation of the reaction system as a combined algebraic-differential equation system. These enhancements may assist in reducing CPU times and thus make simulating fully three-dimensional problems or more complex chemical systems more feasible. One of the more important assumptions in the conceptual model is that oxygen concentrations are always at atmospheric levels at the ground surface and that oxygen is not consumed by root-zone processes. Although field measurements of oxygen in the unsaturated zone at Cambridge support these assumptions, it is noted that in areas with fine-grained soils oxygen diffusion may be restricted during wet periods. Further numerical simulations could be conducted to assess the importance of such transient effects. When modeling the alternative drain field design it was acknowledged that very little is known about the dissolution and nature of *DOC* released from solid organic carbon in the form of wood waste. A better characterization of these factors would allow for more accurate model

predictions and may lead to a carbon source or emplacement method which would not produce *DOC* in excess of that required for denitrification. Finally, the geochemical system within the model could be extended to allow for important oxidation-reduction reactions involving *DOC* and $Fe(III)$- and $Mn(IV)$-bearing minerals, although such an extension would require many additional species and thus would carry with it a significant increase in computational load.

References

Akindunni, F.F., R.W. Gillham and R.V. Nicholson, Numerical simulations to investigate moisture-retention characteristics in the design of oxygen-limiting covers for reactive mine tailings, *Canadian Geotechnical J.*, 28, 446-451, 1991.

Appelo, C.A.J. and D. Postma, *Geochemistry, Groundwater and Pollution*, A.A. Balkema, Rotterdam, 1994.

Aravena, R., M.L. Evans and J.A. Cherry, Stable isotopes of oxygen and nitrogen in source identification of nitrate from septic systems, *Ground Water*, 31(2), 180-186, 1993.

Bae, W. and B.E. Rittmann, A structured model of dual-limitation kinetics, *Biotechnology and Bioengineering*, 49(6), 683-689, 1996.

Baek, N.H., L.S. Clesceri and N.L. Clesceri, Modeling of enhanced biodegradation in unsaturated soil zone, *J. Environmental Engineering*, American Society Civil Engineering, 115(1), 150-172, 1989.

Barry, D.A., C.T. Miller and P.J. Culligan-Hensley, Temporal errors in non-iterative split-operator approaches to solving chemical reaction/groundwater transport models, *J. Contaminant Hydrology*, 22(1/2), 1-17, 1996.

Baveye, P. and A. Valocchi, An evaluation of mathematical models of the transport of biologically reacting solutes in saturated soils and aquifers, *Water Resources Research*, 25(6), 1413-1421, 1989.

Bear, J., *Dynamics of Fluids in Porous Media*, American Elsevier, New York, 1972.

Behnke, J., A summary of the biogeochemistry of nitrogen compounds in ground water, *J. Hydrology*, 27, 155-167, 1975.

Borden, R.C., and P.B. Bedient, Transport of dissolved hydrocarbons influenced by oxygen-limited biodegradation, 1. Theoretical development, *Water Resources Research*, 22(13), 1973-1982, 1986.

Bradley, P.M., M. Fernandez and F.H. Chapelle, Carbon limitation of denitrification rates in an anaerobic groundwater system, *Environmental Science and Technology*, 26(12), 2377-2381, 1992.

Brooks, R.H., and A.T. Corey, Hydraulic properties of porous media, Hydrology Paper No. 3, Colorado State Univ., Fort Collins, Colorado, 1964.

Brown, P.N., G.D. Byrne and A.C. Hindmarsh, VODE, a variable-coefficient ODE solver, *SIAM J. Sci. Stat. Comput.*, 10, 1038-1051, 1989.

Burnett, R.D. and E.O. Frind, Simulation of contaminant transport in three dimensions 2. Dimensionality effects., *Water Resources Research*, 23(4), 695-705, 1987.

Carmichael, P.A., Using wood chips as a source of organic carbon in denitrification: A column experiment and filed study implementing the funnel and gate design, Master of Science thesis, Department of Earth Sciences, University of Waterloo, 1994.

Ceazan, M.L., E.M. Thurman and R.L. Smith, Retardation of ammonium and potassium transport through a contaminated sand and gravel aquifer: The role of cation exchange, *Environmental Science and Technology*, 23(11), 1402-1408, 1989.

Chen, Y.M., L.M. Abriola, P.J.J. Alvarez, P.J. Anid and T.M. Vogel, Modeling transport and biodegradation of benzene and toluene in sandy aquifer material: Comparisons with experimental measurements, *Water Resources Research*, 28(7), 1833-1847, 1992.

Chou, L., R.M. Garrels and R. Wollast, Comparative study of the kinetics and mechanisms of dissolution of carbonate minerals, *Chemical Geology*, 78(2), 269-282, 1989.

Clement, T.P., W.R. Wise and F.J. Molz, A physically based, two-dimensional, finite-difference algorithm for modeling variably saturated flow, *J. Hydrology*, 161, 71-90, 1994.

Cogger, C.G., L.M. Hajjar, C.L. Moe and D. Sobsey, Septic system performance on a coastal barrier island, *J. Environmental Quality*, 17(3), 401-408, 1988.

Colt, J., *Computation of Dissolved Gas Concentrations in Water as Functions of Temperature, Salinity, and Pressure*, American Fisheries Society Publication 14, American Fisheries Society, Bethesda, Maryland, 1984.

Cooley, R.L., Some new procedures for numerical modeling of variably saturated flow problems, *Water Resources Research*, 19(5), 1271-1285, 1983.

Crooks, J.E., Fast and slow proton-transfer reactions in solution, in *Proton-Transfer Reactions*, edited by E. Caldin and V. Gold, Chapman and Hall, London, 153-178, 1975.

DeSimone, L.A., B.L. Howes, Denitrification and nitrogen transport in a coastal aquifer receiving wastewater discharge, *Environmental Science and Technology*, 30(4), 1152-1162, 1996.

Dingman, S.L., *Physical Hydrology*, Macmillian Publishing Company, New York, 1994.

Essaid, H.I., B.A. Bekins, E.M. Godsy, E. Warren, M.J. Baedecker and I.M. Cozzarelli, Simulation of aerobic and anaerobic biodegradation processes at a crude oil spill site, *Water Resources Research*, 31(12), 3309-3327, 1995.

Fipps, G., R.W. Skaggs and J.L. Nieber, Drains as a boundary condition in finite elements, *Water Resources Research*, 22(11), 1613-1621, 1986.

Fipps, G., and R.W. Skaggs, Simple methods for predicting flow to drains, *J. Irrig. Drain. Eng.*, American Society Civil Engineering, 117(6), 881-896, 1991.

Forsyth, P.A., Y.S. Wu and K.Pruess, Robust numerical methods for saturated-unsaturated flow with dry initial conditions in heterogeneous media, *Advances in Water Resources*, 18, 25-38, 1995.

Frind, E.O., W.H.M. Duynisveld, O. Strebel and J. Böttcher, Modeling of multicomponent transport with microbial transformation in groundwater: The Fuhrberg case, *Water Resources Research*, 26(8), 1707-1719, 1990.

Hague, D.N., *Fast Reactions*, Wiley-Interscience, New York, 1971.

Harman, J., W.D. Robertson, J.A. Cherry and L. Zanini, Impacts on a sand aquifer from an old septic system: Nitrate and phosphate, *Ground Water*, 34(6), 1105-1114, 1996.

Harmsen, E.W., J.C. Converse, M.P. Anderson and J.A. Hoopes, A model for evaluating the three-dimensional groundwater dividing pathline between a contaminant source and a partially penetrating water-supply well, *J. Contaminant Hydrology*, 8, 71-90, 1991a.

Harmsen, E.W., J.C. Converse and M.P. Anderson, Application of the Monte Carlo simulation procedure to estimate water-supply well/septic tank-drainfield separation distances in the Central Wisconsin sand plain, *J. Contaminant Hydrology*, 8, 91-109, 1991b.

Harvey, R.W. and M.A. Widdowson, Microbial distributions, activities, and movement in the terrestrial subsurface: Experimental and theoretical studies, in *Interacting Processes in Soil Science*, edited by R.J. Wagenet, P. Baveye, and B.A. Stewart, Lewis Publishers, Boca Raton, Fla., 185-225, 1992.

Henze, M., C.P.L. Grady, W. Gujer, G.V.R. Marais, and T. Matsuo, A general model for single-sludge wastewater treatment systems, *Water Research*, 21(5), 505-515, 1987.

Hindmarsh, A.C., *GEAR: Ordinary differential equation system solver*, Lawrence Livermore National Laboratory Report UCID-30001, December, 1974.

Hindmarsh, A.C. and L.R. Petzold, Algorithms and software for ordinary differential equations, Part II: Higher-order methods and software packages, *Computers in Physics*, 9(2), 148-155, 1995.

Hiscock, K.M., J.W. Lloyd and D.N. Lerner, Review of natural and artificial denitrification of groundwater, *Water Research*, 25(9), 1099-1111, 1991.

Hundsdorfer, W. and J.G. Verwer, A note on splitting errors for advection-reaction equations, *Applied Numerical Mathematics*, 18, 191-200, 1995.

Huyakorn, P.S., S.D. Thomas and B.M. Thompson, Techniques for making finite elements competitive in modeling flow in variably saturated porous media, *Water Resources Research*, 20(8), 1099-1115, 1984.

Huyakorn, P.S., and G.F. Pinder, *Computational Methods in Subsurface Flow*, Academic Press Inc., Orlando, 1983.

Jardine, P.M., F.M. Dunnivant, H.M. Selim and J.F. McCarthy, Comparison of models for describing the transport of dissolved organic carbon in aquifer columns, *Soil Science Society of America J.*, 56, 393-401, 1992.

Jennings, A.A., D.J. Kirkner and T.L. Theis, Multicomponent equilibrium chemistry in groundwater quality models, *Water Resources Research*, 18(40), 1089-1096, 1982.

Kindred, J.S. and M.A. Celia, Contaminant transport and biodegradation 2. Conceptual model and test simulations, *Water Resources Research*, 25(6), 1149-1159, 1989.

Kinzelbach, W., W. Schafer and J. Herzer, Numerical modeling of natural and enhanced denitrification processes in aquifers, *Water Resources Research*, 27(6), 1123-1135, 1991.

Kirkham, D., Flow of ponded water into drain tubes in soil overlying an impervious layer, *EOS Trans. American Geophysical Union*, 30(3), 369-385, 1949.

Korom, S.F., Natural denitrification in the saturated zone: A review, *Water Resources Research*, 28(6), 1657-1668, 1992.

Lacombe, S., E.A. Sudicky, S.K. Frape and A.J.A. Unger, Influence of leaky boreholes on cross-formational groundwater flow and contaminant transport, *Water Resources Research*, 31(8), 1871-1882, 1995.

Lapointe, B.E. and M.W. Clark, Nutrient inputs from the watershed and coastal eutrophication in the Flordia keys, *Estuaries*, 15(4), 465-476, 1992.

Lasaga, A.C., Rate laws of chemical reactions, Chapter 1 in *Kinetics of Geochemical Processes*, edited by A.C. Lasage and R.J. Kirkpatrick, Reviews in Mineralogy Series. Mineralogical Society of America, Vol. 8, 135-169, 1981.

Leggett, D.C. and I.K. Iskandar, Evaluation of a nitrification model, in *Modeling Wastewater Renovation: Land Treatment*, edited by I.K. Iskandar, John Wiley & Sons, New York, 313-358, 1981.

Lensing, H.J., M. Vogt and B. Herrling, Modeling of biologically mediated redox processes in the subsurface, *J. Hydrology*, 159, 125-143, 1994.

MacQuarrie, K.T.B. and E.A. Sudicky, On the incorporation of drains into three-dimensional variably saturated groundwater flow models, *Water Resources Research*, 32(2), 477-482, 1996.

MacQuarrie, K.T.B., E.A. Sudicky and E.O. Frind, Simulation of biodegradable organic contaminants in groundwater 1. Numerical formulation in principal directions, *Water Resources Research*, 26(2), 207-222, 1990.

MacQuarrie, K.T.B. and E.A. Sudicky, Simulation of biodegradable organic contaminants in groundwater 2. Plume behavior in uniform and random flow fields, *Water Resources Research*, 26(2), 223-239, 1990.

Magdoff, F.R., J. Bouma and D.R. Keeney, Columns representing mound-type disposal system for septic tank effluent 1. Soil-water and gas relations, *J. Environmental Quality*, 3(3), 223-234, 1974.

Marzal, P., A. Seco, J. Ferrer and C. Gabaldón. Modeling multiple reactive solute transport with adsorption under equilibrium and nonequilibrium conditions. *Advances in Water Resources*, 17, 363-374, 1995.

Massmann, J., and D.F. Farrier, Effects of atmospheric pressures on gas transport in the vadose zone, *Water Resources Research*, 28(3), 777-791, 1992.

Miller, C.T., and A.J. Rabideau, Development of split-operator, Petrov-Galerkin methods to simulate transport and diffusion problems, *Water Resources Research*, 29(7), 2227-2240, 1993.

Millington, R.J. and J.P. Quirk, Permeability of porous solids, *Trans. Faraday Society*, 15, 1200-1207, 1961.

Molz, F.J., M.A. Widdowson and L.D. Benefield, Simulation of microbial growth dynamics coupled to nutrient and oxygen transport in porous media, *Water Resources Research*, 22(8), 1207-1216, 1986.

Morshed, J. and J.J. Kaluarachchi, Critical assessment of the operator-splitting technique in solving the advection-dispersion-reaction equation: 2. Monod kinetics and coupled transport, *Advances in Water Resources*, 18(2), 101-110, 1995.

Neuman, S.P., Saturated-unsaturated seepage by finite elements, *J. Hydraulics Division*, American Society Civil Engineering, 99(12), 2233-2252, 1973.

Nordstrom, D.K., L.N. Plummer, D. Langmuir, E. Busenberg, H.M. May, B.F. Jones, and D.L. Parkhurst, Revised chemical equilibrium data for major water-mineral reactions and their limitations, Chapter 31 in *Chemical Modeling of Aqueous Systems II*, edited by D.C. Melchior and R.L. Bassett, American Chemical Society, 398-413, 1990.

Odencrantz, J.E., Modeling the biodegradation kinetics of dissolved organic contaminants in a heterogeneous two-dimensional aquifer, PhD thesis, Department of Civil Engineering, University of Illinois, Urbana, Illinois, 1992.

Panday, S., P.S. Huyakorn, R. Therrien and R.L. Nichols, Improved three-dimensional finite-element techniques for field simulation of variably saturated flow and transport, *J. Contaminant Hydrology*, 12, 3-33, 1993.

Postma, D., C. Boesen, H. Kristiansen and F. Larsen, Nitrate reduction in an unconfined sandy aquifer: Water chemistry, reduction processes, and geochemical modeling, *Water Resources Research*, 27(8), 2027-2045, 1991.

Postma, F.B., A.G. Gold and G.W. Loomis, Nutrient and microbial movement from seasonally-used septic systems, *J. Environmental Health*, 55, 5-10, 1992.

Reed, R.C., J.M. Prausnitz and T.K. Sherwood, *The Properties of Gases and Liquids*, Third Edition, McGraw-Hill Book Company, New York, 1977.

Regnier, P., R. Wollast and C.I. Steefel, Long-term fluxes of reactive species in macrotidal estuaries: Estimates from a fully transient, multicomponent reaction-transport model, *Marine Chemistry*, in press.

Reneau, R.B., C. Hagedorn and M.J. Degen, Fate and transport of biological and inorganic contaminants from on-site disposal of domestic wastewater, *J. Environmental Quality*, 18(2), 135-144, 1989.

Robertson, W.D. and D.W. Blowes, Major ion and trace metal geochemistry of an acidic septic-system plume in silt, *Ground Water*, 33(2), 275-283, 1995.

Robertson, W.D. and J.A. Cherry, Hydrogeology of an unconfined sand aquifer and its effect on the behavior of nitrogen from a large-flux septic system, *Applied Hydrogeology*, 1, 32-44, 1992.

Robertson, W.D. and J.A. Cherry, In situ denitrification of septic-system nitrate using reactive porous media barriers: Field trials, *Ground Water*, 33(1), 99-111, 1995.

Robertson, W.D., J.A. Cherry and E.A. Sudicky, Ground-water contamination from two small septic systems on sand aquifers, *Ground Water*, 29(1), 82-92, 1991.

Stan
C
siu
W. K

Rouhi, A. and J. Wright, A new operator splitting method for the numerical solution of partial differential equations, *Computer Physics Communications*, 18, 18-28, 1995.

Saad, Y. and M.H. Schultz, GMRES: A generalized minimal residual algorithm for solving nonsymmetric linear systems, *SIAM J. Sci. Stat. Comput.*, 7, 856-869, 1986.

Sandu, A., J.G. Verwer, M. van Loon, G.R. Carmichael, F.A. Potra, D. Dabdub and J.H. Seinfeld, Benchmarking stiff ODE solvers for atmospheric chemistry problems I: Implicit versus explicit, *Atmospheric Environment*, in press.

Sawyer, C.N. and P.L. McCarty, *Chemistry for Environmental Engineering*, Third Edition, McGraw-Hill Book Company, New York, 1978.

Shackelford, C.D. and D.E. Daniel, Diffusion in saturated soil, I: Background, *J. Geotechnical Engineering*, American Society Civil Engineering, 117(3), 467-483.

Shutter, S.B., E.A. Sudicky and W.D. Robertson, Chemical fate and transport in a domestic septic system: Application of a variably saturated model for chemical movement, *Environmental Toxicology and Chemistry*, 13(2), 223-231, 1994.

Smith, R.E., B.L. Howes and J.H. Duff, Denitrification in nitrate-contaminated groundwater: Occurrence in steep vertical geochemical profiles, *Geochimica et Cosmochimica Acta*, 55, 1815-1825, 1991.

Smithson, A.B., A prescription for performance-based codes, *Small Flows*, 9(4), 12-13, 1995.

Solomon, D.K. and T.E. Cerling, The annual carbon dioxide cycle in a montane soil: Observations, modeling, and implications for weathering, *Water Resources Research*, 23(12), 2257-2265, 1987.

Starr, R.C. and R.W. Gillham, Controls on denitrification in shallow unconfined aquifers, Contaminant Transport in Groundwater - Proceedings of the International Symposium on Contaminant Transport in Groundwater, Stuttgart, edited by H.E. Kobus and W. Kinzelbach, 51-56, 1989.

Steefel, C.I. and A.C. Lasaga, A coupled model for transport of multiple chemical species and kinetic precipitation/dissolution reactions with application to reactive flow in single phase hydrothermal systems, *American Journal of Science*, 294, 529-592, 1994.

Steefel, C.I. and K.T.B. MacQuarrie, Approaches to modeling of reactive transport in porous media, Chapter 2 in *Reactive Transport in Porous Media*, edited by P.C. Lichtner, C.I. Steefel, and E.H. Oelkers, Reviews in Mineralogy Series, Mineralogical Society of America, Vol. 34, 83-129, 1996.

Stone, A.T. and J.J. Morgan, Kinetics of chemical transformations in the environment, Chapter 1 in *Aquatic Chemical Kinetics*, edited by W. Stumm, John Wiley & Sons, New York, 1-42, 1990.

Strang, G., On the construction and comparison of difference schemes, *SIAM J. Numer. Anal.*, 5(3), 506-517, 1968.

Stumm, W. and J.J. Morgan, *Aquatic Chemistry*, John Wiley & Sons, Inc., New York, 1981.

Taylor, G., Dispersion of solute matter in solvent flowing slowly through a tube, *Proc. Royal Society of London*, 219, 186-203, 1953.

Therrien, R., and E.A. Sudicky, Three-dimensional analysis of variably-saturated flow and transport in discretely-fractured porous media, *J. Contaminant Hydrology*, 23, 1-44, 1996.

United States Bureau of the Census, *1990 Census of Housing: Detailed Housing Characteristics*, Housing and Economic Statistics Division, Bureau of the Census, Washington, D.C., 1993.

United States Environmental Protection Agency, *Septic Systems and Groundwater Protection: A Program Manager's Guide and Reference Book*, Office of Groundwater Protection, Washington, D.C., 1986.

Valiela, I., K. Foreman, M. LaMontagne, D. Hersh and J. Costa, Couplings of watersheds and coastal waters: Sources and consequences of nutrient enrichment in Waquoit Bay, Massachusetts, *Estuaries*, 15(4), 443-457, 1992.

Valiela, I., G. Collins, J. Kremer, K. Lajtha, M. Geist, B. Seely, J. Brawley and C.H. Sham, Nitrogen loading from coastal watersheds to receiving estuaries: New method and application, *Ecological Applications*, 7(2), 358-380, 1997.

Valocchi, A.J., R.L. Street and P.V. Roberts, Transport of ion-exchanging solutes in groundwater: Chromatographic theory and field simulations, *Water Resources Research*, 17(5), 1517-1527, 1981.

Valocchi, A.J. and M. Malmstead, Accuracy of operator splitting for advection-dispersion-reaction problems, *Water Resources Research*, 28(5), 1471-1476, 1992.

VanderKwaak, J.E., P.A. Forsyth, K.T.B. MacQuarrie and E.A. Sudicky, WATSOLV sparse matrix iterative solver package; User's guide, Version 1.01, Waterloo Centre for Groundwater Research, University of Waterloo, Waterloo, Ontario, 23 p., 1995.

van der Vorst, H., Bi-CGSTAB: a fast and smoothly converging variant of Bi-CG for the solution of nonsymmetric linear systems, *SIAM J. Sci. Stat. Comput.*, 13, 631-64, 1992.

Vandevivere, P. and P. Baveye, Saturated hydraulic conductivity reduction caused by aerobic bacteria in sand columns, *Soil Science Society of America J.*, 56(1), 1-13, 1992.

van Genuchten, M.Th., A closed-form equation for predicting the hydraulic conductivity of unsaturated soils, *Soil Science Society of America J.*, 44, 892-898, 1980.

Verwer, J.G., Gauss-Seidel iteration for stiff ODEs from chemical kinetics, *SIAM J. Sci. Comput.*, 15(5), 1243-1250, 1994.

Vinsome, P.K.W., ORTHOMIN: An iterative method for solving sparse banded sets of simultaneous linear equations, paper SPE 5729 presented at the Fourth SPE Symposium on Numerical Simulation of Reservoir Performance, Los Angeles, Feb. 19-20, 149-159, 1976.

Viraraghavan, T. and R.G. Warnock, Groundwater pollution from a septic tile field, *Water, Air and Soil Pollution*, 5, 281-287, 1976.

Washington, J.W., A.W. Rose, E.J. Ciolkosz and R.R. Dobos, Gaseous diffusion and permeability in four soil profiles in central Pennsylvania, *Soil Science*, 157(2), 65-76, 1994.

Waterloo Maple Software, *Maple V*, Release 3.0, Waterloo Maple Software, Waterloo, Ontario, 1994.

Weiskel, P.K. and B.L. Howes, Differential transport of sewage-derived nitrogen and phosphorus through a coastal watershed, *Environmental Science and Technology*, 26(2), 352-360, 1992.

Whelan, B.R., Disposal of septic tank effluent in calcareous sands, *J. Environmental Quality*, 17(2), 272-277, 1988.

Whelan, B.R. and Z.V. Titamnis, Daily chemical variability of domestic septic tank effluent, *Water, Air, and Soil Pollution*, 17, 131-139, 1982.

Widdowson, M.A., F.J. Molz and L.D. Benefield, A numerical transport model for oxygen- and nitrate-based respiration linked to substrate and nutrient availability in porous media, *Water Resources Research*, 24(9), 1553-1565, 1988.

Wilhelm, S.R., S.L. Schiff and W.D. Robertson, Chemical fate and transport in a domestic septic system: Unsaturated and saturated zone geochemistry, *Environmental Toxicology and Chemistry*, 13(2), 193-203, 1994a.

Wilhelm, S.R., S.L. Schiff and J.A. Cherry, Biogeochemical evolution of domestic waste water in septic systems 1. Conceptual model, *Ground Water*, 32(6), 905-916, 1994b.

Wilhelm, S.R., S.L. Schiff and W.D. Robertson, Biogeochemical evolution of domestic waste water in septic systems 2. Application of conceptual model in sandy aquifers, *Ground Water*, 34(5), 853-864, 1996.

Wood, B.D., C.N. Dawson, J.E. Szecsody and G.P. Streile, Modeling contaminant transport and biodegradation in a layered porous media system, *Water Resources Research*, 30(6), 1833-1845, 1994.

Yeh, G.T. and V.S. Tripathi, A critical evaluation of recent developments in hydrogeochemical transport models of reactive multichemical components, *Water Resources Research*, 25(1), 93-108, 1989.

Zanini, L., Phosphorous characterization in sediments under four septic systems in Ontario, Master of Science thesis, Department of Earth Sciences, University of Waterloo, 1996.

Zysset, A., F. Stauffer and T. Dracos, Modeling of chemically reactive groundwater transport, *Water Resources Research*, 30(7), 2217-2228, 1994.

Zysset, A. and F. Stauffer, Modeling of microbial processes in groundwater infiltration systems, in *Mathematical Modeling in Water Resources*, Vol. 2, edited by T.F. Russell, R.E. Ewing, C.A. Brebbia, W.G. Gray, and G.F. Pinder, Computational Mechanics Publications, Southhampton, 325-332, 1992.

Appendix A

Reaction Stoichiometry and Rate Expressions for Field Scale Simulations

The various species in the biogeochemical model are related to each other by the following stoichiometric relationships:

$$R_1 : CH_2O + O_{2(aq)} \rightarrow CO_{2(aq)} + H_2O$$

$$R_2 : NH_4^+ + 2O_{2(aq)} \rightarrow NO_3^- + 2H^+ + H_2O$$

$$R_3 : CH_2O + \frac{4}{5}NO_3^- \rightarrow \frac{2}{5}N_2 + \frac{4}{5}HCO_3^- + \frac{1}{5}CO_{2(aq)} + \frac{3}{5}H_2O$$

$$R_4 : CO_{2(aq)} + H_2O \rightleftharpoons HCO_3^- + H^+$$

$$R_5 : CO_{2(aq)} + OH^- \rightleftharpoons HCO_3^-$$

$$R_6 : CO_3^{2-} + H_2O \rightleftharpoons OH^- + HCO_3^-$$

$$R_7 : H_2O \rightleftharpoons OH^- + H^+$$

$$R_8 : CaCO_3 + H^+ \rightleftharpoons HCO_3^- + Ca^{2+}$$

$$R_9 : CaCO_3 + H_2O + CO_{2(aq)} \rightleftharpoons 2HCO_3^- + Ca^{2+}$$

$$R_{10} : CaCO_3 \rightleftharpoons CO_3^{2-} + Ca^{2+}$$

Reactions R_1 to R_{10} are described by the following kinetic expressions:

$$
\begin{aligned}
R_1 &= k_{max}^{ox} X_2 F(X_2) \left[\frac{CH_2O}{CH_2O + K_{CH_2O}}\right] \left[\frac{O_2}{O_2 + K_{O_2}}\right] \\
R_2 &= k_{max}^{nit} X_1 F(X_1) \left[\frac{NH_4}{NH_4 + K_{NH_4}}\right] \left[\frac{O_2}{O_2 + K_{O_2}}\right] \\
R_3 &= k_{max}^{denit} X_2 F(X_2) \left[\frac{CH_2O}{CH_2O + K_{CH_2O}}\right] \left[\frac{NO_3}{NO_3 + K_{NO_3}}\right] \left[\frac{K_{O_2 I}}{O_2 + K_{O_2 I}}\right] \\
R_4^f &= k_{CO_2}^f (CO_{2_{aq}}) \\
R_4^b &= k_{CO_2}^b (HCO_3)(H) \\
R_5^f &= k_H^f (CO_{2_{aq}})(OH) \\
R_5^b &= k_H^b (HCO_3) \\
R_6^f &= k_{HCO_3}^f (CO_3) \\
R_6^b &= k_{HCO_3}^b (HCO_3)(OH) \\
R_7^f &= k_{H_2O}^f \\
R_7^b &= k_{H_2O}^b (OH)(H) \\
R_8^f &= A_{cc} k_1^f (H) \\
R_8^b &= A_{cc} k_1^b (HCO_3)(Ca) \\
R_9^f &= A_{cc} k_2^f (CO_2) \\
R_9^b &= A_{cc} k_2^b (HCO_3)^2 (Ca) \\
R_{10}^f &= A_{cc} k_3^f \\
R_{10}^b &= A_{cc} k_3^b (CO_3)(Ca)
\end{aligned}
$$

where the superscripts *ox*, *nit*, and *denit* indicate organic carbon oxidation, nitrification, and denitrification, respectively. The superscripts f and b indicate forward and backward rates, respectively, and A_{cc} is the reactive mineral surface area per unit volume of porous medium. The nitrifying biomass concentration is X_1, while X_2 is the heterotrophic biomass concentration.

The equations describing the rate of change of the biomass populations are:

$$\frac{dX_1}{dt} = R_2 Y_1 - X_1 k_1{}^d$$

$$\frac{dX_2}{dt} = [R_1 + R_3]\, Y_2 - X_2\, k_2{}^d$$

where it has been assumed that the heterotrophic yield coefficient is the same for organic carbon oxidation and denitrification [*Henze et al.*,1987; *Kinzelbach et al.*, 1991]. The biomass growth inhibition functions are:

$$F(X_1) = \frac{K_{b_1}}{K_{b_1} + X_1}$$

$$F(X_2) = \frac{K_{b_2}}{K_{b_2} + X_2}$$

The parameter values used for simulations at 12°C are given in Table A.1. Values for most parameters have been taken from the wastewater treatment or groundwater modelling literature. The microbial decay rates have been assumed to be zero because the rates for oligotrophic aquifers are very low [*Harvey and Widdowson*, 1992], and because the initial biomass concentrations were chosen to represent background conditions. Thus, setting the microbial decay rates to zero ensures that biomass concentrations do not go below background values. This assumption is supported by the results of several studies in which Monod-kinetic models have been compared to field data [*MacQuarrie and Sudicky*, 1990; *Essaid et al.*, 1995]. Values for the microbial inhibition constants, K_{b_m}, have been selected such that the biomass concentrations do not increase to levels which would cause significant reductions in the saturated hydraulic conductivity. *Vandevivere and Baveye* [1992] have shown that in medium to fine sands, the hydraulic conductivity begins to decrease as aerobic biomass density reaches approximately 4000 *mg/L* of porous medium. The biomass inhibition constants used here are also similar in magnitude to those obtained by *Essaid et al.* [1995] during model calibration to field data from a crude oil spill site.

Table A.1: Kinetic and partitioning parameter values used for field scale simulations.

Parameter	Value	Reference(s)
k_{max}^{ox}	10.0 $1/day$	*Henze et al.* [1987], *Baek et al.* [1989], *Kinzelbach et al.* [1991]
k_{max}^{nit}	1.0 $1/day$	regression equation of *Leggett and Iskandar* [1981]
k_{max}^{denit}	10.0 $1/day$	*Henze et al.* [1987], *Kinzelbach et al.* [1991]
K_{CH_2O}	10.0 mg/L	*Henze et al.* [1987], *Kinzelbach et al.* [1991]
K_{O_2}	0.1 mg/L	*Leggett and Iskandar* [1981], *Henze et al.* [1987]
K_{NH_4}	0.1 mg/L	regression equation of *Leggett and Iskandar* [1981]
K_{NO_3}	0.5 mg/L	*Henze et al.* [1987], *Kinzelbach et al.* [1991]
$K_{O_2 I}$	1.0 mg/L	assumed value
$K_{d_{CH_2O}}$	1.5 cm^3/g	*Jardine et al.* [1992]
$K_{d_{NH_4}}$	0.34 cm^3/g	*Ceazan et al.* [1989]
H_{O_2}	28.2	*Colt* [1984]
H_{N_2}	56.6	*Colt* [1984]
H_{CO_2}	0.95	*Colt* [1984]
Y_1	0.17	*Henze et al.* [1987]
k_1^d	0.0 $1/day$	assumed value
K_{b_1}	1.0 mg/L	assumed value
Y_2	0.5	*Henze et al.* [1987], *Baek et al.* [1989], *Kinzelbach et al.* [1991]
k_2^d	0.0 $1/day$	assumed value
K_{b_2}	0.5 mg/L	assumed value

Table A.1: continued on next page

Table A.1: (continued)

Parameter	Value	Reference(s)
$k^f_{CO_2}$	2592.0 $1/day$	*Stumm and Morgan* [1981]
$k^b_{CO_2}$	$6.818\text{x}10^9$ $1/(M \cdot day)$	computed using equilibrium data of *Nordstrom et al.* [1990]
k^f_H	$7.344\text{x}10^8$ $1/(M \cdot day)$	*Stumm and Morgan* [1981]
k^b_H	8.63 $1/day$	computed using equilibrium data of *Nordstrom et al.* [1990]
$k^f_{HCO_3}$	$1.11\text{x}10^{11}$ $1/day$	*Hague* [1971]
$k^b_{HCO_3}$	$9.22\text{x}10^{14}$ $1/(M \cdot day)$	computed using equilibrium data of *Nordstrom et al.* [1990]
$k^f_{H_2O}$	110.0 $1/day$	*Crooks* [1975]
$k^b_{H_2O}$	$2.46\text{x}10^{16}$ $1/(M \cdot day)$	computed using equilibrium data of *Nordstrom et al.* [1990]
k^f_1	7.69 $\frac{mol}{(cm^2\ day)}$	*Chou et al.* [1989]
k^b_1	$7.69\text{x}10^{-2}$	computed using equilibrium data of *Nordstrom et al.* [1990]
k^f_2	$4.32\text{x}10^{-3}$ $\frac{mol}{(cm^2\ day)}$	*Chou et al.* [1989]
k^b_2	$1.14\text{x}10^2$	computed using equilibrium data of *Nordstrom et al.* [1990]
k^f_3	$5.62\text{x}10^{-6}$ $\frac{mol}{(cm^2\ day)}$	*Chou et al.* [1989]
k^b_3	$1.512\text{x}10^{-3}$	computed using equilibrium data of *Nordstrom et al.* [1990]